NUCLEAR MAGNETIC RESONANCE IN SOME BINARY LIQUID SYSTEMS SHOWING A METAL NON-METAL TRANSITION

DAVID JOHN KIRBY, B.Sc.

A thesis submitted to the University of Warwick for admission to the degree of Doctor of Philosophy

Department of Physics July 1981

TABLE OF CONTENTS

ACKNOWLEDGEMENTS

I wish to express my sincere appreciation of the patient guidance, criticism and friendship of Dr. R. Dupree during his excellent supervision throughout the course of this work. I wish to thank Professor P. N. Butcher and Professor P. W. McMillan, Chairmen of the Department of Physics, University of Warwick for making available the necessary research facilities, and all the members of the Nuclear Magnetic Resonance Group, Department of Physics, University of Warwick for helpful discussions, information and companionship. Special thanks are due to:

Dr. W. Freyland, University of Marburg, Germany, for assistance in caesium alloy containment and provision of some samples.

Dr. J. A. Gardner, Oregon State University, U.S.A. for experimental assistance in the study of selenium-tellurium alloys.

Dr. W. W. Warren, Jr., Bell Telephone Laboratories, U.S.A. for performing independent NMR measurements of caesium-gold alloys and debate as to their interpretation.

The technical support of Mr. T. B. Sheffield is gratefully acknowledged, as is the financial assistance of the Science Research Council, who made this work possible by providing a quota studentship. I am very grateful to Miss S. Callanan for her accurate and speedy typing of this thesis. Finally, I wish to thank my wife, Karen, for her continued support and encouragement during this work, and for practical assistance in the completion of this thesis.

D. J. Kirby

DECLARATION

This thesis is submitted to the University of Warwick in support of my application for admission to the Degree of Doctor of Philosophy. It contains an account of work carried out in the Department of Physics during the period of October 1977 to September 1980 under the supervision of Dr. R. Dupree. No part of this work has appeared in any thesis at this or any other institution. The work reported in this thesis is the result of my own independent research except where specifically acknowledged. Dr. W. W. Warren, Jr., of Bell Telephone Laboratories, U.S.A. independently obtained some of the caesium-gold alloy NMR results presented in Chapter 4.

Some parts of the research reported here have been published as follows:-

1. Dupree, R., Kirby, D. J., Freyland, W., and Warren, W. W. Jr., (1980) Phys. Rev. Lett. 45, 130.
   "Observation of NMR of the Formation of Localised Electronic States in an Ionic Liquid Alloy".

2. Dupree, R., Kirby, D. J., Freyland, W., and Warren, W. W. Jr., (1980), J. de Phys. 41, C8-16.
   "^{133}Cs NMR Investigation of Liquid Cs-Au Mixtures".

3. Dupree, R., Kirby, D. J., and Gardner, J. A., Symposium on Nuclear and Electron Resonance Spectroscopics Applied to Materials Science (Boston 1980). "NMR in Liquid Semiconducting Se_xTe_{1-x}".

It is anticipated that a full report of the caesium-gold system including stoichiometric CsAu will be published. The results of the study of the caesium-antimony system and a more complete report of the selenium-tellurium system will also be published.

D. J. Kirby

ABSTRACT

The results are reported of a pulsed nuclear magnetic resonance investigation at frequencies up to 59 MHz of three binary liquid alloy systems which demonstrate a wide range of electrical properties as a function of composition and temperature. The systems studied are caesium-gold and caesium-antimony, which both show marked deviations from metallic properties at the stoichiometric compositions CsAu and Cs_3Sb, and selenium-tellurium, where increasing temperature or tellurium content give rise to more metallic properties. The aim of the work was to investigate the mechanism of the metal non-metal transition and to determine the nature of the non-metallic states which form. In Cs-Au and Cs-Sb the major emphasis is placed on the concentration dependence of properties at constant temperature, and in Se-Te two concentrations $Se_{0.5}Te_{0.5}$ and $Se_{0.4}Te_{0.6}$ are studied as a function of temperature. Nuclear resonances shifts, spin-lattice T_1, spin-spin T_2, and phase memory T_2^*, relaxation times are measured.

For the system Cs-Au, the addition of gold to caesium has only a small effect on the resonance properties, until for excess mole fraction of caesium = 0.07 a sharp peak is observed in the ^{133}Cs relaxation rate and the shift changes from a nearly free electron behaviour to linear dependence on concentration with only a small shift at stoichiometry. The metal non-metal transition gives rise to strongly localised electron states in the form of F-centres in liquid alloys near the composition CsAu. A thermally generated background concentration of paramagnetic centres is observed near stoichiometry. Addition of large amounts of gold (0.50 mole fraction) to stoichiometric CsAu has negligible effect on the small ^{133}Cs shift. An ionic, molten salt description of liquid CsAu is appropriate.

In contrast to Cs-Au, the addition of small amounts of antimony to caesium causes a rapid decrease in the ^{133}Cs Knight shift. Near stoichiometric Cs_3Sb, the density of states is low and the resonance shift small, (although larger than in caesium salts implying a larger chemical shift contribution). Covalent bonding is much more important in Cs_3Sb than in CsAu. In Cs_3Sb at room temperature a quadrupolar splitting of ^{133}Cs resonance was observed. Neither ^{121}Sb or ^{123}Sb were observed in any of the alloy samples investigated due to the strong quadrupolar interaction which gave rise to extremely rapid spin lattice relaxation times < 3 μs.

For Se-Te near the melting point $T_1 > T_2$ and values of the hyperfine field correlation time are deduced for each nucleus. We find $\tau_{Te} > \tau_{Se}$. The hyperfine field data suggests non-random bonding in these liquids. Shift and relaxation rates for both ^{77}Se and ^{125}Te in both alloys demonstrate similar behaviour and are intrepreted in terms of interaction of the nucleus with a thermally activated concentration of unpaired electrons which localise as chain end defects. ^{77}Se in $Se_{0.4}Te_{0.6}$ demonstrates a change of hyperfine field strength with increasing temperature which is interpreted in terms of a structural transition from a Se-like to a Te-like liquid. This was not observed for other nuclei due to loss of signal with increasing temperature.

CHAPTER ONE

THE METAL NON-METAL TRANSITION IN BINARY LIQUID SYSTEMS

1.1. Introduction

A metal-nonmetal transition occurs in many condensed systems as some thermodynamic parameter such as pressure, temperature or composition is varied (Mott, 1974). Examples are found in crystalline substances like transition metal compounds (Mott, 1974), and also in a great many amorphous solids like highly doped semiconductors (Fritzsche, 1978), metal-halide mixtures (Cheshnovski et al, 1977) and metal-metal mixtures denoted "charge transfer insulators" (Avci and Flynn, 1978).

Liquid systems showing a metal-nonmetal transition include expanded fluid metals (Cusack, 1978) metal-ammonia solutions (Cohen and Thompson, 1968), polar molecular liquids (Hensel, 1977), metal-molten salt solutions (Bredig, 1964, Angell, 1971), liquid semiconductors (Cutler, 1977) and liquid alloys (Enderby, 1978). Hensel (1977) differentiates between fully ionised molten salts and covalent liquid semiconductors on the basis of the electronegativity difference of the constituents, ΔX, and room temperature band gap, E_g. He suggests, on the basis of intermediate ΔX and E_g values, a borderline group containing for example CuI and CsAu. These materials are semiconducting solids but undergo an unusual transition to ionic liquids on melting. The wide ranging recent review of Warren (1980) discusses the metal-nonmetal transition in a variety of liquid systems.

Historically the name "Liquid Semiconductor"was coined by Ioffe and Regel (1960) to describe all non-metallic liquids possessing low electrical conductivity, σ, with a positive temperature coefficient. However, Enderby (1974) has pointed out that the positive sign of $d\sigma/dT$ in liquid alloys is a possible consequence of the temperature dependence of the partial interference

functions, and this serves to emphasise that the increase of conductivity with temperature cannot simply be ascribed to excitation of charge carriers across an energy gap as in a crystalline semiconductor, but more probably indicates a temperature dependent chemical structure. The term 'liquid semiconductor' is now used rather more selectively to refer to only those covalently bonded non-metallic liquids such as In_2Te_3, which have a dominant electronic contribution to conductivity. Liquid semiconductors are the molten phase of semiconducting solid compounds although the converse is not necessarily true since several crystalline semiconductors become metallic on melting: Ge, Si, III-V compounds. This is due to an increase in density and is in accord with the general incompatability of small atomic volume with semiconducting behaviour (Pearson, 1972). A comprehensive review of the electronic properties of liquid semiconductors is provided by Cutler (1977) and the physico-chemical properties by Glazov et al (1969).

In the study of the liquid state it is well to recognise the frequent import of ideas originally applied in related fields. For instance the relatively well understood characteristics of the gaseous and solid states of matter are often used to gain insight to liquid properties. In some ways intermolecular forces dominate giving a solid-like fixed volume, whilst in other ways thermal motion dominates giving a gas-like mobility. For the question of electrical transport in liquids concepts from the wider field of disordered materials are generally invoked (Mott and Davis, 1971, Tauc, 1974), but the greater freedom for temperature promoted changes of chemical structure and the mutual effect on electronic structure must be borne in mind.

The concentration dependence of the electrical transport properties of binary liquid alloy systems can be classified in two broad groups (Enderby, 1974). Many alloys of elemental liquid metals retain metallic values of electrical conductivity and thermopower across the whole range of the phase diagram. However there are some systems which show markedly non-metallic properties in the vicinity of particular fixed compositions.

Frequently one component is a chalcogen element but several examples are known in which both elemental liquids are 'good' metals, yet at compositions corresponding to the satisfaction of chemical valence requirements a sharp change to non-metallic behaviour is observed. Fig. 1.1 demonstrates the conductivity minima that occur as a function of composition at constant temperature in the systems Li-Pb, Mg-Bi, Li-Bi, Cs-Sb and Cs-Au. To facilitate comparison of different systems the concentration scale is quoted in terms of mole fraction rather than atomic fraction. Consider a general system M-A where M is the more electropositive element with valence m and A has valence a. The assumption is made that a molecular group, M_qA_m, forms leaving any excess of either M or A in an unbound state. For example if M is in excess over the compound composition:

$$M_xA_{1-x} \equiv M_y + (M_aA_m)_{1-y} \qquad (1.1)$$

then x represents the atomic fraction of M whilst y represents the mole fraction of M.

The electrical transport data of liquid systems showing non-metallic properties is surveyed by Allgaier (1969). He uses a different classification scheme to that of Enderby, but since a continuous range of properties between liquid metals and liquid non-metals is observed an absolute, definitive categorisation is impossible. Such schemes can never explain the nature of a system but do aid tabulation of behaviour.

Approaches to the understanding of the electronic structure of non-metallic liquids have started with models borrowed from extreme but related classes of materials. Certainly the conventional free electron or semi-conductivity models are unable to describe the sharp conductivity minima observed at stoichiometry in some liquid systems. Appropriate idealised models are adapted from molecular bonding, distorted crystal or metallic models (Cutler 1977). Different non-metallic liquids cover a wide range

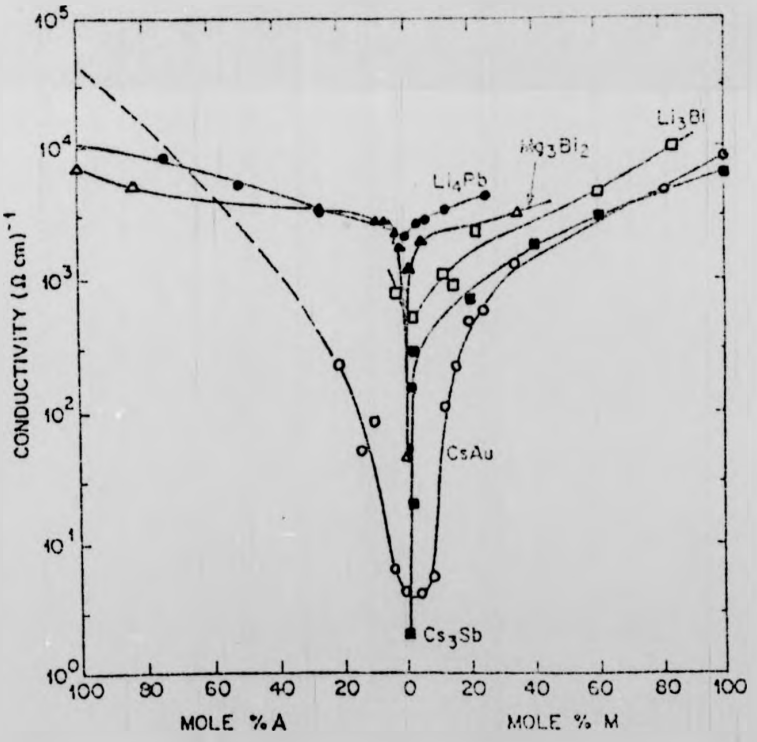

Fig. 1.1: Some examples of conductivity isotherms versus excess concentration in metal-metal solutions where non-metallic behaviour is observed at the stoichiometric composition $M_a A_m$. M is the more electropositive metal.
(After Warren 1980).

- ● Li-Pb @ 800°C, Nguyen and Enderby (1977)
- ▲ Mg-Bi @ 900°C, Ilschner and Wagner (1958)
- △ Mg-Bi @ 900°C, Enderby and Collings (1970)
- □ Li-Bi @ 1150°C, Steinleitner et al (1975)
- ■ Cs-Sb @ 800°C, Freyland and Steinleitner (1977)
- ○ Cs-Au @ 600°C, Schmutzler et al (1976)

of properties and clearly the model most suited to a given system is the one which best emphasises its particular behaviour. For example, liquid Mg_3Bi_2 is relatively highly conducting and a metallic model is probably closest, whilst molten selenium is best described by a molecular bond model. One feature common to all models is the appearance of a dip in the density of states curve near the Fermi Energy, E_F. Such a dip is known as a pseudogap and can be thought of as corresponding to the crystalline semiconductor band gap.

Interest in the electronic structure of non-metallic binary liquids has concentrated experimental research in thermoelectric measurements: conductivity σ, thermopower S, and Hall coefficient R_H. There is a relative paucity of structural, magnetic and optical information which is in no small way associated with the severe experimental difficulties associated with the systems of interest. Low temperature approaches to electronic structure such as electronic specific heat or de Haas van Alphen effect measurements are clearly precluded. The high temperature and chemical nature of many constituents often result in corrosive liquids with appreciable vapour pressure, such that the choice of suitable containment and electrode material requires much auxiliary effort.

This work investigates the composition dependent metal-nonmetal transition in the systems Cs-Au and Cs-Sb, and the temperature dependent metal-nonmetal transition in Se-Te. Each represents a different subgroup of liquid binary alloys: liquid CsAu turns out to be a molten salt composed of Cs^+ and Au^- ions, the liquid semiconductor Cs_3Sb is covalently bonded with electronic conduction, and Se-Te is composed of a covalent extended network. Such differences will be reflected in the electronic structure, but discussion of each system is deferred to the appropriate chapter where a full description of the experimental and theoretical background is presented.

For a metal non-metal transition which occurs as a function of composition in a binary liquid alloy there are three regions of interest. First of all at metal rich compositions the system is metallic and nearly free electron concepts are appropriate. Secondly, the nature of the transition from extended to localised states which often occurs near $y \approx 0.50$ mole fraction excess metal is of considerable interest. It seems unlikely that any one model can adequately explain the roles of disorder, electron-electron correlation and the relative ionicity/covalency of chemical bonding in the many different systems. Thirdly, what is the nature of the localised electron states when the stoichiometric compound has a small excess of metal, and which physical and chemical properties are essential to stabilise localised states in the liquid?

1.2. Bonding

Many binary liquid alloys exhibit anomalous properties at a characteristic composition $M_a A_m$ satisfying common chemical valence requirements. The bonding of a compound is frequently expressed in terms of three extreme models, although in reality the true picture must be intermediate.

1. Molecular or directed covalent bonds: the valence requirements are satisfied within a molecule and the liquid consists of electrically neutral molecules.
2. Ionic bonds: the s- and p- valence electrons are localised on the electro-negative ion.
3. Mixed bonds: a fraction of s- and p- electrons are localised with the remainder involved in an extended covalent network.

Covalent bonding is more familiar in light elements because their intermolecular bonding is weaker and intramolecular stronger than for heavy elements, (Phillips, 1973). Atomic orbitals of heavy elements are not as well separated due to the presence of the large ion core, and so orbitals

other than just those of the valence electrons play a role in bonding. Covalent bonds in heavy element alloys are therefore less directional and can more readily accommodate distortions which alter the bond angle. These effects can be considered to add a partial metallic character to covalent bonding in heavy metal alloys.

Since the electronic character of a material is intimately related to the range of chemical interaction between the constituents a knowledge of bonding might be expected to allow the prediction of the nature of the compound. Generally the greatest difficulty lies in deciding the charge distribution per bonded atom, or the ionicity of the bond. An empirical guide to ionicity is provided by the electronegativity difference (Pauling, 1960)

$$\Delta X = X_A - X_M \qquad (1.2)$$

Electronegativity, X, is a measure of the attraction of an element for a valence electron and as such it is a real property of an element. However it is inexactly defined and various authors dispute the best way of determining electronegativity (Gordy and Thomas, 1956; Pauling, 1967; Phillips, 1970). In particular the value for one element is not independent of the second element in the bond. However the different electronegativity values lead to similar predictions for values of ΔX. The bond ionicity, $I = P/ed$, where P is the dipole moment of the bond and d the bond distance, is related to ΔX by Paulings empirical relationship

$$I = 1 - \exp(-\Delta X^2/4) \qquad (1.3)$$

However the possibility of complex formation complicates the evaluation of ionicity. The complexing ratio R is defined as the ratio of the coordination number of an atom to its valence. Phillips (1973) gives the effective ionicity I_c as

$$I_c = 1 - (1 - I)/R \qquad (1.4)$$

In a liquid, thermal disorder will prevent R having a value greater than six.

At compositions away from stoichiometry the electronic structure is strongly related to the nature of the bonding of the excess element. Cutler (1977) suggests that the best guide is whether, or not the excess element bonds covalently to itself, otherwise metallic bonding of the excess is assumed. For instance in the system M-A if element A is Te and is in excess it can covalently bond to itself, and this will happen even if the M-A bond is ionic.

A further complication is that excess of an element of mixed valence may bond with the mixed valence. For instance, Cu is found with equal preference for its two options 1 and 2. For the case of In a valence of 3 tends to be preferred to 1.

1.3. Liquid Structure

Structural information about liquids is in principle most directly obtained from neutron or X-ray diffraction studies (Enderby, 1974). The quantity obtained from a diffraction experiment is the static structure factor S(Q), but several experimental corrections are required to the raw scattered intensity, see Enderby (1968) for neutrons, Pings (1968) for X-rays. S(Q) is then related to the radial distribution function g(r) by means of a Fourier transform

$$g(r) - 1 = \frac{\Omega}{2\pi^2 N} \int_0^\infty (S(Q)-1) \frac{\sin Qr}{Qr} Q^2 \, dQ \qquad (1.5)$$

In practice truncation errors are introduced since the upper limit is usually $\sim 12\ \text{Å}^{-1}$, and additionally the random error in S(Q) creates a cummulative error at low r after the transform. North et al (1968) describes a suitable correction method. The radial distribution function

g(r) describes the average atomic arrangement of the atoms in the liquid, and is defined so that the average number density of atoms in a spherical shell of radius r about any given atom is given by g(r) multiplied by the average number density of the whole liquid.

In the case of binary liquid alloys M-A it is necessary to introduce three structure factors S_{MM}, S_{MA}, S_{AA}, each of which has a corresponding pair distribution function g_{MM}, g_{MA}, g_{AA}. Experimentally the total coherent scattering intensity must be measured in the same alloy on three separate occasions with different form factors. Two possible methods are; neutron diffraction using isotopically enriched samples (Edwards et al, 1975), or X-ray diffraction of several concentrations relying on the variation of form factor near the absorption edge (Waseda and Tamaki, 1975).

The "bench marking" technique of Enderby (1978) enables structural studies to be interpreted in terms of the bonding near stoichiometry. In this approach structural studies of liquids with reasonably well understood bonding are used as a reference for the liquid alloy under investigation. The reference categories are:-

1. symmetric ionic, NaCl
2. non symmetric ionic, $BaCl_2$
3. incomplete ionic, CuCl
4. molecular, $TiCl_4$
5. extended covalent network, Te.

To date there is little structural information on binary liquid systems, but the ionic character of both CsAu and Li_4Pb has prompted the suggestion that all metal-metal systems are ionic to first order (Enderby, 1978). This is not necessarily at variance with the experimental observation of conductivities greater than expected for a molten salt. For instance, both Li_4Pb and Mg_3Bi_2 have $\sigma = 50\ \Omega^{-1}\ cm^{-1}$ just above the melting point indicating that a significant electronic

contribution is present in addition to any ionic conduction in these systems.

1.4. Metallic Conductors

The distinction between crystalline metals and insulators is based on ideas proposed by Wilson (1931). At absolute zero a metal is a material in which one or more of the energy bands is partly occupied, whereas in an insulator all bands are either completely full or empty and an energy gap separates the occupied and vacant states. The distinction between insulators and semiconductors is less clear and depends upon the magnitude of the energy gap. When the gap is sufficiently small that significant numbers of electrons can be thermally excited the material is termed a semiconductor, whereas insulators have energy gaps of $\gtrsim$ 3eV and negligible carrier densities.

A solid crystal with a periodic lattice has an electronic structure which can be described in momentum space on the basis of the nearly free electron model. (Faber, 1972). The free electron parabolic dispersion curve is modified by long range order which eliminates all the Fourier components of the interaction potential except at $\underline{K} = \frac{1}{2}\underline{G}$ to create an energy gap at the Bragg planes. Consequently the density of states shows a small perturbation which can result in a net decrease in energy $\Delta E \sim |V(G)|^2$ if the Fermi energy, E_F, lies in this region. Fig. 1.2.

In a liquid the atomic arrangement must be represented by an isotomic probability distribution with the destruction of long range order. The simplification of electron band structure results in a spherical Fermi surface, but the electron-ion and electron-electron interactions remain important. See for example the review by March (1968) on electronic properties in liquids.

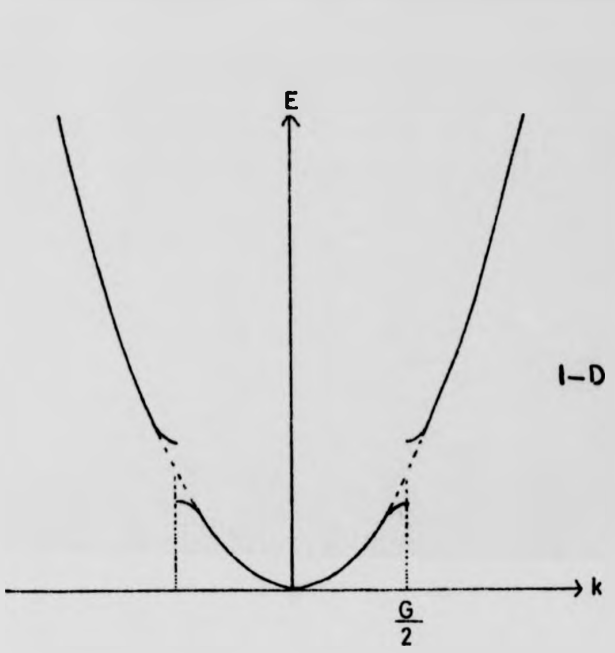

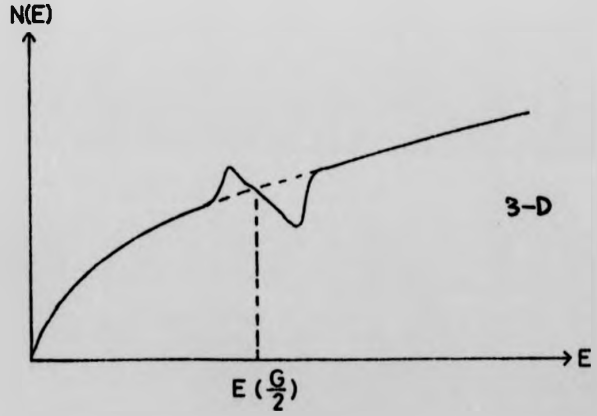

Fig. 1.2: The effect of a Bragg plane reflection on the electron dispersion curve, E(k), and density of states, N(E).

For many liquid metals the nearly free electron theory of Faber and Ziman (1965), (Faber, 1972) is well supported by experimental investigations of electrical conductivity. These materials have values of σ typical of solid metals ($\sigma \gtrsim 3000\ \Omega^{-1}\ cm^{-1}$) and a long mean free path compared to interatomic distance, $\lambda > a$. The weak scattering of electron plane waves is treated by the Born approximation and the main problem is the choice of an appropriate pseudopotential. The conductivity may be expressed as

$$\sigma = \frac{S_F\, e^2 \lambda}{12\pi^3 h} \tag{1.6}$$

where S_F is the Fermi surface area.

The thermopower S is related to σ through

$$S = \frac{\pi^2}{3}\frac{k^2 T}{e}\left(\frac{d\ln\sigma}{dE}\right)_{E=E_F} \tag{1.7}$$

and the elementary equation for the Hall coefficient $R_H = \frac{1}{nec}$ (1.8)

is found satisfactory in pure liq metals, but the situation is less clear for alloys.

1.5. The Pseudogap in Non-Metallic Liquids

Cohen, Fritzche and Ovshinsky (1969) and Davis and Mott (1970) discuss a general model for electron transport in amorphous semiconductors, which was developed for the case of non-metallic liquids by Mott (1971), and is generally referred to as the pseudogap model.

In the study of impurity conduction in crystalline semiconductors it is well known that potential fluctuations at sites of impurity atoms cause the normal band edges to show a smearing or 'band tailing'. (Halperin and Lax, 1966, 1967). If short range order characteristic of covalent bonding exists then the introduction of long range disorder as in amorphous or liquid systems does not necessarily destroy the band gap of a crystalline semiconductor. Instead it results in the smoothing of

Van Hove singularities and a spreading of the density of states into the gap to produce a pseudogap, Fig. 1.3a. This approach; adding disorder to a band structure in which a gap already exists; is known as the distorted crystal model and has been treated theoretically by Gubanov (1965) with emphasis on the amorphous state.

In the metallic approach to the pseudogap model the starting point is the NFE density of states. With the introduction of stronger electron ion interaction and long range disorder the electron mean free path, λ, decreases and the Born approximation is no longer valid. A large dip may develop in N(E) associated with a particular geometric cluster of atoms, stabilised by a structure sensitive decrease in energy if E_F is near the minimum, Fig. 1.3b. In this picture thermal disruption of clusters would lead to an increase of the density of states washing out the pseudogap. With $\lambda \sim a$, where a is the interatomic spacing, Mott (1967) argues that the change in the density of states at the Fermi level becomes the controlling factor for σ, and

$$\sigma = \frac{g^2 e^2}{3ha} \tag{1.9}$$

where

$$g = \frac{N(E_F)}{N(E_F)_{\substack{\text{Free} \\ \text{electron}}}} \tag{1.10}$$

This approach is expected to be valid for $150 < \sigma < 3000\ \Omega^{-1}\ cm^{-1}$ which is called the diffusive regime. Evidence in support of the diffusive mechanism of transport is provided by magnetic measurements where the data fits the predicted equation. E.g. nuclear magnetic resonance shift $\alpha\ \sigma^{\frac{1}{4}}$ (Warren, 1972a), (Seymour and Brown, 1973). The expression for thermopower is also satisfactory,

$$S = \frac{\pi^2}{3} \frac{k^2 T}{e} 2 \left| \frac{d \ln N(E)}{dE} \right|_{E = E_F} \tag{1.11}$$

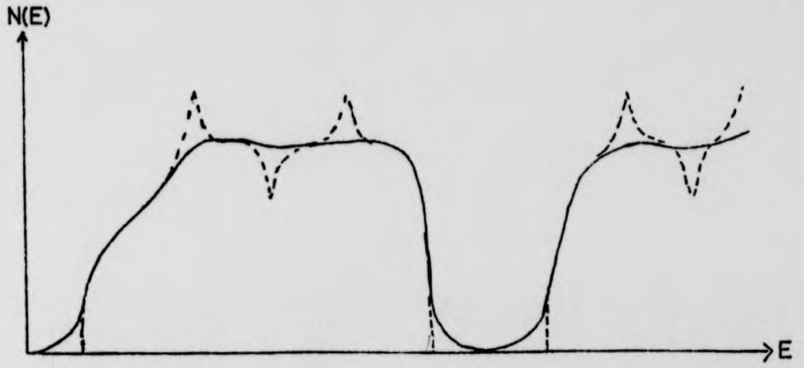

Fig. 1.3a: The smoothing of the density of states, N(E), resulting from loss of crystalline long range order. The pseudogap arises from band tailing due to potential fluctuations.

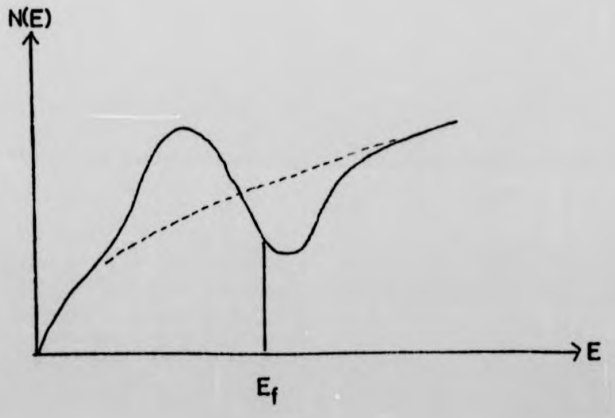

Fig. 1.3b: Pseudogap in the density of states, N(E), due to formation of molecular clusters in the liquid.

but there are problems associated with momentum transfer in the expression for the Hall coefficient. Friedman's theory (1971) accounts only partially for the experimental behaviour.

$$\frac{R}{R_{\substack{\text{Free}\\ \text{electron}}}} = C.g^{-1} \qquad (1.12)$$

The Mott g factor introduced in describing diffusive transport is occasionally troublesome because of the difficulty of knowing just which electrons to count in the free electron approximation. For lower values of σ the spatial character of the electron states acquires great significance.

In a tight binding formulation weakly overlapping atomic states form extended states in a band of width $\Gamma = 2Jz$ where J is the overlap integral and z is the coordination number. Anderson (1958) showed that in the presence of potential fluctuations ΔV, localised states occur when $\Delta V > \eta\Gamma$, where η is some critical value, later evaluated by Mott (1972a) to equal 2. Mott (1968) developed Anderson's theory to consider whether localised and extended states are separated in energy within a band. For a large enough N(E) there will be available sites sufficiently close in energy for an electron to diffuse throughout the volume. For a given ΔV there is a critical density of states below which the tunnelling distance is too large and the electron becomes localised in a given region. Mott suggests that the transition occurs for $g \simeq 1/3$.

It is noteworthy that there is still some dispute as to whether localised states do form as a result of potential fluctuations, (see E.g. Thouless, 1972), but the concensus view is affirmative. Mott (1969) has further suggested that the directional nature of non-s- electrons means they are more likely to become localised than are s-electrons, since they have greater sensitivity to disorder.

Hence there is a value of energy, E_c, which separates localised and extended states and a lower limit for non-activated conductivity must exist. E_c is referred to as the mobility edge, since at finite temperatures the electrical conductivity of localised states is several orders of magnitude smaller than that of extended states. Fig. 1.4. Motts equation (1972a) for the conductivity due to extended states at the mobility edge is

$$\sigma(E_c) = \frac{0.025\ e^3}{ha} = \frac{610}{a^*}\ \Omega^{-1}\ cm^{-1} \qquad (1.13)$$

where $a^*(\mathring{A})$ is the interatomic distance (typically $4\mathring{A}$) and the coordination number $z = 6$. This suggests the minimum metallic conductivity, $\sigma(E_c) \sim 150\ \Omega^{-1}\ cm^{-1}$, is the non-zero lower limit of conductivity in extended states before a discontinuous transition to essentially zero electronic conductivity in localised states occurs. The validity of the minimum metallic conductivity concept is the subject of considerable current interest. As a consequence of the exclusion of the electron wave function from regions of potential fluctuations, Eggarter and Cohen (1970) and Economou et al (1974) have proposed that $\sigma(E)$ decreases more rapidly than $N^2(E)$ and thus goes continuously to zero as $E \to E_c$ from above. It seems likely however that the disputed differences in the shape of $\sigma(E)$ near E_c are unimportant for liquids because they occur on a scale $\leq kT$.

If the density of states at the Fermi Energy, $N(E_F)$, is sufficiently below the free electron value then the observed low conductivity due to localised states is described by the empirical expression (Stuke, 1969)

$$\sigma = \sigma(E_c)\ \exp(-\Delta E/kT) \qquad (1.14)$$

In principle for localised states below the mobility edge two conduction processes are possible.

1. when $1 < \sigma < 150\ \Omega^{-1}\ cm^{-1}$, the predominant mechanism is the excitation of carriers into excited states above the mobility gap.

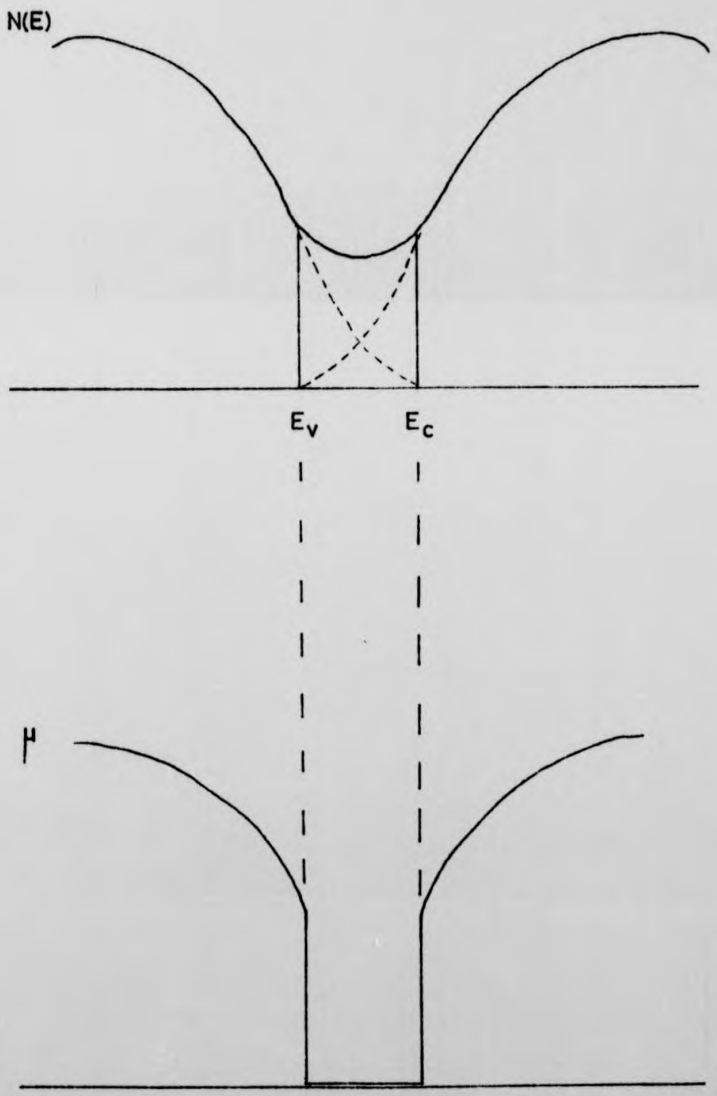

Fig. 1.4: The density of states, N(E), and mobility (μ) near a pseudogap. The energies E_c and E_v define the mobility edges.

2. thermally activated hopping involving the exchange of energy with some source such as phonons.

The first theory of hopping is due to Miller and Abrahams (1960) and the problems are discussed by Butcher (1974). The diffusive motion of charge occurs on a time scale characterised by atomic vibrations to sites that are random in both distance and potential. Nearest neighbour hopping dominates at higher temperatures, but at low temperatures Mott (1969) has shown that variable range hopping is favoured. In this regime the predicted $\sigma \alpha \exp(-\text{const } T^{-\frac{1}{4}})$ is observed in many amorphous solids (Mott, 1978). However, in liquids the continuous diffusive motion of atoms suggests that hopping is not a satisfactory approach. The low mobility of heavy ions in water is an analogous situation.

Transport equations appropriate for E_F in the mobility gap are given by Cutler and Mott (1969)

$$\sigma = \sigma(E_c) \exp(-(E_c - E_F)/kT) \tag{1.15}$$

$$s = \frac{k}{e}\left[1 + \frac{(E_c - E_F)}{kT}\right] \tag{1.16}$$

1.6. Molecular Bond Model for Non-Metallic Liquids

Another approach to the density of states in non-metallic liquids is the bond orbital model which was first applied by Cutler (1971, a,b) to liquid Tl-Te system. Its basis is the assumption of widely separated discrete molecules in which the electronic states of different bonds and non-bonding electrons are independent. The energy and electronic nature of the bond orbitals can be estimated by the semi-empirical methods of structural chemistry. Bringing molecules close together as in real liquid systems broadens the electronic energy levels into bands which can be described by tight binding theory. This method is equally suited to the situation in which network structures or small molecules result from

bonding. Band tailing is expected to create an interband pseudogap. Following the extensive review of Cutler (1977) this model is first illustrated with reference to the Tl-Te system assuming zero ionicity.

The electronic configuration of Te is $5s^2$, $5p^4$ and that of Tl $6p^1$. Bonding of two atoms is assumed to be a linear combination of p orbitals and hybridisation is not considered for simplicity, although in practice the bonding energy is usually increased as a result of mixing of atomic orbitals. Bringing atoms together results in a decrease of energy for the symmetric combination which concentrates charge between atoms and an energy increase for the charge cancelling combination. A Te atom normally forms two bonds; the degeneracy of the original p-orbitals is therefore lifted in the creation of a low energy bonding state σ, and a high energy antibonding state σ^* either side of the remaining non-bonding state π. The four Te p-electrons are distributed so that one p-electron occupies each σ orbital (shared with a bonded atom) and two remain in the π orbital. The σ-σ^* splitting for the Te-Tl bond is different to that of Te-Te due to the larger bond energy. Fig. 1.5 shows schematically the bond orbital process and the associated energy bands for the case of Tl at a Te chain end.

At T = OK pure Te or Tl_2Te has the Fermi energy at the top of the π band. With increased temperature breaking of the Te-Te bond may occur, (Cutler, 1971a). For each dangling bond there will be two extra states and only one extra electron in the π band so that the net effect is to add a hole to the band. Fig. 1.6. Hence this model shows how p-type conduction arises and $N(E_F)$ increases with temperature. Cutler's calculation of conductivity as a function of the fraction of broken bonds shows good agreement with experiment. This approach also describes the Te rich composition range when chains of $Tl-(Te)_n-Tl$ form.

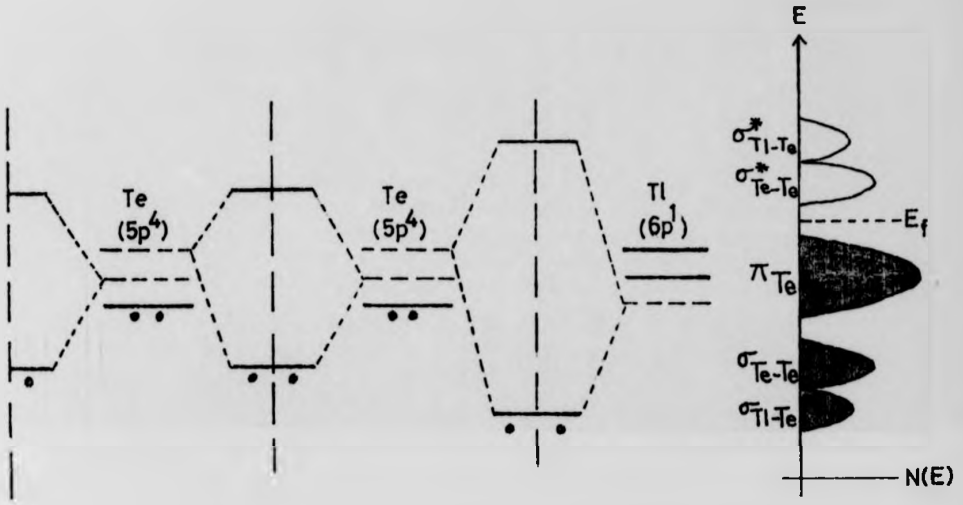

Fig. 1.5: T = OK. Electron ground state energy levels and corresponding tight binding bands for Tl_xTe_{1-x} alloys, $x < 0.67$. Atomic orbitals - - - - are converted to molecular bond orbitals ——— and electron occupancy is represented ●.

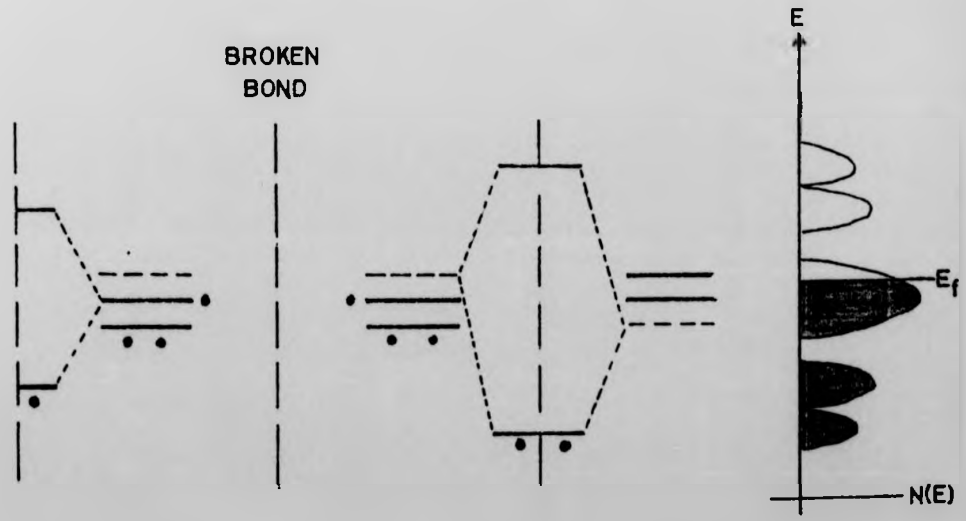

Fig. 1.6: T > OK. Creation of holes in the valence band due to broken Te-Te bonds in Tl_xTe_{1-x} alloys, $x < 0.67$.

Another possible effect of non-zero temperature is a thermal distortion of the bonding configuration. This would have the effect of reversing the level splitting and result in a shift of discrete states toward their original atomic orbital values. Thermal vibrations would therefore cause the σ and σ^* bands to have tails toward the π band as shown in Fig. 1.7. Cutler (1971 (a)) claims that this process may be more important than bond breaking in extended network structures.

A modification to the above molecular bond scheme is necessary in the case of an alloy in which the constitutents have an electronegativity difference such that ionicity might be expected to play a role. For different atoms the initial atomic energy levels will be different, but charge transfer shifts the levels toward each other. (see for example Coulson, 1961). Fig. 1.8 shows schematically the result of charging and of the subsequent σ - σ^* splitting due to bonding. If A is taken to be an element with some non-bonding states such as Te, the tight binding σ and π bonds are likely to overlap strongly as shown. If A is a group V element then there is no π band since all three p-electrons benefit energetically from forming σ bonding orbitals.

1.7. Electronic Structure Away from Stoichiometry

There is a concensus view that a pseudogap exists in the density of states at the stoichiometric composition of some liquid alloys systems. However for compositions away from stoichiometry there is a wide diversity of opinions.

Based on a model of Enderby (1973), the model of Roth (1975) has however gained general acceptance for interpretation of ionic binary systems. The electronic structure of a system M-A as a function of composition is presented in Fig. 1.9. Band tails and possible regions of localised states are shown hatched. With the addition of small amounts

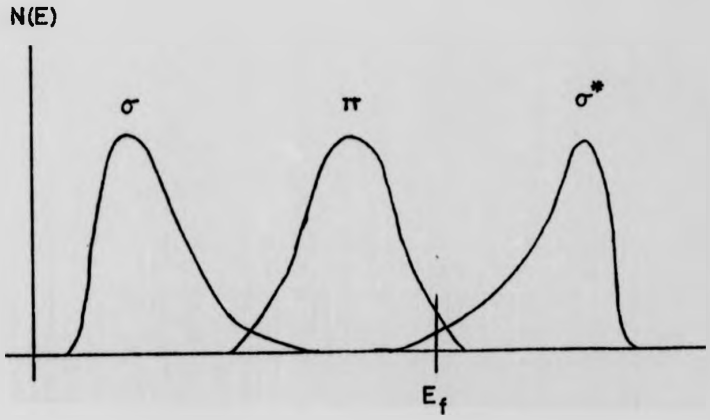

Fig. 1.7: Tailing of the σ and σ* bands towards the original atomic orbitals due to thermal distortion of the bonding configuration in extended network structures.

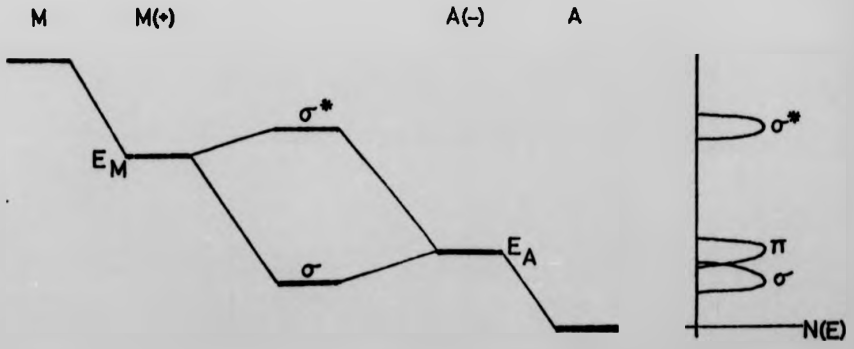

Fig. 1.8: Energy levels and tight binding bands in a partially ionic alloy M-A.

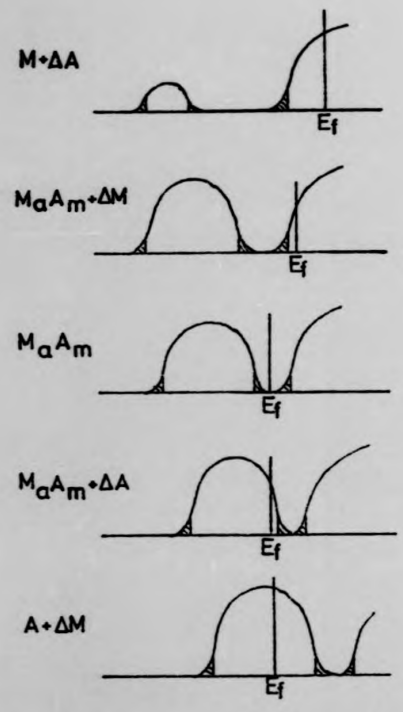

Fig. 1.9: Electronic structure as a function of composition due to Roth (1975) for the liquid ionic system M-A. The lower band is due to A^{a-} ions. Band tails with possible regions of localised states are shown hatched.

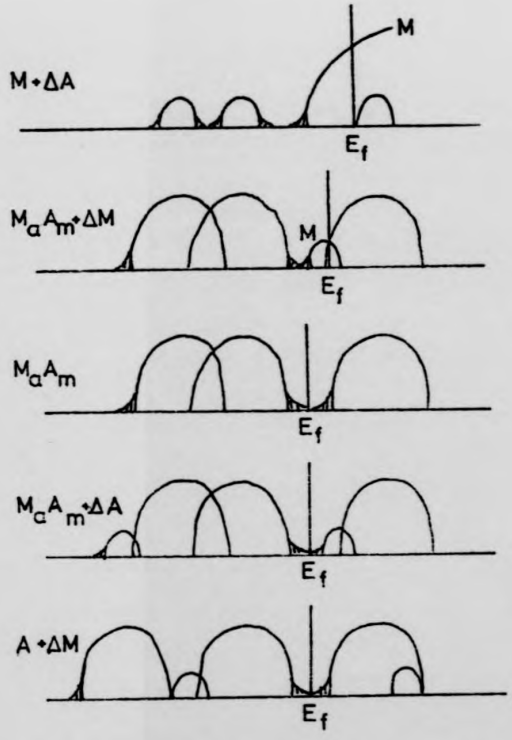

Fig. 1.10: Cutler's (1977) modification of Roth's model for partial covalent bonding. Only in the excess A range is different behaviour from Fig. 1.9 predicted.

of A to M, the bonding electrons form a new band below the Fermi energy which may or may not be separated from the conduction band by a gap. As the concentration of A is increased the A^- band grows and E_F moves down the conduction band since each A atom adds more states than electrons. At stoichiometry E_F is located midway in the pseudogap. Excess of A causes E_F to enter the valence band, which becomes a partly filled band of pure A in the limit of negligible concentration of M. The liquid system Mg-Bi is thought to obey this model.

Cutler (1977) describes a modification of Roth's model for the situation of partial covalent bonding between element M and a chalcogen, A. Fig. 1.10 presents the main features. In M rich alloys the only difference from the ionic case is the splitting of the valence band into σ and π states. Near stoichiometry the reduced M band has become an impurity band which may be absorbed into the σ^* band. At stoichiometry E_F is midway in the pseudogap. If excess A remains unbonded, then E_F moves down the valence band as in the ionic model above. If A atoms bond covalently to each other, then the valence band remains filled and insulator behaviour occurs (at T = OK) as indicated in Fig. 1.10.

An alternative approach is provided by Enderby and co-workers (Enderby and Simmons, 1969; Enderby and Collings, 1970), who speculate that the Hall coefficient is a useful measure of the charge carrier nature and that bound states due to molecular groups at stoichiometry form a band separated in energy below the conduction band. E_F always remains in the conduction band. A peak in R_H at stoichiometry therefore arises from depletion of the number of free electrons arising from either excess M or A. A virtual bound state near E_F was suggested to explain the sign change of thermopower at stoichiometry and the major criticism of this approach is the rather special scattering properties required to reproduce the observed behaviour.

Faber's (1972) model overcomes the thermopower difficulty by assuming the excess element forms an impurity band near the bottom edge of the conduction band, and therefore the N(E) has a different character according to which element is in excess. The impurity band grows into a fully-fledged band in the limit of excess concentration = 1. Although qualitatively satisfactory a separate impurity band is unlikely unless the Eg is large (and σ small). Also impurity band conduction near stoichiometry suggests N(E) would be very sensitive to composition, but Cutler has shown that rigid bands are satisfactory in Tl-Te.

Several authors have approached the electrical properties of non-metallic liquids through non-homogeneous structural models. (Hodgkinson 1971, 1973; Cohen and Jortner, 1973, 1974a; Bhatia and Thornton, 1970; Cutler, 1976c). Density or concentration fluctuations within a sample are considered to create well defined regions and conduction is determined by percolation processes. However thermodynamic considerations do not lend support to this approach (see for example Cutler, 1977).

§1.8: The Effects of Correlation

The disorder-induced Anderson transition and the transition with change of density in divalent metals are both examples of metal-nonmetal transitions permitted in the approximation of non interacting electrons. However the metal-nonmetal transition occuring for example in expanded liquid alkali metals is inexplicable within the classical band model of non interacting electrons. In many systems, if not all involving localised states, electron-electron interactions (correlation) plays an essential role as discussed with different emphasis in the work of Mott and Hubbard.

For a crystalline array of one electron atoms at the absolute zero of temperature Mott (1949, 1961) has shown that a sharp metal-nonmetal transition occurs as the lattice parameter is varied. Defining the number density of electrons as n, and a critical value as n_c, then for $n > n_c$ the ion potential is well screened and a metallic state is formed. However for $n < n_c$ the screening of the long range Coulomb force is insufficient and the free electron gas crystallises into an insulating state. A small number of free carriers is impossible since bound pairs form (Mott and Davis, 1971), and hence a discontinuous change in the number of carriers is predicted. Mott's criterion for the transition is

$$n_c^{1/3} a_H^* \approx 0.26 \qquad (1.17)$$

where a_H^* = effective hydrogen-like radius.

Edwards and Sienko (1978) have shown the applicability of this equation for a variety of materials over a range of n_c equal to 10 orders of magnitude.

The role of the interatomic Coulomb energy was considered formally by Hubbard (1964), who showed that a metal-nonmetal transition was predicted without the need for interatomic Coulomb forces. The Hubbard energy U is defined as the electrostatic repulsive energy of two electrons located on the same atomic site, and for large interatomic separation

$$U = \left\langle \frac{e^2}{r_{12}} \right\rangle = E_I - E_A \qquad (1.18)$$

where r_{12} is the electronic separation

E_I is the ionisation energy

E_A is the electron affinity.

The Hubbard model predicts the splitting of a half filled conduction band of a monovalent metal into two Hubbard bands. The metal-nonmetal transition

occurs when U is approximately equal to the undistorted bandwidth and the lattice parameter is such that the bands separate. At absolute zero the lower band is full and the upper band empty. In the absence of long range Coulomb forces no discontinuous change in the charge density is expected.

The influence of correlation on metal-nonmetal transitions is discussed fully by Mott (1974).

CHAPTER TWO

NUCLEAR MAGNETIC RESONANCE

2.1. Magnetic Susceptibility

The magnetic susceptibility χ, is the most basic magnetic property and may be expressed per mole, per unit mass or per unit volume. For the interpretation of microscopic properties χ_{mole} is the most useful and may for instance be obtained from a combination of density data with χ_{vol}; χ_{mass} is determined by the Gouy Method. Nachtrieb (1962) and Gardner and Cutler (1976) provide examples of the experimental approach necessary for the high temperature study of liquids of interest in this work.

The total measured susceptibility is made up of principally two parts: one due to the ion cores and the other to the conduction electrons

$$\chi_{total} = \chi_{\substack{ion \\ core}} + \chi_{\substack{cond \\ elec.}} \qquad (2.1)$$

The diamagnetic susceptibility of the ion cores is often dominant so that even in liquid metals the net effect may be diamagnetic or only weakly paramagnetic (Dupree and Seymour, 1972). Estimates of the value of $\chi_{\substack{ion \\ core}}$ have been made by direct measurements of ionic salts or by calculation from the free ion wave function, but are not entirely satisfactory. This uncertainty hinders the extraction of $\chi_{\substack{cond \\ elec}}$ which contains information about the electronic structure. The electronic susceptibility itself contains both spin paramagnetism and orbital diamagnetism, and on the free electron model its value is dependent upon the density of states at the Fermi level, $N(E_F)$. However for real metals, electron-electron correlations lead to an enhancement of the static susceptibility (Pines, 1955) producing for example a factor of the order of 2 for alkali metals.

Two cases are of special importance: for nearly free electron metallic liquids a Pauli paramagnetism is expected.

$$\chi^{P}_{elec} = \mu_o \mu_B^2 N(E_F) \qquad (2.2)$$

where μ_B is the Bohr magneton.

For a dilute concentration of localised electrons as found with excess metal in a non-metallic compound or broken covalent bonds a Curie-type susceptibility is appropriate.

$$\chi^{P}_{elec} = \frac{N\mu_o \mu^2}{3kT} \qquad (2.3)$$

where μ is the magnetic moment,

k Boltzmann constant,

T the absolute temperature

2.2. Introduction to Nuclear Magnetic Resonance

Nuclear magnetic resonance (NMR) is the spectroscopy of the nuclear Zeeman energy levels in a static magnetic field, and was first observed by Bloch et al (1946) and independently by Purcell et al (1946). An extensive literature has subsequently arisen on the many different aspects and applications of NMR and therefore this chapter introduces only the material most relevant to this work. A full discussion of the theory of NMR is to be found in Abragam (1961) and Slichter (1978). The use of pulses of power at a discrete frequency in the observation of NMR was first put into practice by Hahn (1950). The behaviour of the spin system is studied after the pulse is turned off, and the same spectral information is obtained as in continuous wave experiments, with the added advantage of direct access to spin relaxation information.

Magnetic resonance phenomena occur in systems possessing both a

magnetic moment $\underline{\mu}$ and spin angular momentum $\hbar\underline{I}$. These quantities are related by the magnetogyric ratio γ according to

$$\underline{\mu} = \gamma\hbar\underline{I} \tag{2.4}$$

The interaction of the magnetic moment with an applied magnetic field $\underline{B}_o$ is given by the Hamiltonian

$$H = - \underline{\mu}.\underline{B}_o \tag{2.5}$$

and this results in the equally spaced Zeeman energies

$$E_m = - \gamma\hbar B_o m \tag{2.6}$$

where m is an eigenvalue of I_z, the component of $\underline{I}$ along $\underline{B}_o$ which is conventionally taken to define the z axis. Transitions can be induced by supplying radiation tuned to the energy difference between neighbouring levels, and thus the resonance condition is given by

$$\omega = \gamma B_o \tag{2.7}$$

Classically the resonance frequency corresponds to the Larmor frequency of gyroscopic precession of a magnetic moment in the applied magnetic field. Strictly the time varying field is a rotating field and the direction of notation must be included

$$\underline{\omega} = - \gamma\underline{B}_o \tag{2.8}$$

For nuclear spins ω corresponds to radio frequencies.

Occupation of the energy levels is described by a Boltzmann distribution when the nuclear spins are in thermal equilibrium with their environment, the "lattice". Despite the equal probability for stimulated upward and downward transitions a net absorption of energy therefore occurs because of the larger number of lower energy spins. To prevent saturation there must be some means of restoring thermal equilibrium when the levels become equally populated, and this is provided by a relaxation interaction

between the spins and the lattice.

Consider a system of N identical nuclei of spin I = ½ in a static magnetic field B_o creating Zeeman levels separated by $2\mu B_o$. Let N_1, N_2 be the occupancy of the lower and upper levels respectively. In thermal equilibrium

$$\frac{N_2}{N_1} = \exp\left(\frac{-2\mu B_o}{kT}\right) \tag{2.9}$$

If the level occupancy is disturbed by an r.f. field then the return to thermal equilibrium when the r.f. field is switched off is characterised by

$$\frac{dn}{dt} = \frac{-(n-n_o)}{T_1} \tag{2.10}$$

where $n_o = N_1 - N_2$ at thermal equilibrium

n = instantaneous population difference

$1/T_1 = (W\downarrow + W\uparrow)$ = the sum of the probabilities per second for spin lattice transitions up and down.

T_1 is therefore a characteristic time associated with the approach to thermal equilibrium and is related to the microscopic details of the spins and the lattice. The study of T_1 provides much information concerning the dynamic nature of the nuclear environment.

Spin-spin couplings allow the establishment of thermal equilibrium among the spins. Such processes vary the relative energies of the spin levels and are characterised by a relaxation time T_2.

The non-zero 'natural' width and shape of a resonance absorption line arise from a combination of the finite lifetime (T_1 process) and energy level fluctuations (T_2 process). The line shape function for Lorentz lines common in liquids is

$$g(\omega) = \frac{T_2}{\pi} \frac{1}{1+T_2^2(\omega-\omega_o)^2} \tag{2.11}$$

where the half width at half height is given by

$$\Delta\omega_{\frac{1}{2}} = \frac{1}{T_2} \tag{2.12}$$

The observed experimental linewidth $^1/T_2^*$ may have an additional contribution due to magnetic field inhomogeneity, which causes spins in different parts of the sample to precess at slightly different frequencies.

$$\frac{1}{T_2^*} = \frac{1}{T_2}_{\text{natural}} + \frac{1}{T_2}_{\text{magnet}} \tag{2.13}$$

The effect of motion in a non-viscous liquid is to reduce all couplings with the nuclear spin, such that the r.m.s. local field is much less than in the rigid lattice. The dominant contribution to the linewidth is therefore due to lifetime broadening and in the limit of extreme motional narrowing, $\omega\tau << 1$, T_2 increases until $T_2 = T_1$. For viscous liquids in which $T_1 > T_2$ a long correlation time τ is indicated, and the T_1/T_2 ratio enables τ to be determined. A generalised form of the T_1 and T_2 dependence on τ, valid for any interaction, is presented in Fig. 2.1. (see for example Slichter, 1978).

In condensed matter there is an ensemble of spins and for each the actual field experienced is modified from B_o by an average internal field associated with the nuclear environment. The resonance condition can thus be written

$$\omega = \gamma(B_o + \Delta B) \tag{2.14}$$

and measurement of the nuclear resonance shift provides information about the static aspects of interactions with the nuclear spin. These will generally include nuclear dipole-dipole interactions, magnetic couping of electrons to nuclei, and the strong electrostatic effects between electrons and nuclei possessing electric quadrupole moments.

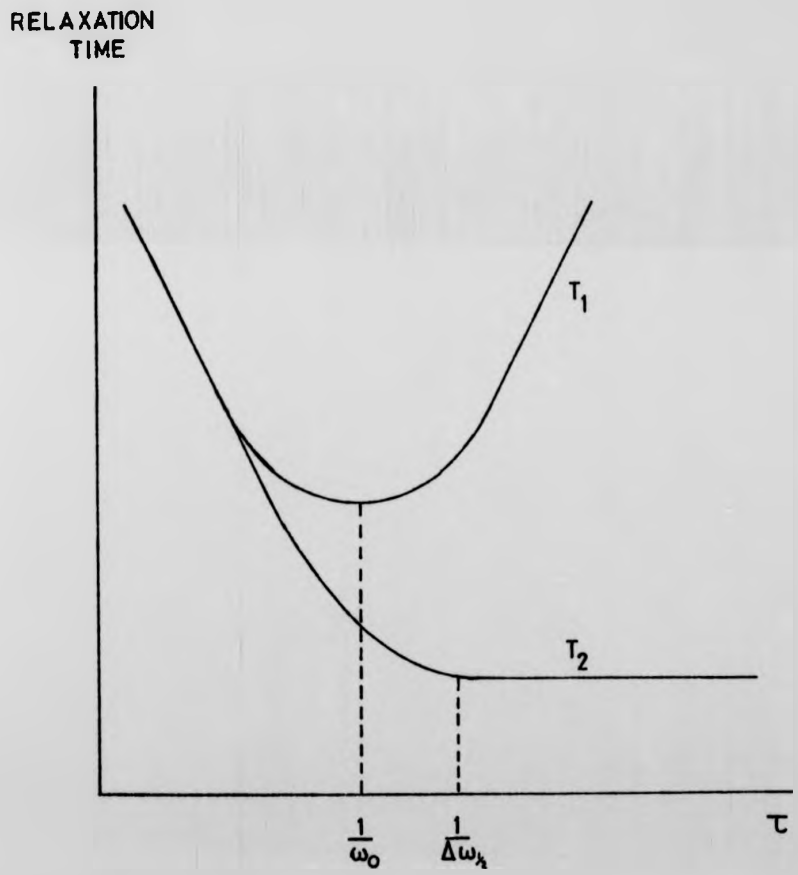

Fig. 2.1: Generalised form of the spin-lattice relaxation time, T_1, and spin-spin relaxation time, T_2, as a function of the correlation time for the interaction causing relaxation, τ. ω_0 is the nuclear Larmor frequency and $\Delta\omega_{\frac{1}{2}}$ the rigid-lattice linewidth in angular frequency units.

An important consideration for NMR in metals is the exclusion of r.f. magnetic fields by the r.f. skin effect, described by

$$\delta = \left(\frac{2}{\omega\sigma\mu}\right)^{\frac{1}{2}} \qquad (2.15)$$

where δ is the skin depth

σ is the electrical conductivity

μ is the magnetic permeability.

Frequently metallic samples are divided into particles smaller than the calculated skin depth, but it is sometimes convenient to work with bulk samples. When the skin depth is less than the particle size the nuclear resonance is confined to only nuclei near the surface and a reduction of signal size results. The shape of the resonance line is also distorted due to the interaction of nuclear spins with the induced eddy currents. A further problem is the reduction of the Q factor of the r.f. coil caused by such a lossy sample which also reduces the signal to noise ratio.

2.3. Resonance Shifts and Relaxation Data

A classical description of the net magnetisation during a pulsed nuclear magnetic resonance is now presented. The validity of a classically precessing magnetisation in a quantum mechanical system possessing only $(2I + 1)$ states along $\underline{B}_o$ is explained by the fact that the expectation value of $\underline{\mu}$ has an exactly similar time dependence to that of the magnetisation vector $\underline{M}$ (see for example Slichter, 1978).

A static magnetic field $\underline{B}_o$ produces a preferred orientation of the nuclear spins and a net magnetisation $\underline{M}$ along the z axis. An additional $\underline{B}_1$ rotating in the x-y plane at frequency ω causes M to precess about the direction of the effective field. It is convenient to pursue the description in a rotating frame of reference, in which the z^1 axis is coincident with

the laboratory z axis but the x^1-y^1 plane rotates at ω. (Rabi et al, 1954). In the rotating frame the spin behaves as though subjected to an effective field given by

$$\underline{B}_{eff} = \underline{B}_o + \frac{\underline{\omega}}{\gamma} + \underline{B}_1 \qquad (2.16)$$

Hence for the 'on-resonance' situation of $\underline{B}_1$ rotating in the laboratory frame at the Larmor frequency ω_o, the effective field is in the direction of $\underline{B}_1$. Assuming $\underline{B}_1$ to be directed along the x^1 axis then the magnetisation rotates in the y^1-z^1 plane of the rotating frame as shown in Fig. 2.2. In a time t_p the angle θ through which M precesses is given by

$$\theta = \gamma B_1 t_p \qquad (2.17)$$

Two pulse lengths are particularly important:

1. The 90° pulse, τ_N, which causes $\underline{M}$ to tip into the x^1y^1 plane and point along the y^1 axis.

$$\frac{\pi}{2} = \gamma B_1 \tau_N \qquad (2.18)$$

2. The 180° pulse, τ_{180}, which causes a precession of $\underline{M}$ until it points in the -z direction.

$$\pi = \gamma B_1 \tau_{180} \qquad (2.19)$$

The generation of a component of magnetisation in the x^1-y^1 plane induces a voltage at frequency ω_o in a receiver coil placed in the plane and so enables resonance to be detected.

In the simplest theory, pulses are assumed to be so short that no spin relaxation processes occur during the pulse. Following the end of the pulse the interaction of the spins with each other and the lattice causes the magnetisation to return to its equilibrium value $\underline{M}_o$. The relaxation of the M_{z^1} component is characterised by the spin-lattice or longitudinal relaxation rate $R_1 = {}^1/T_1$, and that of the $M_{x^1y^1}$ component by the spin-

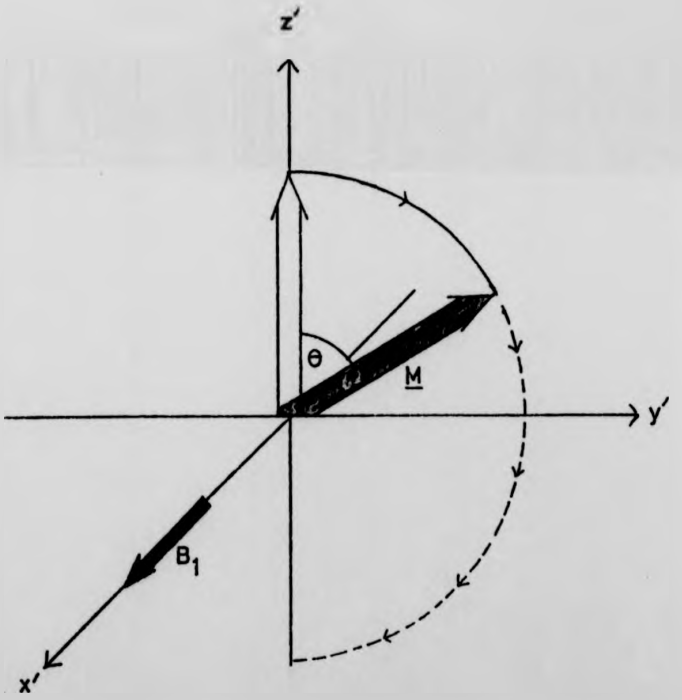

Fig. 2.2: On resonance rotation of the magnetisation vector in the rotating frame of reference. The B_1 field is applied along the x′ axis and precession occurs in the z′-y′ plane. In a time t_p, the angle swept out, $\theta = \gamma B_1 t_p$.

spin or transverse relaxation rate $R_2 = {}^1/T_2$. The decay to zero of the initial signal amplitude created by M_{x1y1} is due to spin dephasing and is known as the free induction decay (F.I.D.). For a sample not in a perfectly uniform magnetic field such dephasing is increased and the signal decays with the characteristic time T_2^* .

For the 'off resonance' situation of the r.f. at a slightly different frequency to the Larmor value, M rotates relative to the rotating frame, and the F.I.D. shows wiggles within the decay envelope at a beat frequency corresponding to the difference from resonance frequency.

The measurement of the F.I.D. following a 90^o pulse is the basic way of determining spectral information. The position of the resonance may be obtained by noting both the frequency of operation and the beat frequency evident in the F.I.D. wiggles. Repeating this procedure at a different operating frequency yields a unique value for the resonance frequency. Nuclear magnetic resonance shifts are then determined by taking as reference the resonant frequency of the same nucleus at infinite dilution in a suitable solution at the same field, or equivalently the resonant field of the reference at the same frequency.

Alternatively, the resonance lineshape can be obtained using pulsed NMR as pointed out by Clark (1964). This relies on the fact that the steady state unsaturated absorption χ'' is proportional to the Fourier cosine transform of the F.I.D. envelope and the disperison χ' is proportional to the Fourier sine transform. (Lowe and Norberg, 1957). By sweeping either frequency or field the output of a boxcar integrator sweeps out the resonance lineshape as discussed further in chapter 3. Calibration of the sweep thus enables the resonance position to be obtained.

It is generally necessary to distinguish three relaxation times characterising nuclear magnetic resonance:

$$T_2^* \leq T_2 \leq T_1$$

The phase memory time, T_2^* is directly obtained from the exponential F.I.D. envelope. This approximation is usually made even though the mangetic field inhomogeneity can result in a non-exponential F.I.D. Equivalently, line-shapes obtained from the boxcar integrator give T_2^*, once gatewidth distortions are accounted for. In rapidly relaxing liquids the magnetic field contribution to T_2^* can be sufficiently small that $T_2^* = T_2 = T_1$, and the simpler determination of T_2^* is used to determine the spin lattice relaxation time. It is necessary to check the validity of this assumption by determining T_1 directly for some data points.

The relaxation times T_1 and T_2 are obtained from observation of the F.I.D. following more complex pulse sequences. A 180°-τ-90° pulse sequence is used for the determination of the spin-lattice relaxation time T_1. The initial 180° pulse tips the magnetisation from the equilibrium value of $+\underline{M}_o$ to $-\underline{M}_o$. After time τ relaxation has changed the z component of magnetisation according to

$$M_\tau = M_o \left[1 - 2 \exp\left(\frac{-\tau}{T_1}\right)\right] \qquad (2.20)$$

Application of a 90° pulse samples the instantaneous magnitude of M_τ by tipping it into the x^1y^1 plane where it is detected by the receiver coil. A series of measurements of M_τ as a function of τ enables T_1 to be determined from a graph of

$$\ell n(M_o - M_\tau) = -\frac{t}{T_1} + \text{const.} \qquad (2.21)$$

A large value of B_1 is required so that there is neglegible relaxation during the pulses and the PRF is limited by the need to allow recovery to thermal equilibrium between pulses. The value of the equlibrium magnetisation M_o at large τ is measured several times during the course of the T_1 measurement to ensure that there have been no changes in the system. (For weak signals the output from the receiver may show random drift due to external radiation being detected).

In solids and viscous liquids the correlation time for nuclear interaction is long enough to distinguish $T_2 < T_1$. The determination of T_2 without the magnetic field inhomogeneity contribution is achieved by the use of Hahn's (1950) 90°-τ-180° spin echo sequence. Following the 90° pulse the spins in the x^1y^1 plane are allowed to dephase for a period τ before a 180° pulse causes precession about the x^1 axis. Refocussing of the spins then occurs at time 2τ along the $-y^1$ axis to create the so-called echo. A series of echo amplitude measurements as a function of 2τ allows the determination of T_2.

$$A_{2\tau} \propto \exp\left(\frac{-2\tau}{T_2}\right) \tag{2.22}$$

The simple spin-echo technique is limited in applicability because of molecular diffusion which reduces the echo amplitude by a term dependent upon magnetic field gradients G, and the diffusion coefficient D. (Carr and Purcell, 1954).

$$A_{2\tau} \propto \exp\left(-\frac{2\tau}{T_2} - \frac{2}{3}\gamma^2 G^2 D\tau^3\right) \tag{2.23}$$

The strong τ dependence has most influence on measurements of long T_2, but must be borne in mind in situations where T_2^* is artifically reduced in order to make the echo visually sharper. Problems are indicated when the echo amplitude is seen to decrease faster than exponentially.

2.4. Nuclear Resonance Shifts

In a fixed magnetic field nuclear magnetic resonance in metals generally occurs at a higher frequency than for the same nucleus in a diamagnetic sample. Equivalently at a fixed frequency the static field required for resonance is lower in a metal. The fractional shift is called the Knight shift, K (Knight, 1949).

$$K = \frac{\Delta\omega}{\omega_d} = \frac{\Delta B}{B_m} \tag{2.24}$$

where ω_d is the resonance frequency in a diamagnetic sample

B_m is the resonance field in the metal.

K is typically $\sim$ 1% and is independent of the value chosen for ω_d (or B_m). A paramagnetic shift is taken to be positive.

In metals the dominant contribution to the local magnetic field at the nuclear site, ΔB, arises from the magnetic contact hyperfine interaction which couples nuclear and electronic magnetic moments

$$H = A\underline{I}.\underline{S}\delta(\underline{r}) \tag{2.25}$$

where A is the hyperfine coupling constant

$\delta(\underline{r})$ is a delta function.

S-type conduction electrons have a net polarisation due to the external field B_o, and because of their finite probability density at the nuclear site they produce an extra magnetic field proportional to B_o. The Knight shift can be expressed as (Townes et al, 1950)

$$K = \frac{\Delta B}{B_m} = \frac{2}{3} \langle|\psi(0)|^2\rangle_F \, \Omega \, \chi_V^P \tag{2.26a}$$

$$= \frac{A\chi_V^P}{\mu_o n \gamma_e \gamma_n \hbar^2} \tag{2.26b}$$

where $\langle|\psi(0)|^2\rangle_F$ is the electronic probability amplitude at the nucleus averaged over states at the Fermi level

Ω is the electron normalisation volume

χ_V^P is the Pauli paramagnetic susceptibility per unit volume.

n is the number density of electrons.

In principle equation (2.26) can be used to obtain the density of states at the Fermi level since χ_V^P is proportional to $N(E_F)$. However

problems arise due to the difficulty of determining $\langle|\psi(0)|^2\rangle_F$. Electron spin resonance experiments can yield this factor directly, but this has only been achieved for alkali metals, (Schumacher and Slichter, 1956; Ryter, 1960). Values of $|\psi_A(0)|^2$ from atomic optical hyperfine structure can be used together with some estimate of the penetration factor, ξ.

$$\xi = \frac{\langle|\psi(0)|^2\rangle_F}{|\psi_A(0)|^2} \tag{2.27}$$

ξ is typically $\sim$ 0.5 (Knight, 1956), and therefore tends to cancel the further problem of the electron-electron susceptibility enhancement, leading to agreement with calculated values of K within about $\pm$ 30%.

The nuclear resonance shift is a measure of the contact interaction but this cannot generally be obtained unambiguously due to the presence of other contributions to the observed shift. For instance, polarisation of the s-electron in the core by the conduction electrons creates an additional resonance shift, S_{cp}, called the core polarisation shift. This is difficult to evaluate since the effect of s, p and d fractional character of the conduction electrons on each core state has to be individually determined. Some contributions may be negative producing a reduction in the observed shift, but S_{cp} is unlikely to be greater than $\pm$ 15% of K.

The nuclear resonance shift, S_o, due to the orbital motion of the conduction electrons is approximately described by Noer and Knight (1964)

$$S_o = \chi_o \frac{\mu_o}{2\pi} \left\langle \frac{1}{r^3} \right\rangle \Omega \tag{2.28}$$

where χ_o is the orbital susceptibility

r is the mean electron orbit radius.

Except for transition metal nuclei S_o is small compared to K and will be neglected.

In different non-metallic compounds there exists a small range in the

observed resonance position of a given nucleus, creating further difficulties in the extraction of the conduction electron contribution to the observed shift. The shifts in insulators are known as chemical shifts and arise from the orbital motion of bonding electrons (Ramsey, 1950). This changes the charge distribution around an atom and mixes high states into the ground state. A diamagnetic shift is defined to be positive.

$$\frac{\Delta B}{B} = -\delta = \frac{2\mu_o e^2 \hbar^2 z}{3m\Delta E} \left\langle \frac{1}{r^3} \right\rangle \qquad (2.29)$$

where z is the number of valence electrons

ΔE is the energy difference between ground and excited state. Chemical shifts are generally at least an order of magnitude smaller than Knight shifts and are dependent upon the molecular environment, (being anisotropic in solid compounds). A chemical shift can in principle be related to electronegativity since a purely ionic closed shell configuration will create no shift.

Finally, localised paramagnetic centres in an insulating system create a shift due to the hyperfine contact interaction which is characterised by a Curie susceptibility

$$\frac{\Delta B}{B} = \frac{\mu_o}{2\pi} czA \frac{\gamma e}{\gamma n} \frac{S(S+1)}{3kT} \qquad (2.30)$$

where A is the contact hyperfine coupling constant with a centre of spin S

c is the concentration of paramagnetic centres

z is the co-ordination number of a paramagnetic centre

For this work, a salient feature of this shift is the linear dependence on concentration which should be contrasted with the (number density)$^{1/3}$ dependence of shift in a metallic system. Furthermore, both expressions for the shift due to the contact hyperfine interaction show that the shift

is proportional to the electronic susceptibility through a constant term involving the coupling constant A. An estimate of A is therefore obtained from the gradient of a shift versus susceptibility graph, and this may aid interpretation of relaxation data as discussed in §2.5.

2.5. Spin Lattice Relaxation

On a semiclassical picture any time dependent transverse component of nuclear spin-lattice interaction with a non zero Fourier component at the resonance frequency ω_o will induce transitions and allow the spin to relax. (Bloembergen et al, 1948). Quite generally the spin-lattice relaxation rate, R_1, can be written

$$R_1 = (\text{interaction strength})^2 . f(\tau) \qquad (2.31)$$

and various approaches to express R_1 in terms of the lattice parameters are discussed by Abragam (1961).

The concept of a spin temperature can be used in the case where spin-spin coupling is much stronger than the coupling of the spin to the lattice. The strong interaction establishes a common temperature for the spins which is then changed by interaction with the lattice. However, in the case of motionally narrowed resonances the density matrix formalism is most appropriate. Here the lattice parameters are taken to be random functions of time and are described by their probability distribution using the density matrix, ρ: a quantum operator which performs the role of the classical density of points in phase space. This approach is exactly equivalent to time dependent perturbation theory but provides a more convenient way of computing thermal equilibrium properties of a system (Slichter, 1978).

In metals the most effective interaction by which nuclei relax is

the scalar contact interaction between nuclear spins and conduction electrons. The correlation time is of the order of the time for a Fermi surface electron to cross the unit cell (Bloembergen, 1949)

$$\tau_c \simeq \frac{\hbar}{E_F} \simeq 10^{-15}\text{s} \tag{2.32}$$

The contact relaxation rate is given by

$$(R_1)_{\text{contact}} = \frac{4}{9} \mu_o^2 \gamma_e^2 \gamma_n^2 \hbar^3 \pi \Omega^2 \langle|\psi(0)|^2\rangle_F N^2(E_F) kT \tag{2.33}$$

The common origin of $(R_1)_{\text{contact}}$ and the Knight shift leads to a relation between these two parameters, first derived by Korringa (1950) for free non-interacting electrons. The Korringa relation is expressed as

$$TK^2 (T_1)_{\text{contact}} = \frac{\hbar}{4\pi k} \frac{\gamma_e^2}{\gamma_n^2} \tag{2.34}$$

This is useful since it allows the conduction electron contribution to the total observed relaxation rate to be determined from observed nuclear resonance shifts, and also allows comparison of experimental K and T_1 with independently determined parameters. It is found that agreement of experiment with equation 2.34 is not always satisfactory, and an additional multiplicative parameter, $K(\alpha)$, is introduced on the right hand side of the above Korringa expression to take into account electron-electron effects. Experimental values of $K(\alpha)$ are near to 0.7 for a number of liquid metals, but the uncertainty in the dynamic part of the spin susceptibility responsible for relaxation makes theoretical estimates of $K(\alpha)$ difficult.

Other magnetic interactions in liquid metals usually make negligible contribution to spin lattice relaxation. For example a Korringa-type relation exists between the shift and relaxation due to core polarisation. However the rate is reduced by a factor of between $^1/_5$ and 1 due to the degeneracy of non s-states at the Fermi surface (Yafet and Jaccarino, 1964).

$$T\, S_{cp}^2 (T_1)_{cp} \geq \frac{h}{4\pi k} \frac{\gamma_e^2}{\gamma_n^2} \qquad (2.35)$$

Note that even if $S_{cp} \simeq 0.15$ K then $(R_1)_{cp} \simeq 0.02 (R_1)_{contact}$. Mitchell (1957) has shown that provided the conduction electron wavefunction has at least 50% s-character then relaxation due to orbital motion of conduction electrons is at least two orders of magnitude less effective than the contact interaction. Interactions such as dipole-dipole and indirect exchange similarly contribute little to R_1 because of their small size and the motionally narrowed regime of most liquids. (Bhoembergen et al, 1948).

Modulation of the hyperfine interaction of localised paramagnetic centres can however be responsible for significant relaxation, as is familiar from the presence of Mn^{2+} ions in water. Except in the case of very strong hyperfine interactions (Ichikawa and Warren, 1979), the relaxation rates are given by (Abragam, 1961).

$$R_1 = \frac{2}{3} \frac{S(S+1)}{h^2} czA^2 \frac{\tau}{1+(\omega_s-\omega_I)^2\tau^2} \qquad (2.36a)$$

$$R_2 = \frac{1}{3} \frac{S(S+1)}{h^2} czA^2 \left(\tau + \frac{\tau}{1+(\omega_s-\omega_I)^2\tau^2} \right) \qquad (2.36b)$$

where c is the concentration of paramagnetic centres,

z is the coordination number of a paramagnetic centre,

A is the hyperfine coupling constant with a centre of spin S,

ω_s and ω_I are the electron and nuclear Larmor frequencies resp.

τ is the nuclear correlation time with an unpaired electron.

When $T_1 \neq T_2$, values for τ can be estimated from the ratio of the observed relaxation times

$$\frac{T_1}{T_2} = 1 + \frac{(\omega_S - \omega_I)^2 \tau^2}{2} \qquad (2.37)$$

An additional important source of spin lattice relaxation for systems with $I \geq 1$ is the interaction of the nuclear quadrupolar moment with a fluctuating electric field gradient (see Gaskell, 1978). This may be caused by the diffusional or vibrational thermal motions of ions or atoms as discussed by Sholl (1967). In addition rotations also modulate local field gradients in liquids composed of relatively stable atomic clusters. If the local environment has cubic symmetry this interaction vanishes, and normally the rapid motion in a liquid leads to time averaged spherical symmetry and hence the absence of quadrupolar shift or splittings. However, there remains a contribution to relaxation as observed for example in liquid Bi (Heighway and Seymour, 1971). In the short correlation time limit

$$(R_1)_Q = \frac{3}{4} F(I) \left(\frac{e^2 Qq}{h}\right)^2 \tau_c \qquad (2.38)$$

where $F(I) = \dfrac{(2I+3)}{I^2(2I-1)}$

eQ = nuclear quadrupole moment

eq = electric field gradient = $\partial^2 v/\partial z^2$

Generally it is not possible to separate magnetic and electric contributions to the observed relaxation rate. One method is to recognise the rapid decrease in $(R_1)_Q$ with increased temperature and so assume that quadrupolar relaxation is negligible at the highest temperatures measured. The experimental high temperature Korringa product TK^2T_1 is then used to estimate the quadrupolar contribution to relaxation at low temperatures.

A more satisfactory determination of $(R_1)_Q$ is provided by the technique of isotopic separation (Warren and Clark, 1969), and is applicable when spin-lattice relaxation rates R_A and R_B can be determined at the same temperature for two isotopes, A and B, of the same atomic species in a

given sample. By defining

$$\alpha = \left(\frac{\gamma_A}{\gamma_B}\right)^2 \tag{2.39}$$

$$\beta = \frac{F(I_A)Q_A^2}{F(I_B)Q_B^2} \tag{2.40}$$

it is straightforward to resolve the observed R_A and R_B into the electric and magnetic contributions provided $\alpha \neq \beta$.

$$R_{AQ} = \beta \frac{(R_A - \alpha R_B)}{(\beta - \alpha)} \quad ; \quad R_{AM} = \alpha \frac{(R_A - \beta R_B)}{(\alpha - \beta)} \tag{2.41a}$$

$$R_{BQ} = \frac{R_{AQ}}{\beta} \quad ; \quad R_{BM} = \frac{R_{AM}}{\alpha} \tag{2.41b}$$

The quadrupolar relaxation rate is determined by instantaneous fluctuations in the electric field gradient, δV_{ij} $^{i,j=x,y}$ and the correlation time of a particular arrangement of neighbouring atoms, τ_c. If δV_{ij} can be obtained from static quadrupolar effects in the solid of a similar system then the experimental $(R_1)_Q$ enables an estimate of τ_c to be made. This is clearly sensitive to the formation of chemical bonds and τ_c is likely to be the rotational time if covalent molecular groups persist for times longer than typical diffusional times, 10^{-12}s. The larger $(R_1)_Q$ is then due to the large τ_c and large value of eq associated with covalent bonds. This $(R_1)_Q$ may be a measure of the degree to which local structural order is perserved above the melting point.

2.6. Investigation of Electronic Structure

The effective use of NMR techniques in the study of electron structure was first demonstrated by Warren (1971). Compared to measurements of bulk transport properties NMR has the advantage that it is a microscopic probe which is sensitive to the local atomic environment, selective with respect to atomic species within an alloy or compound and can be applied to a

wide variety of elemental constituents.

In a metal the Korringa relaxation process is independent of the details of electron transport since the time a conduction electron spends near a particular nucleus is independent of the long free path. Warren (1971) obtains the approximate expression

$$R_M \simeq \frac{16\ kT\ \gamma_n^2}{h\ \gamma_e^2}\ K^2\ \frac{\tau_c}{\hbar N(E_F)} \tag{2.42}$$

when $\lambda > a$, $\tau_c \simeq a/v_F \simeq \hbar N(E_F)$ and the relaxation rate reproduces the Korringa formula to within a factor of $4/\pi$.

When scattering becomes sufficiently strong that $\lambda \simeq a$ or electron localisation occurs then the situation is very different. The "residence time" of an electron at a particular nucleus is increased and nearly free electron concepts are not valid. The factor $\tau_c/\hbar N(E_F)$ increases from unity and the relaxation rate is enhanced

$$\eta = \frac{R_{m_{obs}}}{R_{m_{Korr}}} \simeq \frac{\tau_c}{\hbar N(E_F)} \tag{2.43}$$

Since $R_{m_{Korr}}$ may be computed from experimental values of K, η may be determined from $R_{m_{obs}}$. This is a relatively direct measure of localisation in terms of the time an electron resides at a particular site but there exists no precise criterion to distinguish just when localisation occurs. Fig. 2.3 reproduces Warren's compilation for various liquid metals and semiconductors which reveals how the Korringa enhancement parameter is correlated with the conductivity regimes discussed in chapter one.

The density of states as described by Motts g-factor can be obtained by comparing the Knight shift observed in the non-metallic liquid to the value for the same nucleus in a system of similar composition for which $N(E_F)$ is known. As an example, if there is a temperature or concentration range for which the system of interest is a sufficiently good metal it can be assumed that $N(E_F)$ is given by the free electron value

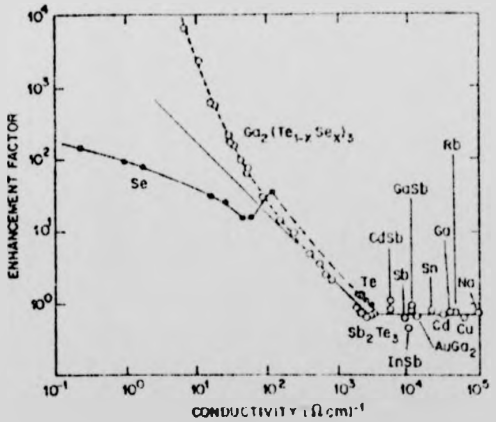

Fig. 2.3: (After Warren and Dupree, 1980b). The Korringa enhancement factor, η, of nuclear relaxation rate versus electrical conductivity for some liquid metals and semiconductors. η is approximately constant in the N.F.E. regime, and $\eta \propto \sigma^{-1}$ is shown for the diffusive transport regime.

$$g = \frac{N(E_F)}{N(E_F)_{\substack{\text{Free}\\ \text{elec}}}} = \frac{K_{obs}}{K_{metal}} \qquad (2.44)$$

Assumptions implicit in this approach are the similarity of penetration factor ξ, electron-electron effects and fractional s-character in both the metallic and 'non-metallic' systems. Further problems may arise from volume changes and the basic difficulty associated with the definition of g discussed in chapter one.

CHAPTER THREE

EXPERIMENTAL

3.1. Sample Preparation

3.1.1. Caesium-Gold and Caesium-Antimony Alloys

Chemicals used in this work were obtained from

caesium: Koch-Light Laboratories Ltd., 99.98%

gold: Koch-Light Laboratories Ltd., 99.999%

antimony: Halewood Chemicals Ltd., 99.999%

The high chemical reactivity of caesium with oxygen and water necessitated the handling of caesium within a well controlled dry, inert atmosphere during the preparation of these alloy samples. Nitrogen gas was passed through molecular sieve types 3A and 4A, silica gel pellets and over a large surface of phosphorous pentoxide, P_2O_5, before being continuously flushed through a glove box. Within the glove box open dishes of phosphorous pentoxide were used to provide further drying of the atmosphere, and a usually sealed container of Titanium tetrachloride, $TiCl_4$ was available to provide a final check on the quality of the atmosphere. No quantitative estimate of moisture content was attempted, but experience showed that several minutes were required for any visible surface tarnish to appear on thin layers of caesium which formed on the base of the glove box after being dropped whilst molten from a surgical syringe.

Target alloy compositions were prepared by weighing required amounts of the elemental metals inside the glove box. Antimony in the form of shot and gold as wire presented no problems, but caesium was transferred from the supplied one gram quartz ampoule to the NMR sample cell whilst molten. Since the efficiency of transfer was clearly unknown in advance and it was considered desirable to have the caesium exposed to the glove box atmosphere for the shortest possible time, the following procedure was adopted.

1. $\sim \frac{1}{4}$ of the pre-weighed target mass of gold (antimony) was placed in the pre-weighed NMR cell.
2. The NMR cell, caesium ampoule and surgical syringe were warmed to 323 K by placing in a suitably drilled, electrically heated brass block.
3. The caesium ampoule was opened and liquid transferred quickly (< 15 sec) to NMR cell, which was temporarily sealed to allow determination of amount of caesium transferred.
4. The correct amount of gold (antimony) was then added to the NMR cell, which was immediately re-sealed.

The strong tendency for caesium and antimony to form the intermetallic compound Cs_3Sb (discussed in Chapter 5) was sufficiently exothermic to cause the destruction of several cells during the production of antimony rich alloys. Caesium-gold alloys did not present this problem. W. Freyland collaborating at the University of Marburg, Germany provided some samples for NMR experiments and was involved in the design of the NMR sample cells which will now be discussed.

Containment of the highly corrosive, high temperature liquid alloys in a form suitable for an NMR experiment is a non-trivial problem. A sectioned diagram of a typical cell is shown in Fig. 3.1. High purity single crystal alumina (sapphire) of wall thickness 1 mm formed the lower part of the cell. This was bonded to a Niobium collar and sealed by means of a re-usable Molybdenum cone compression joint. Problems of leakage arose only at the Niobium-alumina bond due to the corrosion of the glaze by caesium, which has a significant vapour pressure at the temperature of interest, (at 1000 K P_{cs} = 1100 torr, Kaye and Laby, 1968), and a totally inert glaze has not been found. The most successful cells have been produced by the following technique: a preliminary chemical cleaning of the sapphire and Niobium, followed by baking at 1573 K under diffusion

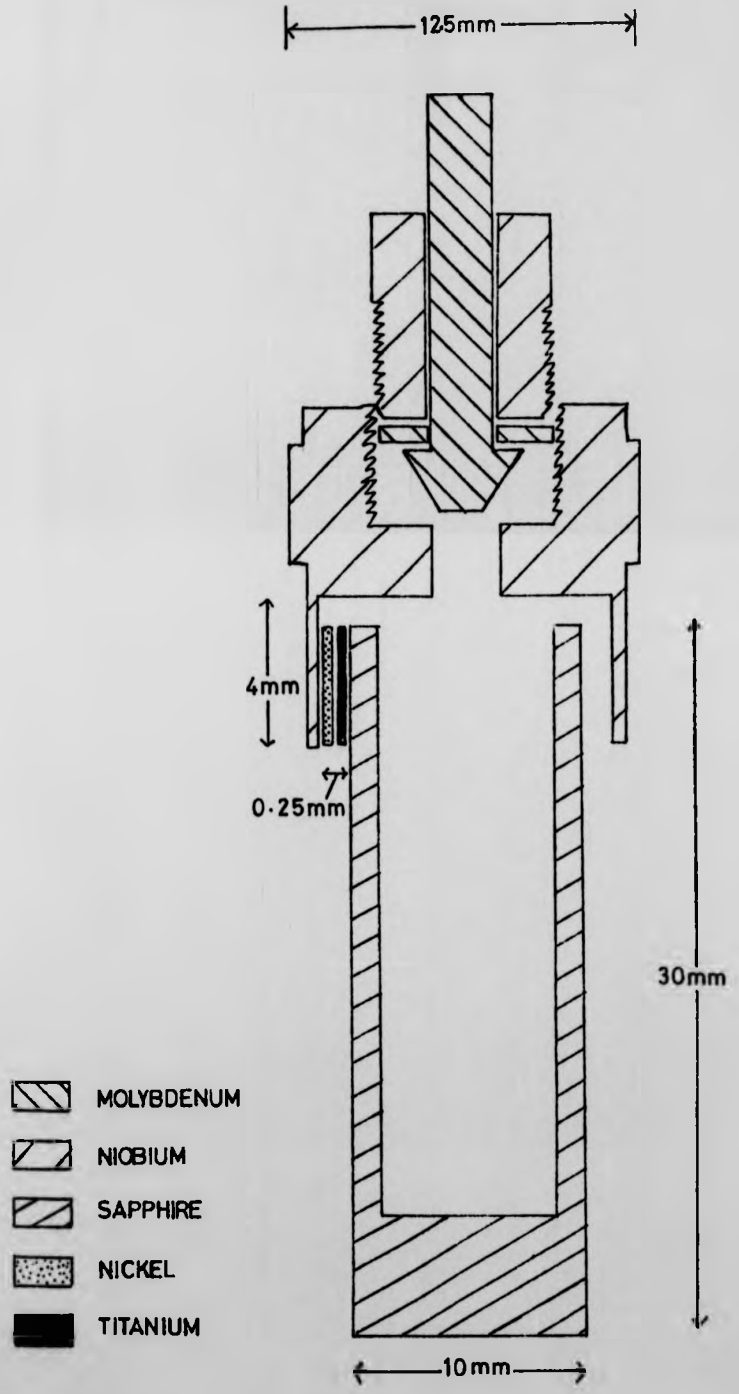

Fig. 3.1: Sectioned representation of an NMR cell used for containment of caesium alloys.

pump vacuum of 10^{-6} torr. After cooling to room temperature, 0.025 mm thick foil strips of Nickel and Titanium (Goodfellow Metals, Ni 99.9%, Ti 99.6%) in the atomic ratio 50:50 were wrapped alternately round the sapphire cylinder to a total foil thickness $\sim$ 0.25 mm, and the total assembly force-fit into the Niobium collar. This was then heated under a vacuum of 10^{-6} torr, and held at 1633 K for only two minutes before cooling. Room temperature helium-gas leak-detection of the resulting seal showed no leak within the instrument sensitivity of 10^{-10} torr ℓ/sec. Recently a new technique has been developed by W. Freyland which requires no glaze. A diffusion bond is achieved between sapphire and Niobium using compression techniques at elevated temperatures.

A filled cell removed from the glove box contained an atmosphere of nitrogen in addition to the alloy composition required. This was removed using the vacuum closure device shown in Fig. 3.2. The cell is prevented from rotating by the internal design and so the cone seal separates when the upper nut is rotated. The gas tight seal of the closure device is preserved by the sliding 'O' rings and so the nitrogen gas from the cell is removed by the rotary vacuum pump. Tightening of the nut by $\sim 30^{o}$ beyond the original fiducial mark then enables a good seal to be obtained.

3.1.2. Selenium-Tellurium Alloys

Chemicals used in this work were obtained from:-

selenium: Koch-Light Laboratories Ltd., 99.998%

tellurium: Apache Chemicals Inc., 99.999%

Despite the toxicity, the experimental constraints are rather more relaxed with this alloy system due to the lack of oxidation problems and the suitability of quartz as a containment material. Operation with the super-conductive magnet requires the generation of a horizontal B_1 field and for

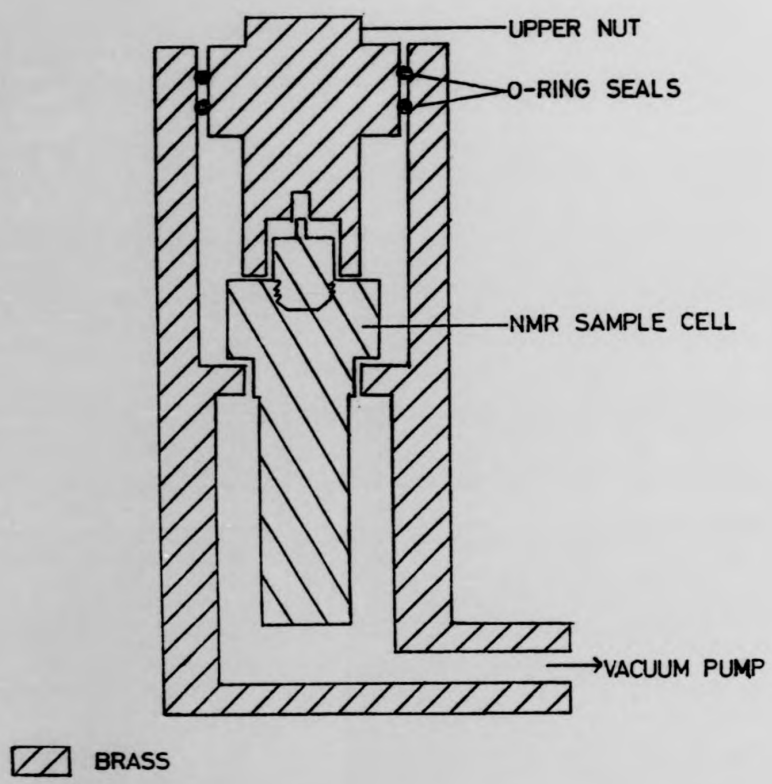

Fig. 3.2: Vacuum closure device used with casesium alloy sample cells.

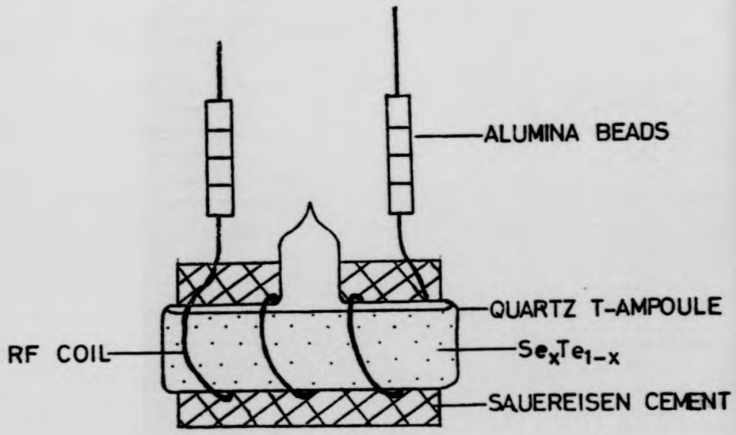

Fig. 3.3: Quartz "T-ampoule" for selenium-tellurium alloys.

reasons to be discussed in §3.5 the desirability of using a solenoidal r.f. coil suggested the use of the 'T-shaped' quartz ampoules shown in Fig. 3.3. Again, specific compositions were obtained by weighing of elemental constituents. Sealing of the quartz was accomplished with the sample under rotary pump vacuum and the ampoule cooled by immersion in water. Unlike the independent r.f. coils used with cells described in 3.1.1., a three turn r.f. coil of silver wire was wound directly onto the Se-Te 'T-ampoule' and cemented in position (§3.5).

3.2. D.C. Magnetic Field

Early work on the caesium-gold system and stoichiometric Cs_3Sb was undertaken using a Varian Associates 15 inch electromagnet. The pole face gap was 1¾ inch (44.5 mm) and static fields up to 2.3 T were controlled by a Varian Associates Field dial unit fitted with variable field sweep facility.

All work on the selenium-tellurium system and the remaining caesium alloys was undertaken using an Oxford Instruments Superconductive magnet with a Niobium-Titanium winding, which makes available static fields up to 7.75 T with uniformity of 6 ppm over a sample volume of 1 cm^3. A 54 mm bore provided room temperature access to the Bo field. A field sweep facility of maximum range ± 0.02 T proved inefficient due to the low permitted rate of change of field, the non-linear start and end to the sweep, and the unequal rate of change when increasing and decreasing the field. These effects originate in the large inductance, 75 H, associated with a superconductive magnet system, and the Lenz Law tendency to oppose any change in the magnetic flux. The low quiescent liquid helium boil-off of 16.5 cm^3/hr was increased to 120 cm^3/hr during magnetic field sweep, due mainly to thermal contact via the (demountable) current leads.

3.3. The NMR Furnace

In order to achieve the elevated temperatures required to melt the alloy samples, and to study the temperature dependence of the NMR properties, a furnace was used for containment of the sample cell and r.f. coil within the region of static magnetic field. Different designs were required for use in the electromagnetic and superconductive magnet, but general principles required of both situations were as follows.

1. The need to fit in the confined magnet space.
2. The control of atmosphere and therefore all seals to be gas and vacuum tight. Metals like Molybdenum and Niobium (used in the r.f. coil and sample cells) react readily with oxygen at high temperatures and experiments must therefore be done under on Argon atmosphere.
3. A non inductive heater winding supplied with dc electrical power.
4. A central hot zone well insulated from the water-cooled outer jacket to protect the solder connections.
5. Continuous temperature mointoring via a thermocouple in the vicinity of the sample.
6. An r.f. input connection.

Fig. 3.4. shows the way in which these requirements are met for a furnace designed for the superconductive magnet. In addition to the furnace body itself, all connections are also constrained to fit within the 54 mm bore. All non-soldered joints are 'O' ring protected for gas tightness. The concentric brass furnace tubes have a spacing of $\sim$ 0.5 mm and the ends are hard-soldered to brass flanges. Copper pipes (6 mm dia.) in the top flange allow water to flow into and out of this cooling jacket space at a rate of $\sim$ 0.5 ℓ/min, and the circulation is controlled by a wire spiral soldered to the inner tube. The heater winding of Nichrome was non-inductively wound on thermally re-crystallised alumina tube of 1 mm wall-thickness and potted in Sauereisen cement of typical thickness 2 mm.

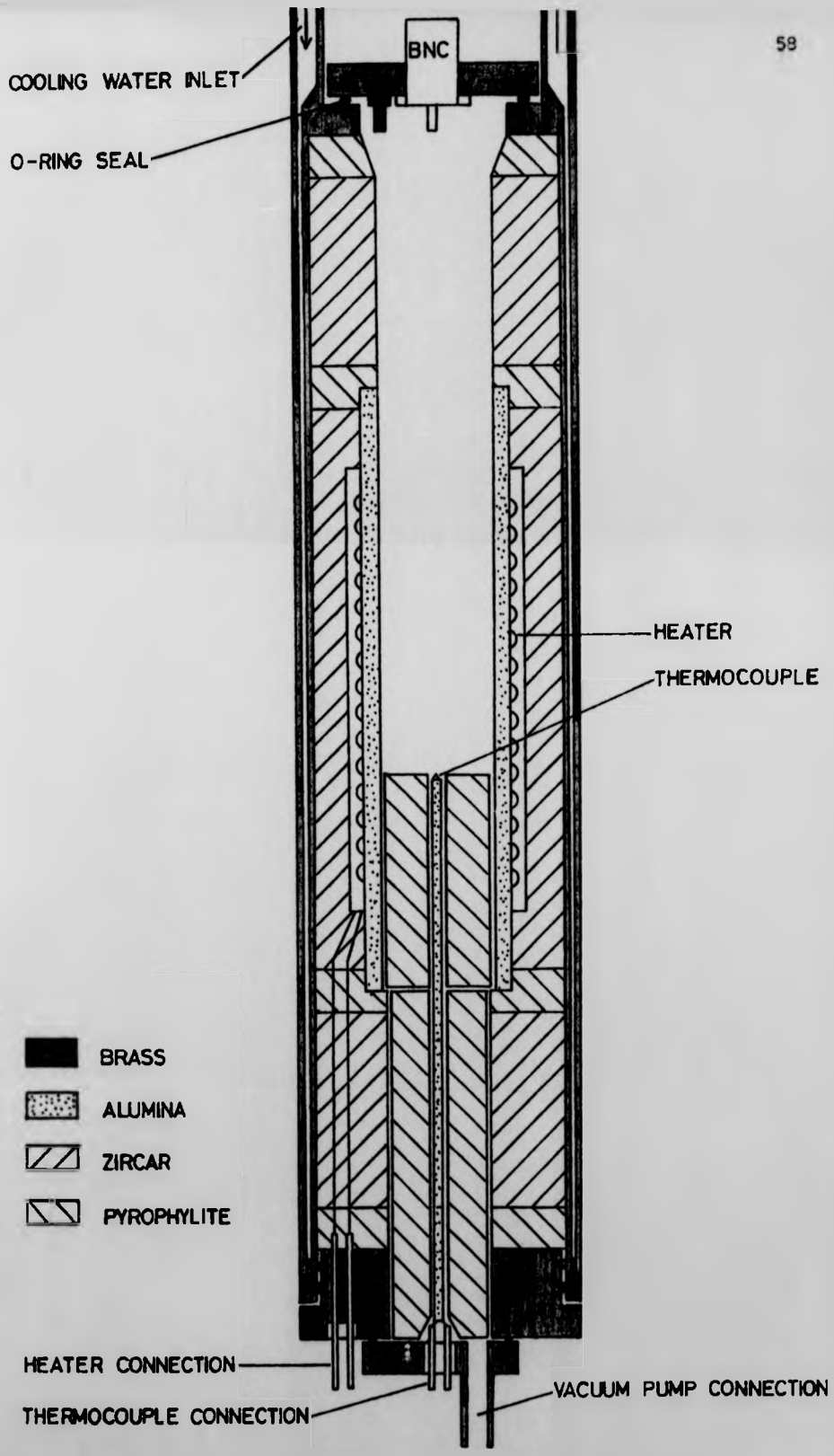

Fig. 3.4: NMR furnace used in the superconductive magnet.

Pyrophylite was machined and fired to create the annular shape necessary to support the alumina heater element centrally within the furnace. Thermal insulation was achieved using Zircar cloth and ½ inch board and the uppermost and lowest stacking pieces produced of pyrophylite for physical strength. Heater leads were fed down through the lower stacking sections and attached by a screw connection to the lead-through connectors in the lower brass flange. A final lower plate contains a vacuum/gas entry pipe and a two pin glass to metal seal to which the chromel-alumel thermocouple was soldered. Within the furnace the thermocouple was insulated in alumina and centred within cylindrical pieces of phrophylite. The furnace top cap had a central BNC connector for contact between the capacitor tuning unit and the r.f. coil, and a glass to metal seal, furnished with an additional thermocouple during calibration of the furnace, but normally with a simple aerial wire to detect the magnitude of the transmitted r.f. pulse. The r.f. coil and sample are suspended from the furnace top cap at a height corresponding to the centre of the furnace hot zone.

Under an argon atmosphere at 873 K the temperature gradient in the absence of a sample showed 5K over a range of 30 mm. This is the worst possible case, and line width evidence from samples with strongly temperature dependent shifts suggests an upper limit not greater than 3 K variation over the sample. During an NMR experiment a conducting sample is stirred by the r.f. magnetic field and consequently the temperature homogeneity is likely to be considerably improved over these estimates.

Continuous thermocouple monitoring allowed observation of the temperature on a WPA direct reading galvanometer and the thermocouple voltage also provided temperature control by means of a modified Thor Cryogenic temperature controller and a Kingshill 50 V, 5 A programmable power supply. Additional noise was often created on the receiver signal by these furnace connections and empirical noise reduction involved elimination of earth loops and connection of capacitors across input terminals.

3.4. The NMR Pulse Spectrometer

In order to undertake pulsed nuclear magnetic resonance investigations the following general requirements must be satisfied:

1. A stable, homogeneous d.c. magnetic field.
2. A stable radio frequency generator and flexible pulse programmer.
3. An r.f. transmitter capable of generating μs bursts of KW of power but no irradiation in the absence of the pulse. The r.f. pulse envelope must have rise and fall times << pulse length.
4. A probe, or sample circuitory, to contain the sample and couple to both the transmitter and receiver efficiently. The transmitter power must generate a large B_1 field over the sample volume and ring-down quickly after the end of the pulse. Having withstood the large r.f. voltages (kV) the probe must be able to respond to the weak nuclear signals (μV) with high sensitivity.
5. A receiver, well isolated from the transmitter, which recovers quickly from overload created by the B_1 pulse to create the maximum signal-to-noise ratio from the nuclear induction.
6. Signal recovery and processing by means of a transient recorder or a box car integrator (when a field or frequency sweep is available) or computer facility.

The instrumentation used in this work is represented schematically in the block diagram, Fig. 3.5. A commerical Polaron pulsed NMR spectrometer, originally supplied for operation at 7, 12 and 21 MHz, was used as the transmitter and receiver stages. Transmitter drive and output stages were rebuilt to facilitate operation at frequencies up to 60 MHz. The radio frequency was obtained from either a crystal or signal generator (for example Marconi Instruments TF 2008) and the frequency determined using a CSC 100 MHz counter. The system coherence was derived from the r.f. carrier used as

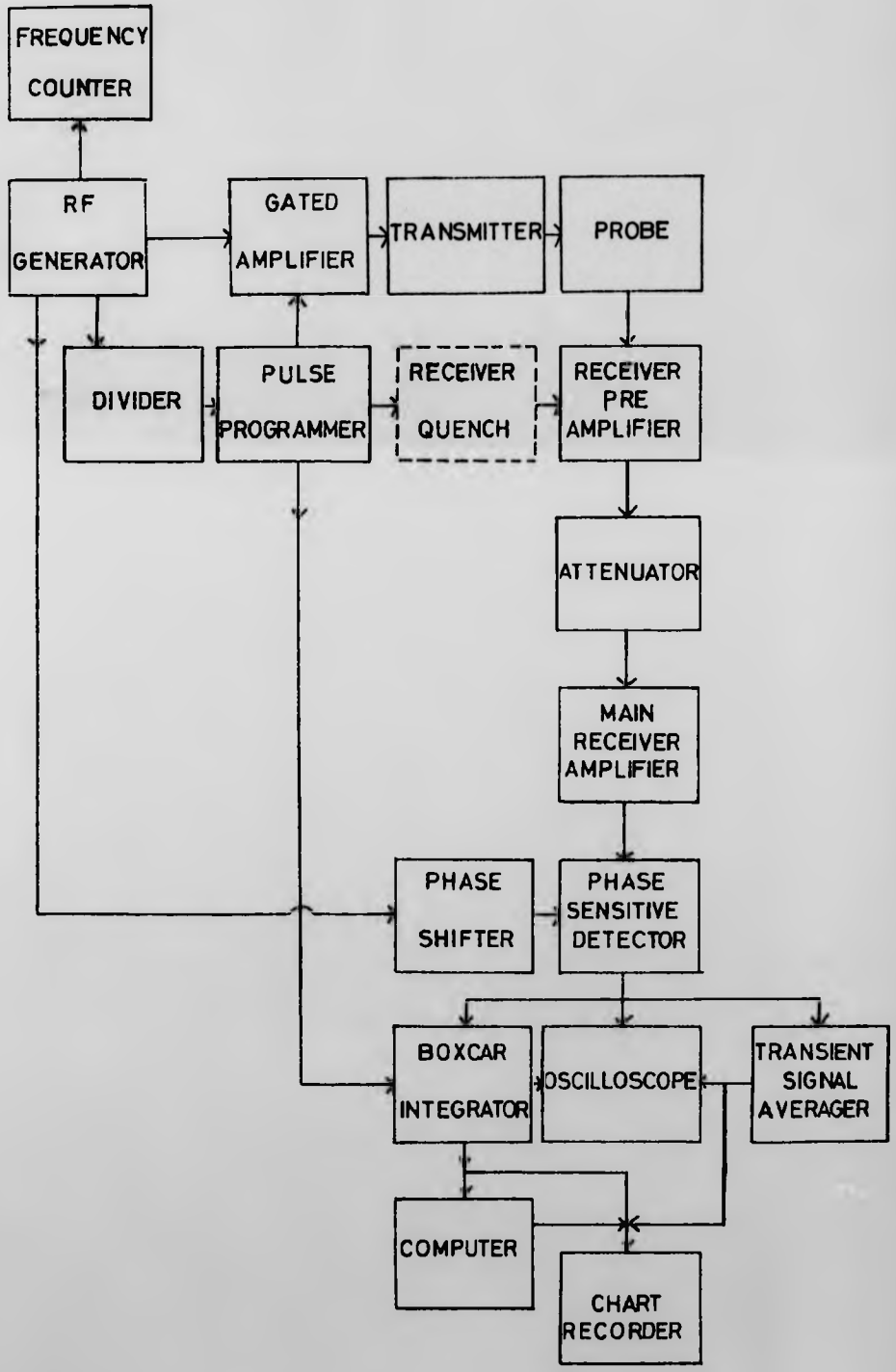

Fig. 3.5: Block diagram of the NMR pulsed spectrometer.

input to the divider chain, and pulse generation accomplished with a home-built programmer capable of a range of pulse widths and spacings from 0.2 μs - 270 ms.

3.5. The Sample Probe

A single coil has been used for both the transmitter and receiver coils in all experiments in this work. This has advantages over two orthogonal coils in terms of mechanical simplicity in a confined space and, more importantly, in the generation of the largest B_1 r.f. field within the given sample volume. Clark (1964) shows

$$B_1 \propto \left(\frac{PQ}{\omega_o V_c}\right)^{\frac{1}{2}} \qquad (3.1)$$

where P is transmitter pulse power

Q is the quality factor of the resonant circuit

ω_o is the resonance frequency

V_c is the coil volume.

The coil needs to be close over the sample and the ratio of sample volume to coil volume is described by the filling factor, η, which needs to be high for greater sensitivity. A large Q is seen to be desirable in the creation of large B_1 fields. The advantages of the single coil are however obtained at the expense of some complexity in the isolation of transmitter and receiver circuits. Further, the recovery from overload arising from the tuned sample circuit rings down with a time constant $\sim 2Q/\omega_o$, and thus a large Q gives rise to a poor transient response to the excitation pulse. The apparently mutually exclusive requirements can be overcome by damping the receiver tuned circuit for the duration of the pulse, but this approach was not used since the switching effects introduced noise such that the overall signal to noise was less than obtained by simply

delaying detection until after the transient behaviour. Considerations in the design of the sample probe are therefore the achievement of a maximum, uniform B_1 field, a short rise and fall time of the power and the maximum signal to noise ratio.

Since the d.c. magnetic field geometry is different for the electro- and superconductive magnets, different r.f. coils were used in the respective probes. The electromagnet has a horizontal B_o, and so a single layer solenoid with vertical axis was used to create a vertical B_1 r.f. field. The vertical B_o field of the superconductive magnet necessitates a horizontal B_1 field created using a Helmholtz or saddle-shaped coil. (see for example Warren and Clark, 1968). An alternative approach suitable in a wide bore furnace in the superconductive magnet is to employ a solenoidal coil with horizontal axis and this is especially attractive from the point of view of sensitivity.

The sensitivity of NMR to frequency was originally thought to be proportional to $\omega_o^{3/2}$. (Abragam, 1961).

$$\frac{S}{N} = K\eta M_o \left(\frac{\mu_o Q \omega_o V_c}{4FkT_c \Delta\nu}\right)^{\frac{1}{2}} \qquad (3.2)$$

where S/N is the signal to noise ratio

K is a dimensionless factor describing the coil geometry

η is the filling factor

M_o is the nuclear magnetisation

μ_o is the permeability of free space

V_c is the coil volume

F is the noise figure of the preamplifier

T_c is the coil temperature

$\Delta\nu$ is the receiver bandwidth

The expected signal to noise improvement prompted the use of high magnetic fields, but in practice results were disappointing. Resonance shift resolution was of course also improved, being proportional to ω_o. A

significant factor in the less-than-expected improvement in sensitivity was the use of Helmholtz type coils in the superconductive systems necessary for high fields. Hoult and Richards (1976) have presented a general derivation of S:N for any coil configuration, which reproduces equation 3.2 in the special case of a solenoidal coil. For this discussion their expression is summarised as:

$$\frac{S}{N} \alpha V_s B_1 \left(\frac{r}{\ell}\right)^{\frac{1}{2}} \omega_o^{7/4} \qquad (3.3)$$

where V_s is the sample volume

B_1 is the r.f. field per unit current

r is the wire radius

ℓ is the length of wire

The signal to noise ratio is shown to be broadly independent of the number of turns within given overall coil dimensions. Fig. 3.6 shows Helmholtz and solenoidal coils on which are defined the parameters: r = wire radius, 2a = coil diameter, 2g = coil length. The Helmholtz coil is shown with angular width 120° which gives the optimum B_1 homogeneity. Because of the reduced wire radius and significantly greater length of wire per unit turn in the Helmholtz coil, the signal to noise performance of the solenoid is, for example, 3 times better when a = g and 4½ times better when 2a = g. An important consequence is that correspondingly longer pulses are required by the Helmholtz arrangement. Finally in terms of coil design it is worth noting that in an ideal coil the noise arises solely from the resistance and therefore the connecting leads should be kept as short as possible.

The signal to noise ratio obtainable from bulk metallic samples with increasing frequency is also reduced when the sample size exceeds the skin depth, δ, given by

$$\delta = \left(\frac{2}{\omega\sigma\mu}\right)^{\frac{1}{2}} = 5 \times 10^{-4} \left(\frac{\rho}{\nu}\right)^{\frac{1}{2}} \qquad (3.4)$$

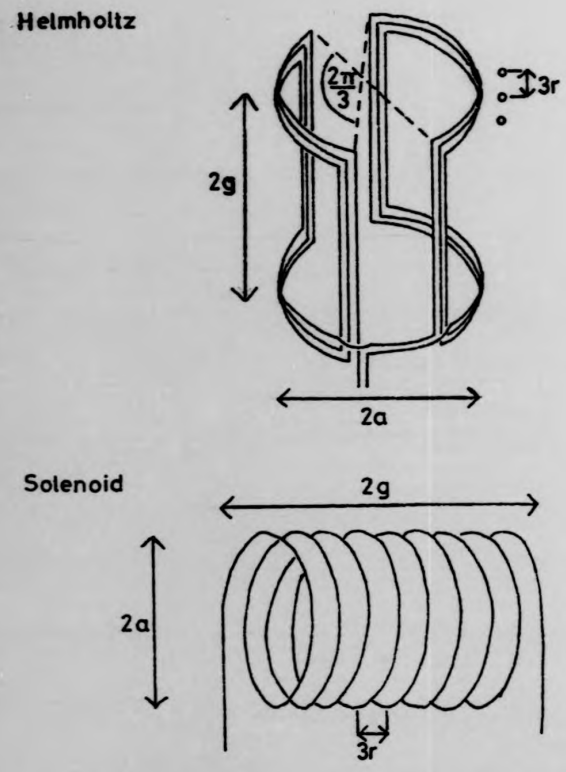

Fig. 3.6: Helmholtz (saddle-shaped) and solenoidal coil geometries.

r = wire radius
2a = coil diameter
2g = coil length.

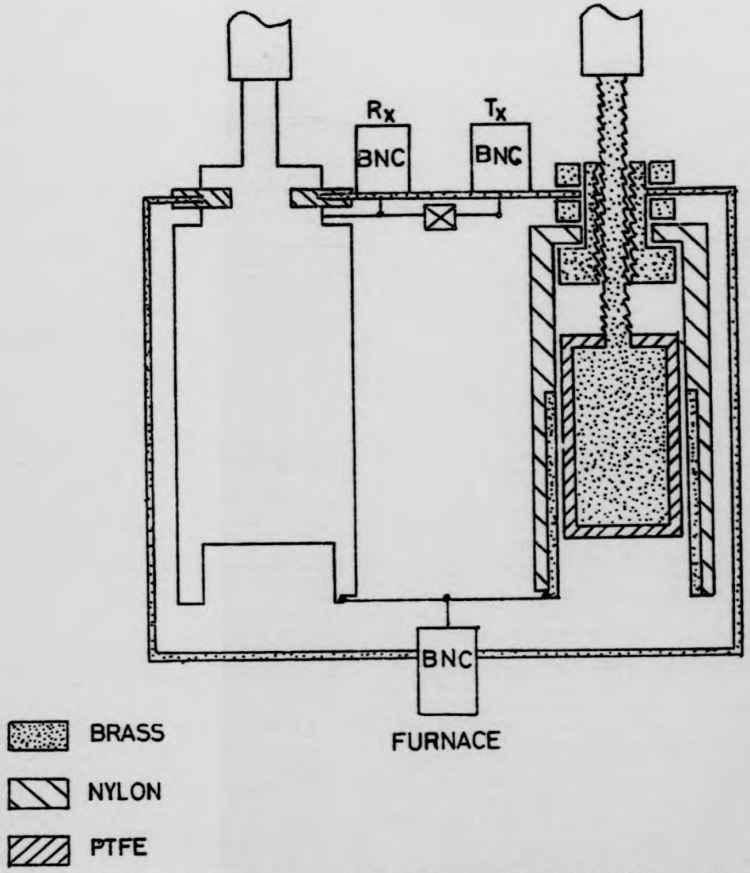

Fig. 3.7: High voltage tubular variable capacitor and schematic representation of match-tune box for direct connection to NMR furnace.

where $\omega = 2\pi\nu$ is the frequency (MHz)

$\rho = 1/\sigma$ is the electrical resistivity ($\mu\Omega m$).

Production of r.f. coils employed a lost wax method, in which a wooden cylindrical former was coated with a wax layer. This was turned on a lathe to leave a uniform thickness of $\sim$ 1 mm. For solenoidal coils a screw thread $\sim$ 0.05 mm deep was cut into the wax, and wire typically 0.3 mm diameter wound into the groove. Sauereisen cement was then used to pot the winding. Helmholtz coils were would in planar form before being curved to the shape of the wax former. Having allowed the cement to dry, gentle heating allows removal of the coil from the former. Excess wax was dissolved with a suitable solvent. Coil leads were insulated with alumina beads and twisted together to reduce their contribution to the total inductance. Internal coil dimensions were typically 10 mm diameter, 15 mm long and coils had inductance of $\sim$ 0.3 μH. Platinum wire was not suitable for use in the coil since any caesium leaking from the samples reacted readily with this metal. Silver and molybdenum were most commonly used; silver being limited by its relatively low melting temperature and occasionally by ringing for several tens of microseconds. The parameters controlling ringing, both mechanical and electrical, are not well described in the literature and empirical attempts to determine the optimum experimental coil configuration proved inconclusive.

In order to have the shortest possible coaxial cable connection between the NMR furnace and the matching and tuning capacitors, the capacitor unit was connected directly to the BNC plug on the furnace top cap. High voltage tubular capacitors were designed and built to fit within the bore of the superconductive magnet, and Fig. 3.7 shows the capacitor arrangement used. Each capacitor was constructed from brass, P.T.F.E. dielectric and a nylon outer, and gave a range of capacity of

approximately 2-45 pF.

The circuit of Fig. 3.8 represents the capacitor configuration used in the probe and also shows the connections with transmitter and receiver used to effect isolation. This relies on the transformation properties of quarter wavelength cables (Lowe and Tarr, 1968) and the non-linear characteristic of diodes. With the transmitter pulses "on", the crossed diodes D_1 and D_2 both conduct, and the short circuit provided by D_2 to earth is transformed to an open circuit by the quater wavelength cable to protect the receiver. With the pulses "off" D_1 and D_2 do not conduct when the voltage level falls below $\sim$ 1V and the weak nuclear signal passes to the pre-amplifier.

The impedance of the coil must be transformed by the capacitors so that the probe is power matched to the transformer. C_t serves to tune the coil at the resonant frequency and C_m to match the probe to the output impedance of the transmitter, in this case 50 Ω. C_t and C_m are related by

$$C_m = \left(\frac{C_t}{50Q\omega_o}\right)^{\frac{1}{2}} \qquad (3.5)$$

Experimentally the probe was brought to this condition by feeding the low level r.f. carrier into the probe via a V.S.W.R. device (anzac CH136), Fig. 3.9. A reflected voltage on the monitor socket measures impedance mis-match between the probe and a $\sim$ 50 Ω reference resistor. A minimum reflection occurs when the probe is properly matched. Simultaneously the furnace aerial wire was monitored for a maximum in the voltage pick up. When the nuclear resonance signal was strong enough the final tuning adjustment was made by observation of the signal on the oscilloscope, but it was generally found that only a small correction was required.

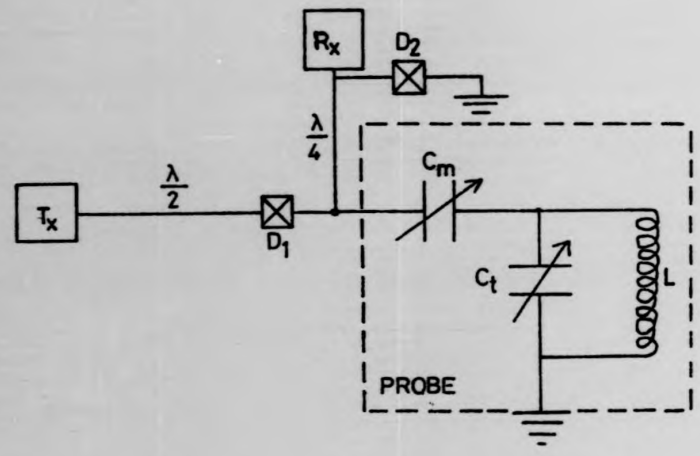

Fig. 3.8: Transmitter-receiver isolation network and probe capacitor configuration.

D_1, D_2 = crossed diodes

C_m, C_t = capacitors

L = r.f. coil.

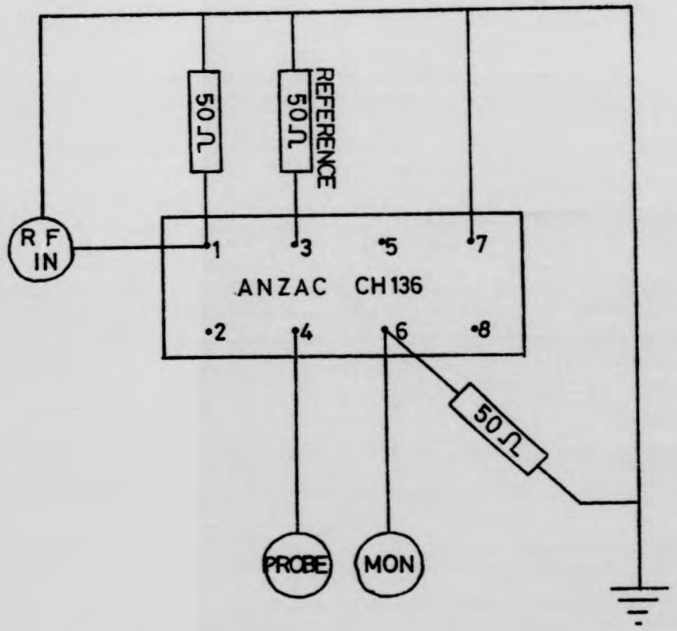

Fig. 3.9: Voltage Standing Wave Ratio device. Minimum monitor voltage occurs when probe is correctly matched to reference impedance.

3.6. Signal Processing

After each pulse the FID signal is detected by the coil, then amplified and phase sensitively detected by the receiver system. Observation of the resonance amplitude by either a transient recorder or boxcar integrator, or directly on an oscilloscope with larger NMR signals, enabled the pulse length to be set to τ_N. A Bruker transient recorder, TMC-600, and averager, MSO-E, with 2K word memory and time resolution 50ns/word has been used in this work to record the FID signal at the receiver output. Cummulative storing of the N-times repeated signal under the same conditions of field and frequency gives the familiar $N^{\frac{1}{2}}$ improvement factor in signal to noise ratio, since only the synchronous signal voltages add constructively. The averaged signal was plotted on a y-t chart recorder after a maximum of 2^{14} = 16 K counts. The normalisation carried out by the Bruker restricted signal recover to situations where the S:N ratio was not less than $\sim$ 1:30. After 2^m counts, where $8 \leq m \leq 14$ and m is an integer, the available Bruker output was normalised to give an output signal of the same size as achieved after 128 = 2^7 counts. Consequently the noise became smaller with each increase in the number of counts and the limit of applicability was reached when digitization noise appeared on the trace (due to the 8-bit size of the ADC). The Bruker averager is an early version of a new range, and is to be returned to the manufacturer for modification.

A large pulse repetition frequency (PRF) is desirable in order to obtain the data in the shortest possible time, but an upper PRF limit is set by the need to allow the spin system to return to thermal equilibrium between pulses. A time interval of $5T_1$ achieves this to within 0.7%. In conducting samples the saturation constraint was superceeded by that of r.f. heating. In this case the controlling factor is the product of PRF and pulse length, called the duty factor. Generally duty factors below $\sim$ 0.001 were found to create negligible heating. The effect of r.f. heating was most accurately

determined for samples which showed significant temperature dependence of the resonance properties. A calibration of shift versus furnace temperature for negligible pulse length can then be used to predict sample temperatures when the duty factor is high - as occurs when using multiple pulse sequences at low transmitter power.

An alternative method of obtaining the NMR data involves the use of a boxcar integrator (Clark, 1964). This is essentially a gate and integration network positioned so as to sample some or all of the FID signal. As the field or frequency is swept through the resonance condition the boxcar output sweeps out a representation of the resonance lineshape, which may well display distortion if the sampling gate is short or delayed from the end of the pulse by ringing in the receiver circuit. A further potential source of distortion is due to the time-constant. An effective time constant less than 0.1 of the time taken to sweep through the resonance line is required for no distortion;

$$TC_{eff} = \frac{TC_{BOX}}{\tau_{BOX}\, PRF} \tag{3.6}$$

where TC_{eff} is the effective time constant

TC_{BOX} is the time constant of the boxcar

τ_{BOX} is the time of the boxcar gate pulse.

The resonance lineshape is usually a mixture of absorption and dispersion but can be adjusted to show only absorption by change of the phase delay in the reference line to the PSD. This zero phase position can also be set by obtaining a maximum signal for the on-resonance FID.

In work with the superconductive magnet it was found convenient to sweep the frequency rather than the field. An external narrow sweep mode of the r.f. generator was computer controlled and the simultaneous boxcar

output stored on computer files. Multiple sweeps were again used for signal to noise enhancement. The many tuned circuits in the system gave rise to frequency dependent responses, and the greatest experimental difficulty associated with sweeping the frequency was the usual absence of a flat baseline in the boxcar output. Indeed many of the "bumps" were very resonance-like, even having temperature dependence, but could be distinguished from a true nuclear resonance by their continued presence in a magnetic field $\sim$ 100 G different from before, and most conclusively by their failure to appear on a magnetic field sweep. Calibration of the frequency sweep enabled the resonance positions to be determined, and resonance amplitudes relative to the baseline gave relaxation data. Based on the assumption of Lorentzian lineshapes, a computer programme written by Professor J. A. Gardner was used to fit the resonance lineshape data and calculate values of position, T_2^* and phase. This programme took into account the use of non-90° pulse lengths and relaxation during the pulse, in addition to gatewidth distortion.

CHAPTER FOUR

THE CAESIUM-GOLD SYSTEM

4.1. Introduction

The phase diagram of the caesium-gold alloy system Cs_xAu_{1-x} reported by Schmutzler (1978) disputes the liquidus line obtained by Kienast and Verma (1961) as shown in Fig. 4.1. Nonetheless there exists only one congruent melting compound with a very narrow range of stoichiometry at the equiatomic composition $Cs_{50}Au_{50}$. Melting temperatures deduced from changes in the resonance properties during the course of NMR experiments were found to agree within experimental error with those of Schmutzler. He found that the liquidus temperature rises from 300 K for pure caesium to 856 K at $Cs_{50}Au_{50}$, and did not observe a decrease at the eutectic composition $Cs_{58}Au_{42}$. The unusual shape of the liquidus line in the region of pure gold (T_m = 1336 K) deserves further investigation since it is most unlikely that even a small mole fraction of caesium in gold produces such a minor effect. (Lewis, 1980). The strong lack of symmetry of melting temperature either side of the CsAu compound means that at, say, 873 K caesium-rich alloys are well above the melting temperature and CsAu is also molten, but for concentrations of atomic fraction Cs, $x \leq 0.35$, the system is still solid. The rapidly increasing liquidus in gold-rich alloys coincides with a region of metallic behaviour, and this formed the basis of the decision not to undertake NMR investigations below $x = 0.35$. The short range order revealed by neutron diffraction studies (Martin et al, 1980) and the partial molar volume analysis of Hensel (1979) provide strong evidence for the assumption that the bonds between caesium and gold are essentially unchanged across the whole of the concentration range. Non-stoichiometric alloys are therefore considered to be a pseudo-binary mixture of pure metal and the compound CsAu, and alloy concentrations will be generally expressed using the excess mole fraction y introduced in Chapter one.

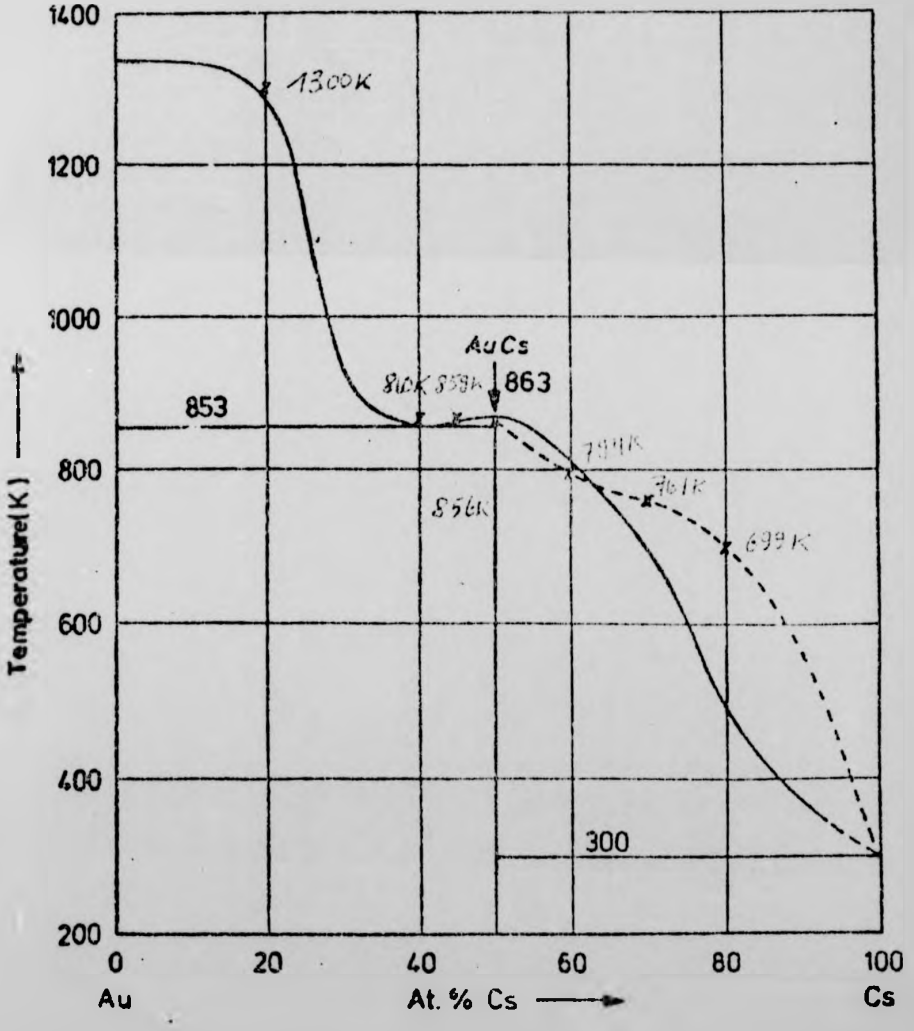

Fig. 4.1: The phase diagram of the caesium-gold system.
----- Schmutzler (1978)
——— Hansen (1958)

For all concentrations the sample was prepared in situ and was not dispersed. NMR studies were restricted to measurements of the ^{133}Cs nucleus since the ^{197}Au nucleus is particularly unfavourable for this technique. ^{133}Cs NMR shifts were measured at 12 MHz and 44 MHz relative to an aqueous CsCl solution corrected to infinite dilution (Deverell and Richards, 1966). The spin lattice relaxation time, T_1, was found to equal the spin phase-memory time, T_2^*, in the liquid samples.

The main focus of interest of this work is the metal-nonmetal transition which occurs as a function of composition in the liquid caesium-gold alloy system. However it is first instructive to consider the behaviour of the compound CsAu in both the solid and liquid states.

4.2. NMR in The Stoichiometric Compound CsAu

Fig. 4.2 presents the relaxation rate data obtained as a function of temperature for a variety of samples, all of which were nominally composed of $Cs_{50}Au_{50}$. In all cases the data on the solid were taken after heating of the sample above the melting temperature. Relaxation data taken after recycling of the temperature showed reproducibility within the experimental uncertainty of typically 10%. Features common to all such samples are

1. the low temperature observation that $T_2 < T_1$
2. the motional narrowing with increased temperature above 550K
3. above about 750 K $T_2 = T_1$
4. the sharp 25 fold increase in relaxation rate on melting
5. the positive temperature coefficient of relaxation rate in the liquid.

Below about 500 K a two component exponential was observed in measurements of T_1 in all except one sample. The exception was one of the samples produced and measured by our collaborator W. W. Warren, which gave a single T_1 exponential with the lowest room temperature relaxation rate of 1.5 s^{-1} and the smallest measured resonance shift of 0.036%. The preparation of this

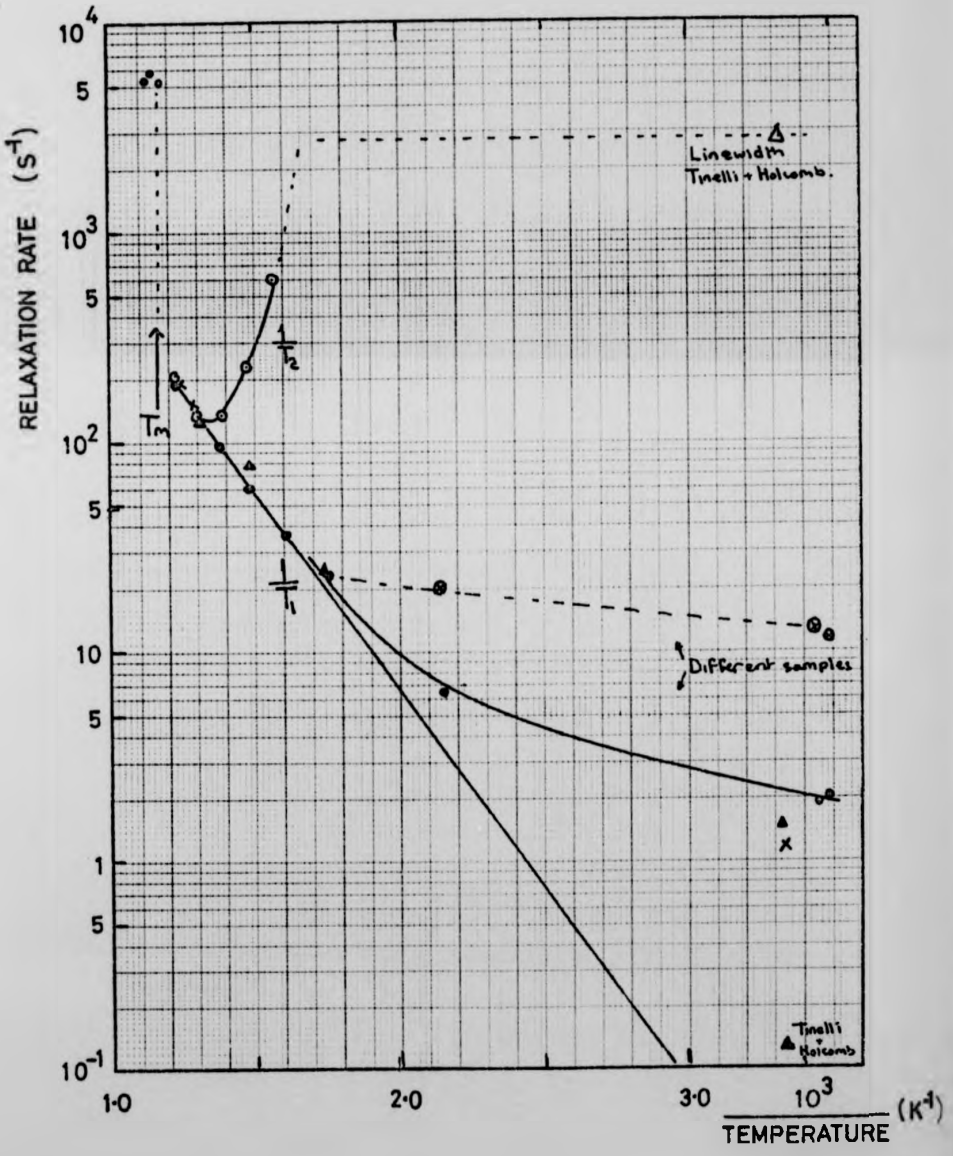

Fig. 4.2: ^{133}Cs relaxation rate as a function of reciprocal temperature in stoichiometric CsAu.

sample followed Tinelli and Holcomb (1978), who have shown that the room temperature spin lattice relaxation rate is particularly sensitive to doping of the compound CsAu by excess metallic caesium. To overcome the problem of non-stoichiometry a mixture of elemental constituents in the nominal composition Cs_{505} Au_{495} were allowed to react at 533 K for a period of 8 hours whilst being continuously pumped on a rotary vacuum system. The stability of CsAu allows excess caesium to be removed during this process. Although this was the 'best' sample in the sense that it was closest to stoichiometry, the room temperature relaxation time of T_1 = 650 ms is an order of magnitude smaller than the 7.5 s observed in the best sample of Tinelli and Holcomb. An estimate of the carrier concentration necessary to produce the observed shift and relaxation can be made by assuming the same effective hyperfine coupling constant in CsAu as in caesium metal. Then $^1/T_1 \propto n^{2/3}$ where n is the electron density (Korringa, 1950).

	T_1/s	n/cm^{-3}
metallic Cs (Carver et al 1967)	370×10^{-6}	8×10^{21}
CsAu (Tinelli and Holcomb 1978)	7.5	2.8×10^{15}
CsAu (this work)	0.65	1.1×10^{17}

On the assumption that each excess caesium atom contributes one conduction electron our most nearly stoichiometric sample is therefore adjudged to possess $\sim 10^{-5}$ mole fraction of excess caesium.

At higher temperatures the spin lattice relaxation of solid CsAu becomes progressively stronger and the linewidth decreases, until eventually the high temperature solid is completely motionally narrowed. This thermally activated relaxation process is presumably related to diffusion - possibly of excess metal, but is much stronger than any corresponding process in

CsI (Sotier and Warren, 1980). In this region there is a gradual increase in resonance shift and at the melting point $K_{solid} \approx K_{liquid}$.

Liquid CsAu shows a resonance shift of (0.075 ± 0.002)%, which is noticeably larger than the 0.036% found in the room temperature crystalline solid. The relaxation rate, $^1/T_1 \approx 200\ s^{-1}$ is also markedly increased over the solid and is furthermore significantly greater than found for ^{133}Cs in the typical molten salt CsI, where $^1/T_1 \approx 10^{-1}s^{-1}$ (Sotier and Warren, 1980). Both the shift and relaxation rate in the liquid have a positive temperature coefficient, and we suggest that the data indicate the presence of a small temperature dependent concentration of paramagnetic centres, even in the molten compound CsAu. Such paramagnetic centres are most likely to be due to thermal generation of electron-hole pairs which is a consequence of the small band gap of molten CsAu, and may explain the appreciable optical absorption at low energies (Minster and Freyland, 1979). In contrast, the large band gap of molten alkali halides such as CsI precludes the thermal generation of background paramagnetism as a source of nuclear interaction.

A molar concentration of paramagnetic centres, $C_o \approx 0.004$, is obtained by extrapolation to zero of the relaxation rate in samples near to stoichiometry and of the shift to the chemical shift of the crystal. The observed temperature dependence of the resonance properties imply an activation energy of 0.2 eV - 0.3 eV for the electron-hole creation process, which can be summarised as

$$Cs^+ + Au^- \rightarrow Cs^o + Au^o$$

$$(e) \quad (h)$$

$$\text{vacancy } Au^{-2}$$

Further evidence is provided in §4.3 that the free electron will localise in a lattice vacancy as an F-centre analogue (Pitzer, 1962). The associated hole is localised as a V_k centre on the dimeric Au^-_2 ion.

The marked 25-fold increase of relaxation rate on melting may possibly be interpreted as evidence of an Anderson transition in the sense that increased disorder in the liquid gives rise to strongly localised states, which influence nuclear relaxation through a corresponding increase in the correlation time.

4.3. NMR in Caesium-Gold Liquid Alloys

Fig. 4.3 presents the experimental resonance shift isotherm obtained as a function of concentration in liquid caesium-gold alloys at 873 K. The shift is always paramagnetic and ranges from the 1.403% Knight shift of pure caesium to a minimum of (0.075 ± 0.002)% for stoichiometric CsAu. In caesium rich alloys the shift decreases monotonically from pure caesium, and Fig. 4.4 demonstrates that below about mole fraction of caesium, $Y_{Cs} = 0.07$ the approach to stoichiometry is characterised by a linear dependence of shift on caesium concentration. In marked contrast the alloys on the gold rich side of stoichiometry show a shift which is nearly independent of concentration and only slightly larger than for CsAu, even at concentrations where the conductivity has reached clearly metallic values. For reference, the conductivity data of Hoshino et al (1975) is shown across the upper axis.

The variation of the shift over most of the liquid alloy concentration range Cs - CsAu is well described by the nearly free electron model, (Faber, 1972). For a metal the Knight shift is described by equation (2.26)

$$K = \frac{\Delta B}{B} = \frac{2}{3} \langle |\psi(0)|^2 \rangle_F . \Omega . \chi_V^P$$

Neglecting any changes in the probability amplitude due to perturbations of electron charge density associated with Au^- ions, and also the electron-electron enhancement of susceptibility, then $\chi_V^P \propto n^{1/3}$, where n is the density of free electrons. The density data of Schmutzler (1978) were

The marked 25-fold increase of relaxation rate on melting may possibly be interpreted as evidence of an Anderson transition in the sense that increased disorder in the liquid gives rise to strongly localised states, which influence nuclear relaxation through a corresponding increase in the correlation time.

4.3. NMR in Caesium-Gold Liquid Alloys

Fig. 4.3 presents the experimental resonance shift isotherm obtained as a function of concentration in liquid caesium-gold alloys at 873 K. The shift is always paramagnetic and ranges from the 1.403% Knight shift of pure caesium to a minimum of (0.075 ± 0.002)% for stoichiometric CsAu. In caesium rich alloys the shift decreases monotonically from pure caesium, and Fig. 4.4 demonstrates that below about mole fraction of caesium, $Y_{Cs} = 0.07$ the approach to stoichiometry is characterised by a linear dependence of shift on caesium concentration. In marked contrast the alloys on the gold rich side of stoichiometry show a shift which is nearly independent of concentration and only slightly larger than for CsAu, even at concentrations where the conductivity has reached clearly metallic values. For reference, the conductivity data of Hoshino et al (1975) is shown across the upper axis.

The variation of the shift over most of the liquid alloy concentration range Cs - CsAu is well described by the nearly free electron model, (Faber, 1972). For a metal the Knight shift is described by equation (2.26)

$$K = \frac{\Delta B}{B} = \frac{2}{3} \langle |\psi(0)|^2 \rangle_F . \Omega . \chi_V^P$$

Neglecting any changes in the probability amplitude due to perturbations of electron charge density associated with Au^- ions, and also the electron-electron enhancement of susceptibility, then $\chi_V^P \propto n^{1/3}$, where n is the density of free electrons. The density data of Schmutzler (1978) were

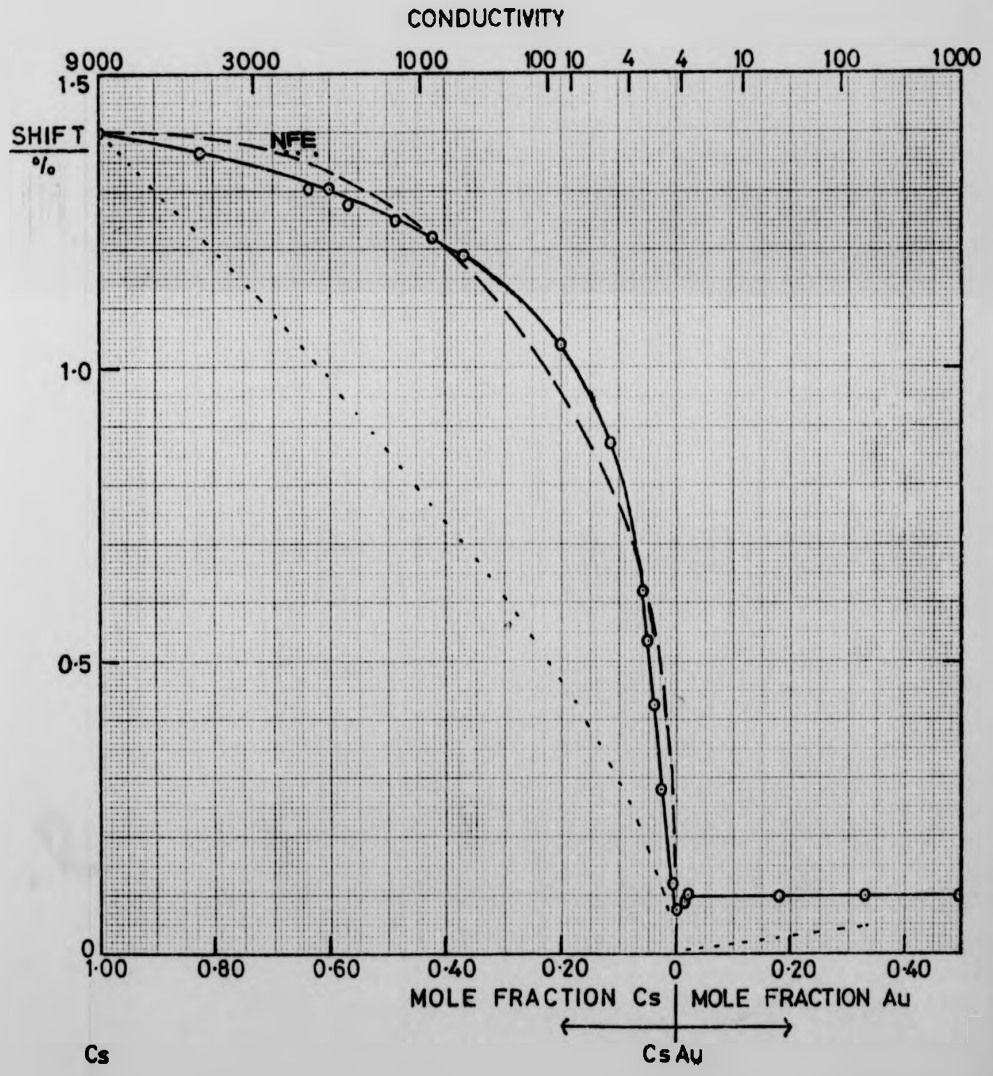

Fig. 4.3: ^{133}Cs resonance shift as a function of composition in Cs-Au liquid alloys at 873 K. The dotted line is the theoretical prediction of Franz et al (1980) (§4.4).

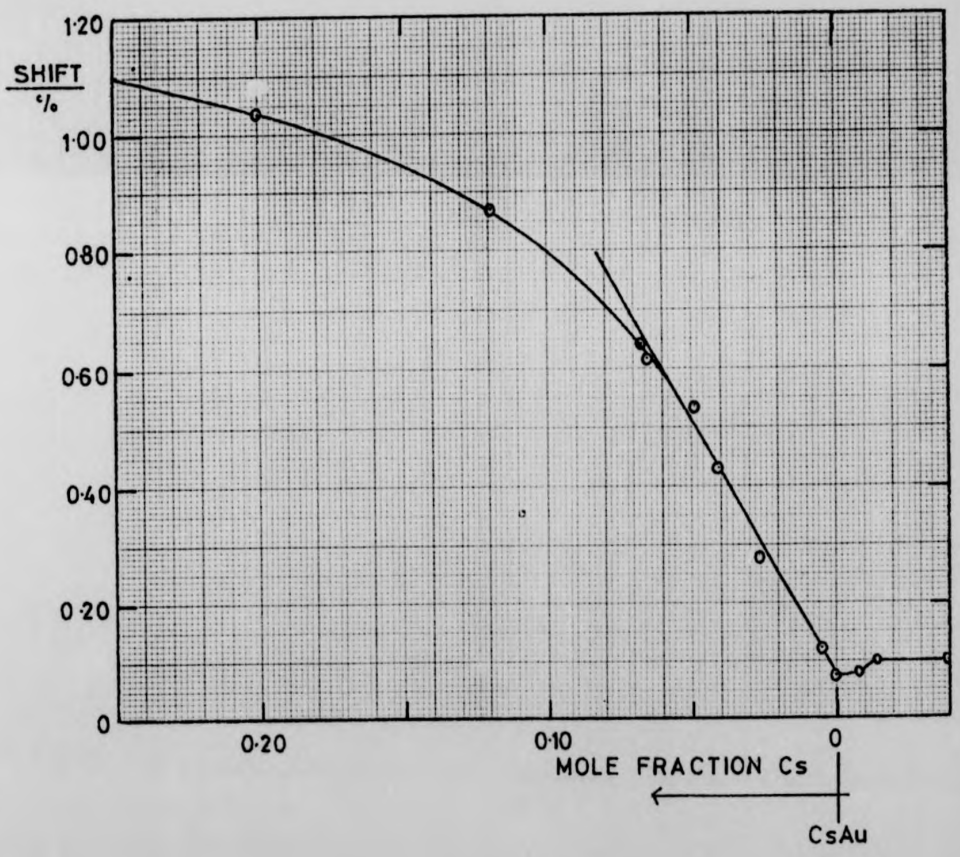

Fig. 4.4: Linearity of ^{133}Cs resonance shift as a function of caesium mole fraction near stoichiometry at 873 K.

used together with the assumption of one conduction electron per excess caesium atom to calculate the concentration dependence of χ_V^P. Normalised to the shift of pure caesium, the free electron shift is plotted as a dashed line on Fig. 4.3 and is seen to provide a good representation of the gross features of the data. However Fig. 4.5 shows that although the shift follows $n^{1/3}$ above $y_{cs} = 0.07$ it deviates markedly near stoichiometry and clearly a nearly free electron approach is no longer appropriate.

In particular, the large shifts which occur when the d.c. conductivity $\sim 10\Omega^{-1}cm^{-1}$ together with the linear dependence of shift on concentration for alloys on the caesium rich side of CsAu suggest that the electron states are no longer extended. Localised electrons characterised by a Curie Law susceptibility are described by eqn. (2.30)

$$\frac{\Delta B}{B} = c\,\bar{A}\left(\frac{\gamma_e}{\gamma_n}\right)\frac{S(S+1)}{3kT}$$

where $\bar{A} = zA$

The simple interpretation of c as the concentration of excess caesium is belied by the background paramagnetism of CsAu, shown in §4.2 to be consistent with a molar concentration $C_o = 0.004$ of localised electrons. Hence the total concentration of paramagnetic centres is given by $c = c_o + y_{Cs}$. The experimental resonance shift then gives a mean hyperfine coupling of $\bar{A} = (8.68 \pm 0.72) \times 10^{-25}$ J or in frequency units (1.31 ± 0.11) GHz. This value is approximately 60% of the 6s atomic value suggesting an interpretation of the localised states created by excess caesium as atomic-like with a 40% reduction in probability amplitude at the nucleus. Alternatively, (Pitzer, 1962) the excess electron may form an 'F-centre' analogue with equal amplitude on z Cs^+ ions. If z = 6 as found by Martin et al (1980) for the coordination number in neutron diffraction experiments, then the hyperfine field on a particular neighbouring ^{133}Cs nucleus is

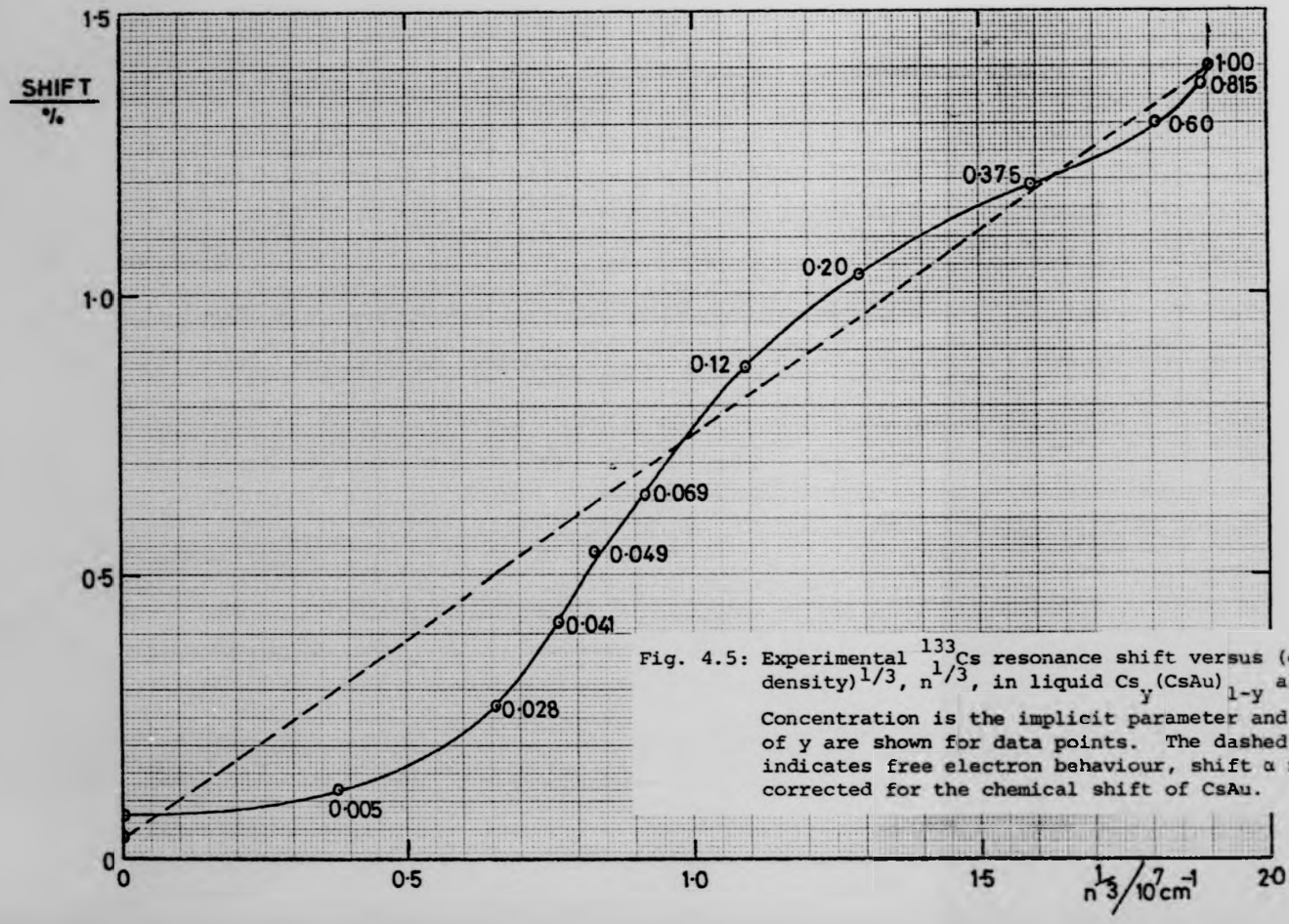

Fig. 4.5: Experimental ^{133}Cs resonance shift versus (electron density)$^{1/3}$, $n^{1/3}$, in liquid $Cs_y(CsAu)_{1-y}$ alloys.

Concentration is the implicit parameter and values of y are shown for data points. The dashed line indicates free electron behaviour, shift α $n^{1/3}$, corrected for the chemical shift of CsAu.

$\sim$ 10% of the free atom value. This is a typical magnitude for the nearest neighbour hyperfine field around F centres in caesium halide crystals (Seidel and Wolf, 1968).

The variation of the nuclear resonance shift in the concentration range Cs - CsAu enables a determination of the density of states at the caesium site to be made. Expressed in terms of the Mott g factor, Fig. 4.6 shows the result of dividing the experimental nuclear resonance shift due to the s-conduction electron susceptibility by the calculated free electron shift.

$$g = \frac{N(E_F)}{N(E_F)_{\substack{\text{Free}\\\text{elec}}}} = \frac{K_{expt} - K_{\substack{\text{chem}\\\text{shift}}}}{K_{\substack{\text{Free}\\\text{elec}}}}$$

g is seen to be more or less constant in the range from pure caesium to values of $y_{Cs} < 0.10$. The small variations in this range can be assumed to be attributable to possible variations in $\Omega < |\psi(0)|^2 >_F$ for which no allowance has been made. The hatched region is drawn to illustrate the concentration where NMR properties suggest that the metal-nonmetal transition occurs and at this concentration $g \simeq 0.7$. This is a markedly different value from $g = 0.3$, predicted by Mott for the transition.

Addition of gold to CsAu causes only very small changes in the NMR properties implying that excess gold enters solution as a diamagnetic species such as Au^-. Certainly the consistently low value of the ^{133}Cs shift in the gold rich range implies that the s-electron density at the Cs^+ nucleus remains small, even though the alloy attains metallic conductivities. Why this should be is not clear but one might speculate that the nearest neighbour ionic environment of the caesium retains an essentially similar character to that which it possessed at stoichiometry.

The temperature derivative of the shift is presented in Fig. 4.7.

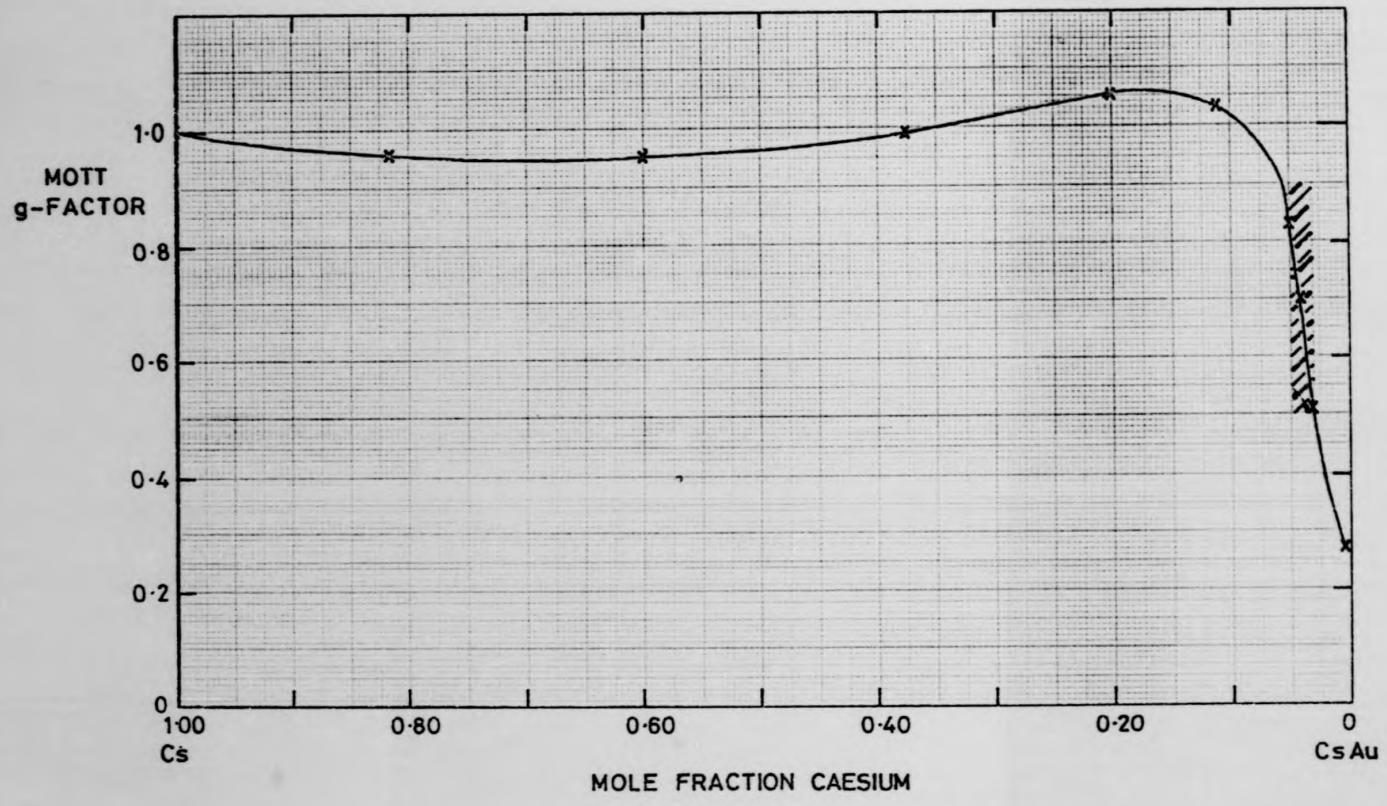

Fig. 4.6: The reduction in caesium density of states as a function of mole fraction caesium described by the Mott g-factor. The hatched region corresponds to the metal-nonmetal transition observed by NMR.

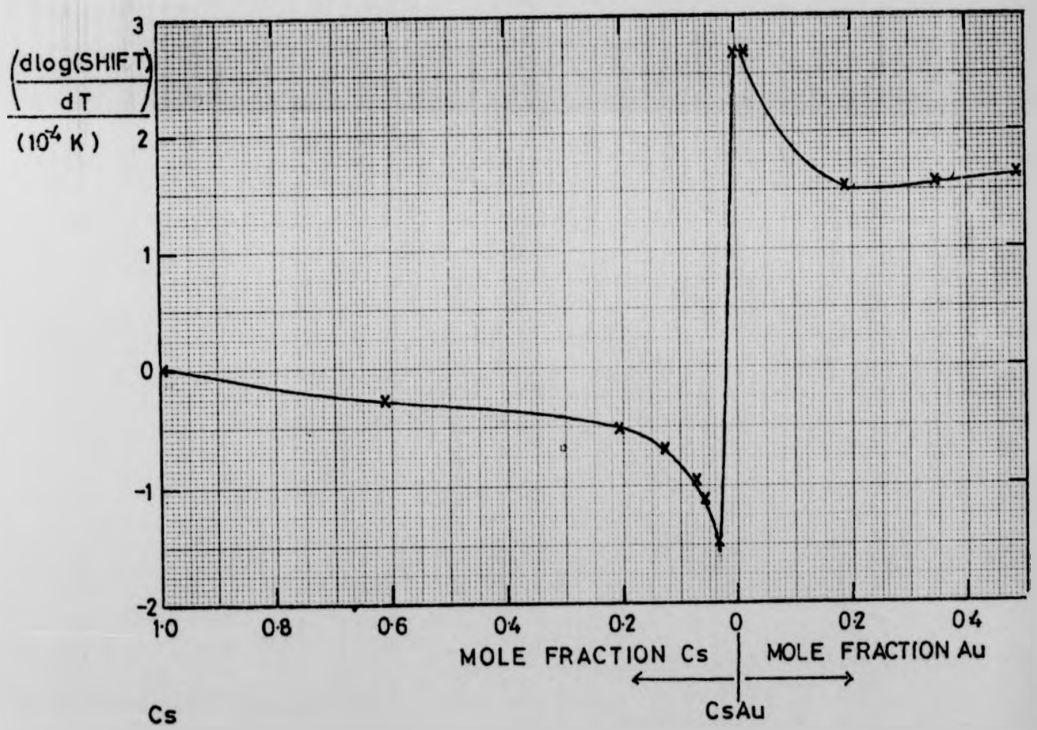

Fig. 4.7: The temperature coefficient of ^{133}Cs resonance shift $\left(\frac{d \ln \text{shift}}{dT}\right)$ versus composition in liquid alloys at 873 K.

It is marginally positive for pure caesium, but is negative over most of the caesium rich range and becomes stronger as the caesium content is reduced. Very close to stoichiometry there is an abrupt change of sign and relatively large positive values are reached for CsAu and gold rich alloys. The negative coefficient is consistent with a reduction in the conduction electron probability amplitude at the ^{133}Cs site due to increasing molar volume. Near to stoichiometry this effect is countered by the thermally driven increasing concentration of paramagnetic entities.

The spin lattice relaxation rate $^{1}/T_{1}$, at 873 K varies only slowly over most of the liquid Cs - CsAu concentration range as shown in Fig. 4.8. However the rate rises sharply at mole fraction of caesium, $y_{Cs} = 0.07$ to reach a peak value of $1.2 \times 10^{4}\ s^{-1}$ near $y_{Cs} = 0.04$. At stoichiometry the rate of $\simeq 200\ s^{-1}$ is still about $^{2}/3$ of that in pure liquid caesium, and $^{1}/T_{1}$ remains similar in gold rich alloys, further implying that excess gold in CsAu does not give rise to any additional paramagnetism at the ^{133}Cs site.

For excess caesium concentrations, $y_{Cs} \geq 0.07$ the conduction electrons are mobile, but Warren (1971) has shown that incipient localisation leads to an enhancement of $^{1}/T_{1}$ with respect to the nearly free electron Korringa rate $(^{1}/T_{1})_{Korr}$ according to equation (2.43)

$$\left(\frac{1}{T_1}\right)_{obs} = \frac{\tau}{h\ N(E_F)} \left(\frac{1}{T_1}\right)_{Korr}$$

Enhancement is slight, showing for example the values of only 2.4 at $y_{Cs} = 0.20$. The open data points on Fig. 4.8 show the values of τ calculated from the observed relaxation rates allowing $N(E_F)$ to vary with composition according to free electron theory in the range $y_{Cs} \geq 0.07$. For pure caesium, the correlation time is taken to be $\tau = a/V_F$ where a

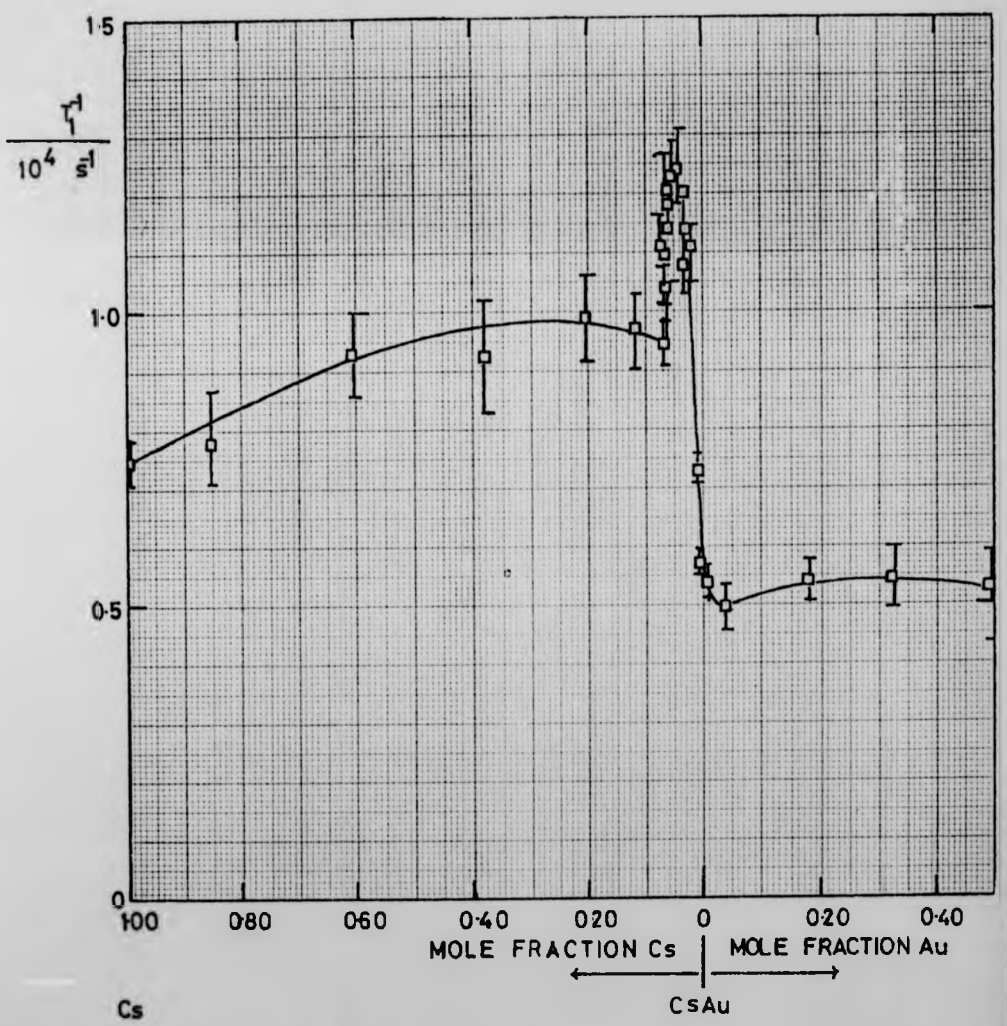

Fig. 4.8: ^{133}Cs nuclear relaxation rate $^1/T_1$ as a function of composition in Cs-Au liquid alloys at 873 K.

is the mean interatomic spacing and V_F is the Fermi velocity.

The dramatic increase in relaxation rate for $0.04 < y_{cs} < 0.07$ could be caused by a concomitant increase in any of the factors controlling $^1/T_1$. These are summarised in the general equation (2.31)

$$\frac{1}{T_1} \simeq n \overline{A^2} \tau$$

where n is the number of unpaired electrons responsible for nuclear relaxation

$\overline{A^2}$ is the mean square value of hyperfine coupling

τ is the correlation time of the local hyperfine field.

However, the smooth variation of the resonance shift precludes the possibility that the first two named factors are responsible, and the only explanation is therefore a sudden increase in the correlation time of the hyperfine field created by a particular paramagnetic centre. The system is now localised and equation (2.36) describes the relaxation rate in the short correlation time limit $\omega\tau << 1$, when $^1/T_1 = {}^1/T_2$

$$\frac{1}{T_1} = \frac{2}{3} \frac{s(s+1)}{\hbar^2} c \overline{A^2} \tau$$

where $\overline{A^2} = zA^2$

The closed data points on Fig. 4.9 show the values of τ obtained when the experimental spin lattice relaxation rates are substituted in eqn. (2.36) on the basis of two different models: z = 1 for atomic like states and z = 6 for 'F-centre' analogues. It is observed that the increase in τ at low caesium concentration best joins the curve for the extended model with the assumption z = 6, and provides strong evidence in favour of Pitzer's F centre model. The correlation time is thus seen to rise by about three orders of magnitude from pure caesium to molten CsAu and reaches a value of a few times 10^{-13} s at stoichiometry. τ is most sensitive to concentration for small amounts of caesium in CsAu,

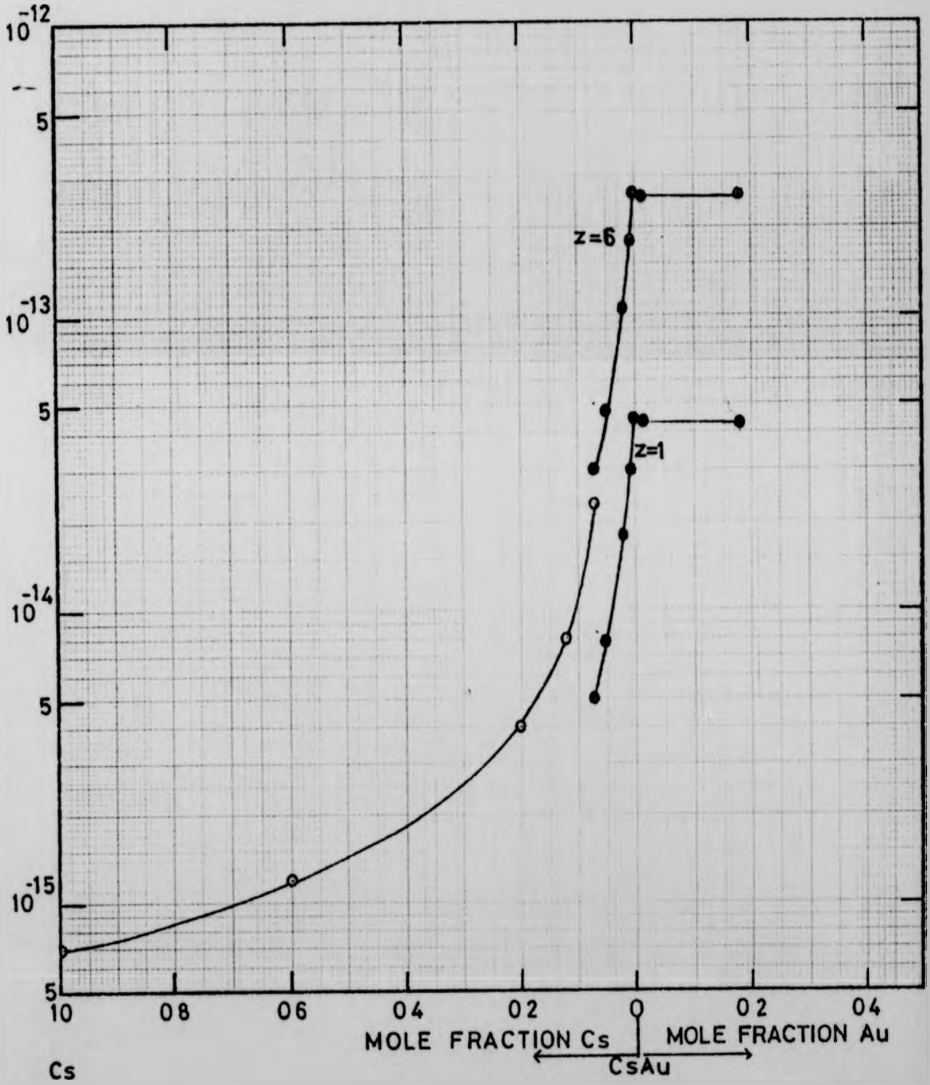

Fig. 4.9: The hyperfine field correlation time, τ, as a function of composition in Cs-Au liquid alloys at 873 K.

o deduced from relaxation enhancement in the extended regime

● deduced from relaxation by localised electrons for atomic states (z=1) and F-centre analogues (z=6).

but remains large on the gold rich side of stoichiometry. The sharp peak in relaxation rate on the caesium side of stoichiometry arises from the competing effects of rapidly increasing correlation time but decreasing concentration of localised electrons.

4.4. Relation to Other Properties

All theoretical attempts to calculate the band structure of solid CsAu are consistent with a semiconductor description in which the ionicity of the bonding plays an important role. Hensel (1979) provides a brief survey of the relativistic K.K.R. approach of Overhof et al (1978), the self consistent A.P.W. method of Hasegawa and Watabe (1977) and the combined K.K.R. - quantum defect calculation of Huang and Liu (1971).

Extensive experimental investigations provide a broad base of evidence in support of the semiconducting nature of the solid stoichiometric compound CsAu. Electrical conductivity (Spicer et al, 1959; Wooten and Condas, 1963) and thermopower measurements (Schmutzler et al, 1975) indicate that solid CsAu is an extrinsic n-type semiconductor. The actual value of σ, 5 - 100 Ω^{-1} cm^{-1}, depends critically upon the concentration of excess metal in the compound and has almost no temperature dependence. As opposed to 'metallic' alloying, charge transfer drives compound formation as indicated by the room temperature molar volume of 46.63 cm^3, which shows a negative excess volume of 42% compared to that predicted for ideal mixing. The stoichiometric compound crystallises in the typically ionic CsCl structure with a lattice constant of 4.263 x 10^{-10} m (Kienast and Verma, 1961, Tinelli and Holcomb, 1977), and has an optical gap of 2.6 eV at 298 K (Spicer et al, 1959).

This work supports the above description of room temperature CsAu and confirms the dopant role played by excess caesium at low temperatures

as evidenced by resonance shift and, more sensitively, by spin lattice relaxation. At high temperatures the rigid lattice picture is no longer appropriate since an intrinsic thermally activated relaxation process occurs.

On melting, stoichiometric CsAu undergoes a solid semiconductor - ionic liquid transition, in which the electrical conductivity decreases to about 3 Ω^{-1} cm^{-1} (Schmutzler et al, 1976). The positive temperature coefficient of conductivity of liquid CsAu yields an apparent activation energy of 0.2 eV, but it is worth noting that the temperature driven increase of ion diffusion in molten salts can be influenced strongly by the thermal expansion of the liquid, and so the apparent activation energy of mass transport need not have a simple interpretation in terms of atomic theory. (see for example, Hensel, 1977). The electromigration experiments of Krüger and Schmutzler (1976) established that Faraday's Law of Electrolysis is obeyed and provide direct evidence that liquid CsAu conducts ionically. The recent theoretical and experimental structural studies of Evans and Telo da Gama (1980) on molten CsAu are consistent with an ionic structure characterized by a preference for unlike nearest neighbours and short range order similar to molten salts. Further supporting evidence for the ionic, molten salt-like nature of liquid CsAu includes the large negative thermopower - 1500 μVK^{-1} and the absence of an n-type to p-type transition as the concentration is varied through stoichiometry. (Schmutzler et al, 1976; Krüger et al, 1977). The optical gap of the solid compound decreases with increasing temperature and shows a discontinuous decrease from 2.1 eV to 1.3 eV on melting (Schmutzler et al, 1976). Such a sharp change is found in many molten salts (Mollwo, 1948). The gram magnetic susceptibility χ_g (Freyland and Steinleitner, 1976, 1977) shows a large diamagnetic deviation from the linear interpolation between

pure liquid metals, and in the neighbourhood of CsAu the temperature coefficient of χ_g is small and negative. Intepretation of the susceptibility is consistent with the presence of ionic species in the liquid, and a simple ionic Born-Haber thermodynamic cycle adequately explains the measured heat of formation of CsAu (Schmutzler, 1978, Sommer et al, 1979).

This work complements the molten salt nature of CsAu and indicates the presence of localised paramagnetic centres even at stoichiometry. The nearest neighbour coordination number deduced from NMR is in agreement with the neutron diffraction results of Martin et al (1980).

The non metallic properties which occur near the equiatomic composition CsAu represent a dramatic transition from the nearly free electron behaviour of pure liquid caesium and gold. The concentration dependent metal-nonmetal transition has a similar character to that observed in many metal-molten salt solutions such as Cs-CsI (Warren, 1980) and K-KBr (Bredig, 1964). In the Cs-CsAu system the conductivity is relatively insensitive to excess caesium in molten CsAu up to approximately y_{Cs} = 0.15, (Hoshino et al, 1975). This behaviour is to be contrasted with the strong dopant effect of excess metal in liquid semiconductors such as Mg_3Bi_2, Tl_2Te, Cs_3Sb. The thermopower results (Schmutzler et al, 1975) for caesium rich alloys show typically small metallic values, but in salt rich solutions large negative values characteristic of molten salts are observed. The concentration dependence of magnetic susceptibility (Freyland and Steinleitner, 1976,1977; Steinleitner and Freyland, 1975) in salt rich solutions shows the same trend as found in Cs - CsI (Steinleitner, 1978). The rapid reduction of diamagnetism with increasing excess metal concentration in both cases suggests that any localised paramagnetic centres formed in Cs - CsAu are similar to those occuring in the alkali

metal-molten salt solution. Again we can contrast electronically conducting liquid semiconductors where a slower variation of susceptibility is observed, eg. Cs_3Sb (Freyland and Steinleitner, 1977).

Electrical transport data for the liquid Cs-Au alloy system have shown the occurrence of a metal-nonmetal transition in the neighbourhood of mole fraction of caesium, $y_{Cs} \approx 0.18$, but this work recognises a transition in the nature of electronic states from extended to localised at $y_{Cs} = 0.07$. The most obvious cause of such a discrepancy is experimental concentration error due to the difficulty of handling the reactive materials. However, our NMR results were reproduced independently by W. W. Warren collaborating in the U.S.A. and a large measure of confidence in their reliability is therefore in order. A satisfactory physical explanation of the discrepancy has not been achieved. It is possible that the nature of the experimental probe can determine whether or not electron states appear to be localised. For instance, Holcomb (1978) discusses the occurence of electron spin resonance line narrowing in the semiconductor Si:P at a donor concentration a factor 3.5 smaller than that required for d.c. charge transport delocalisation. The explanation is an electron exchange coupling large enough to average out the hyperfine interaction with donor nuclei, but not large enough to overcome the correlation barrier to charge transport. However, it is possible that the non-coincidence of delocalisation detected by NMR and conductivity in the caesium-gold system is due to an experimental artifact, and further investigation is advised.

Fig. 4.10 shows our experimental nuclear resonance shift in caesium rich alloys at 873 K plotted against the magnetic susceptibility of a gram-atom of caesium, deduced from the gram susceptibility data of Freyland and Steinleitner (1976). The gradient yields the hyperfine field per paramagnetic centre, but quantitative analysis is not appropriate because

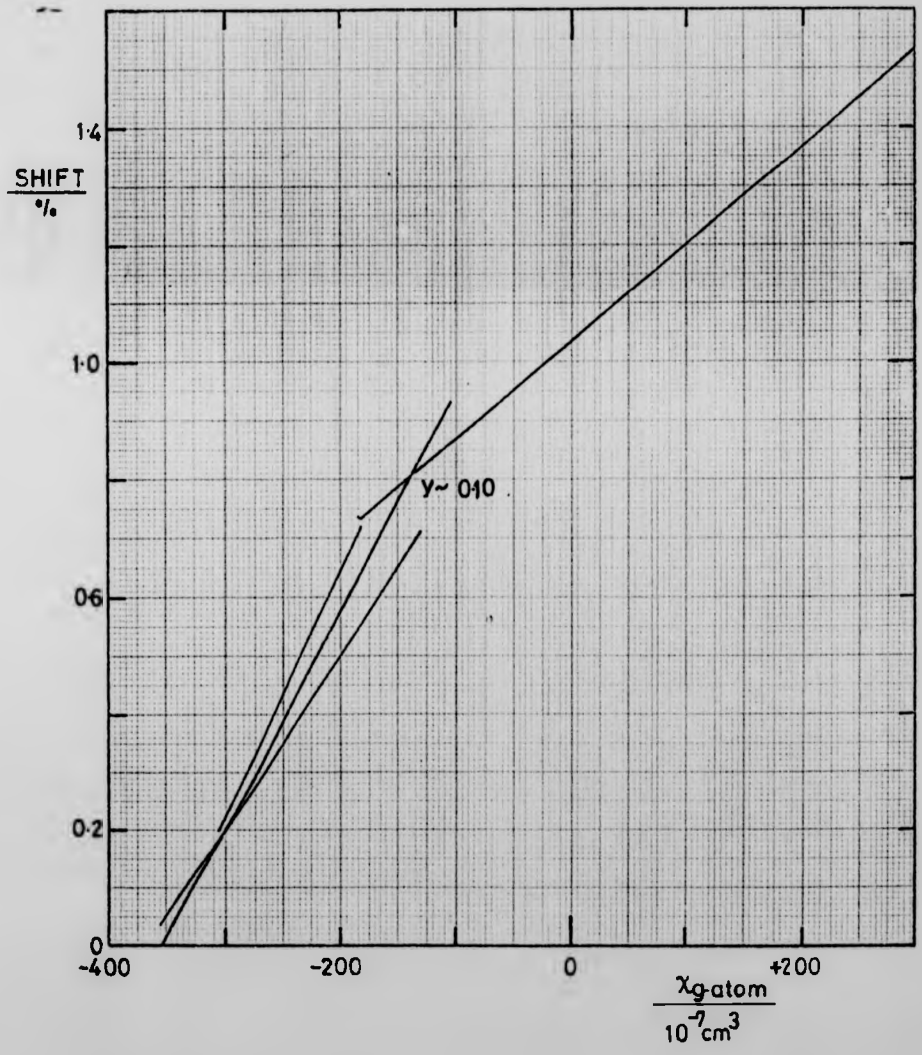

Fig. 4.10: ^{133}Cs resonance shift at 873 K versus the magnetic susceptibility of one g-atom of caesium. Concentration is the implicit parameter.

of the large uncertainty in the susceptibility data and the further difficulty of estimating the gold contribution to the measured susceptibility. Qualitatively, the hyperfine coupling increases at the transition from extended to localised states near $y_{C_s} \simeq 0.10$. For completeness $^{A}/h = (2 \pm 1)$ GHz in the localised region, in only approximate agreement with the value of 1.3 GHz derived from eqn. 2.30 describing the linear dependence of shift on concentration of localised centres.

Recent attempts to calculate the electron density of states in liquid ionic alloys have included particular reference to the caesium-gold system. Kittler and Falicov (1976) used a solid state model based on the Cluster-Bethe Lattice to study the effect of short range order. Ten Bosch et al (1976) used an adapted truncated fraction method and found an energy gap due to charge transfer when the short range order was high. Roth (1977) calculated the concentration dependence of transport properties in addition to the density of states, but did not include the effects of ionic mobility. Most recently Franz et al (1980), Brouers et al (1980) and Holzey et al (1981) have included short range order and charge transfer self consistently within a tight binding approach in order to investigate liquid alkali metal-gold systems. Liquid LiAu and NaAu are metallic but CsAu and RbAu undergo a metal-nonmetal transition near stoichiometry, whilst KAu has intermediate properties, and their model satisfactorily accounts for the wide range of electrical behaviour found in the alloy series LiAu to CsAu (Nicoloso et al, 1978). This theory shows that the essential factors generating the metal-nonmetal transition are the size of the alkali constituent (and hence the different bandwidths) and the interatomic Coulomb interaction. The electronegativity difference is relatively unimportant. In the particular case of Cs-Au the later papers correct an earlier error such that at stoichiometry the local order parameter now has a very large magnitude consistent with an ionic structure, $\sigma_{SR} \leq -0.9$. Holzey et al (1981) claim that other quantities

remain "nearly the same", and the density of states at the Fermi energy looks similar, although there may be a steeper rise on the caesium side of stoichiometry in the revamped calculation. Franz et al (1980) demonstrate the good agreement with experiment found for σ, $d\sigma/dT$ and χ_g for Cs-Au alloys and predicts the dependence of Knight shift on concentration. This curve is plotted as the dotted line on Fig. 4.3 and is seen to give only qualitative agreement with experiment. In particular the calculation underestimates the rapid dependence of shift with excess caesium in the compound CsAu. Noteworthy however is the correct prediction of the negligible effect of excess gold on the ^{133}Cs resonance.

The calculated liquid density of states (Franz et al, 1980) is presented in Fig. 4.11 and is observed to be of a similar form to the generalised model (Fig. 1.8) for the electronic structure of an ionically bonded system due to Roth (1975). In caesium rich alloys, increasing gold concentration serves to broaden the lower band but the energy gap is preserved by the increasing short range order. At the equiatomic composition the mixing of gold and caesium states is at a maximum and the Fermi level is at the centre of the gap. In gold rich alloys local order decreases and broadening of the gold band quickly destroys the gap.

4.5. Summary of the Caesium-Gold System

^{133}Cs NMR results in liquid caesium-gold alloys demonstrate a sharp metal-non metal transition at mole fraction of caesium $y_{Cs} \simeq 0.07$. Dissolution of Au in Cs has only very small effects on the resonance properties and nearly free electron behaviour is observed. Close to the stoichiometric composition CsAu a sharp drop in the Knight shift is observed, accompanied by a sharp peak in the spin-lattice relaxation rate, which arises from the competing effects of a rapidly increasing correlation time

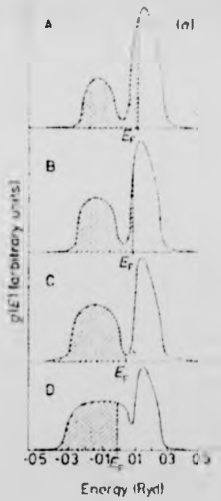

Fig. 4.11: The density of states N(E) for liquid $Cs_x Au_{1-x}$ alloys at 600°C at different compositions (Franz et al 1980).

(a) x = 0.7 (b) x = 0.6 (c) x = 0.5 (d) x = 0.4.

and a decreasing concentration of excess electrons. Near stoichiometry the shift has a linear dependence on concentration.

This data is interpretted as direct evidence of strong localisation of excess electrons in caesium doped CsAu in the form of F centre analogues for $y_{Cs} < 0.07$. The composition dependent transition from localised states to extended states takes place when overlap of individual F-centres occurs, and is therefore a Mott-Hubbard transition (Littlewood 1981). This is the first report of F-centres in an ionic liquid alloy.

Stoichiometric CsAu crystallises in the typically ionic CsCl structure and has a room temperature band gap of 2.6 eV. Electronic contribution to conduction is therefore negligible, but the compound is readily doped with excess caesium. Caesium-gold is the most ionic metal alloy known (Robertson 1981 calculates a charge transfer of ± 0.96 e), and becomes a typical molten salt on melting. (See for example Freyland and Steinleitner 1976).

The resonance shift of room temperature CsAu, 0.036%, is typical of caesium salts (CsI, 0.027% Haase et al 1977) and increases to 0.075% at the melting point, where we deduce the presence of a thermally generated concentration of electron-hole pairs to explain the background paramagnetism. A sharp 25-fold increase in spin-lattice relaxation rate accompanies melting indicating increases disorder in the liquid. Excess gold in CsAu must exist in a diamagnetic form, Au^-, since the ^{133}Cs resonance properties remain similar to their values at stoichiometry.

The observed properties of Cs-Au liquid alloys reflect the extreme situation of complete ionic bonding and it would be most interesting to extend this work by investigating other alkali-gold systems. RbAu has a smaller band gap and is thought to be at the border of metal-nonmetal behaviour and is therefore an excellent candidate for study. In other fields there is a broad base of information, but noticeably absent are measurements of Hall effect and viscosity.

CHAPTER FIVE

THE CAESIUM-ANTIMONY SYSTEM

5.1. Introduction

The phase diagram for the caesium antimony system Cs_xSb_{1-x} is presented in Fig. 5.1 (Elliott 1965) and its complicated nature reflects the large number of intermetallic compounds which are thought to form. In particular, the region $0.5 < x < 0.75$ is least well defined. From the melting point of pure caesium at 300 K the liquidus temperature rises steeply with the addition of very small amounts of antimony, and for only 2 atomic % of antimony in caesium reaches ~ 700 K. The liquidus temperature continues to rise with increasing antimony content to a maximum of 998 K at the stoichiometric compound Cs_3Sb. Liquid alloy concentrations in the region Cs-Cs_3Sb cover a continuous range of electrical properties from metallic to semiconducting, Fig. 5.2, (Steinleitner 1978), and provide the major focus of NMR investigation in this work, although some concentrations in the vicinity of compounds or eutectic composition with $x < 0.75$ have also been studied. Assuming the ready formation of molecular Cs_3Sb, data is often presented in terms of the excess mole fraction of caesium, y, above stoichiometric Cs_3Sb. It is important to bear in mind that relative to the atomic concentration scale, x, the excess concentration scale, y, is greatly expanded in the vicinity of Cs_3Sb. For example $Cs_{.76}Sb_{.24}$ corresponds to $y \approx 0.14$.

Alloy samples were prepared in situ and were not dispersed. A strongly exothermic reaction between solid antimony and liquid caesium occurred at the melting point of caesium and caused the destruction of several NMR cells. This problem was most severe for antimony rich solutions. By not adding all of the antimony at once and by reducing the antimony surface area the reaction was inhibited, but nevertheless sample temperatures

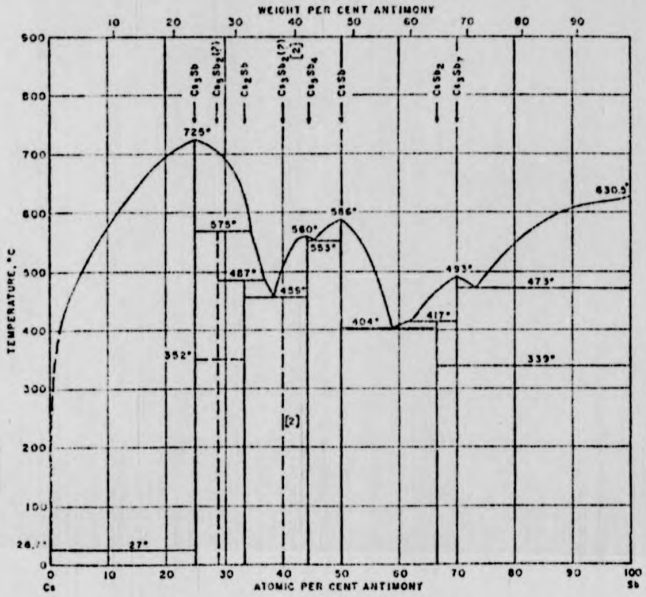

Fig. 5.1: The phase diagram of the caesium-antimony system (Elliott 1965).

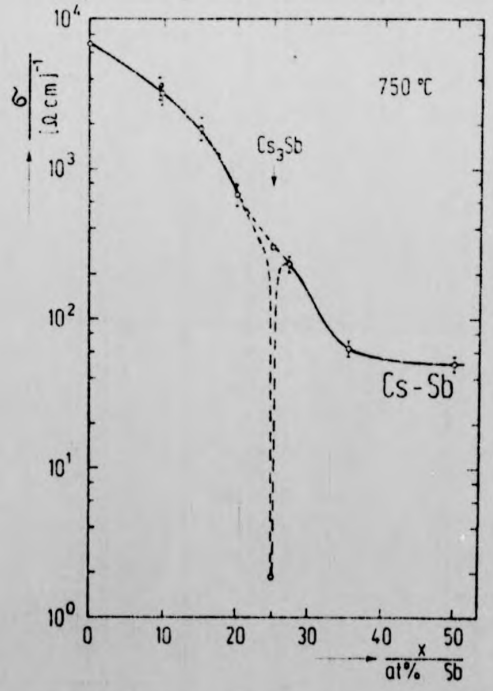

Fig. 5.2: Electrical conductivity as a function of composition in Cs-Sb liquid alloys at 1023 K (Steinleitner 1978).

spontaneously reached ∿ 370 K. The reaction product is uncertain since the heats of formation of the various caesium-antimony compounds are unknown, but it is thought likely to be CsSb. Caesium-antimony alloys proved to be much more corrosive to the sample containers than caesium-gold alloys (due in part to the ∿ 100 K higher temperatures required), and until the latter stages of this work data collection was usually curtailed by sample leakage. The diffusion bonded cells produced by Freyland at Universität Marburg have proved particularly successful.

Both caesium and antimony nuclei are amenable to investigation by NMR. ^{133}Cs was studied at frequencies of approximately 12 MHz in the gap of the electromagnet, and 24,32,40 MHz in the superconductive magnet. Caesium resonance shifts were measured relative to an aqueous solution of CsCl corrected to infinite dilution. The low temperature solid compounds Cs_3Sb and CsSb demonstrated a caesium spin-lattice relaxation time greater than the spin-spin relaxation time, $T_1 > T_2$, but relaxation data in the liquid indicated that the extreme motional narrowing criterion was satisfied, $\omega\tau << 1$ and $T_1 = T_2$. Often the spin phase memory time T_2^* was measured and a field inhomogeneity correction applied where appropriate to obtain the true relaxation times. In principle, the antimony isotopes ^{121}Sb and ^{123}Sb are prime candidates for the investigation of nuclear relaxation by the technique of isotopic separation of magnetic and quadrupolar contributions (Warren and Clark 1969) (Equations 2.41), and it was hoped that much additional information would be obtained from their study. Also, comparison of the Sb resonance shift with that of Cs would enable a comparison of the respective densities of states to be made. As discussed later, however, it was not found possible to observe NMR for either antimony isotope in any of the caesium-antimony alloys studied.

The data for non-stoichiometric Cs_xSb_{1-x} liquid alloys is presented in §5.2 and that for the stoichiometric compounds Cs_3Sb and CsSb in §5.3.

5.2. NMR in Caesium-Antimony Liquid Alloys

Fig. 5.3 presents the ^{133}Cs nuclear resonance shift at 1023 K as a function of concentration in caesium-antimony liquid alloys. For $x_{Cs} \geq 0.75$ an excess mole fraction scale is used for concentration (left hand side), and for $x_{Cs} \leq 0.75$ the atomic fraction is used (right hand side). (The excess concentration scale cannot be used for $x_{Cs} \leq 0.75$ since in the solid many phases are possible). From the value of pure caesium (Warren, this work), the shift is seen to fall sharply with the addition of antimony. The shift reaches a minimum of $\sim$ 0.16% at Cs_3Sb, before rising to a small maximum and falling again to even smaller values at CsSb and $Cs_{385}Sb_{615}$, 0.11%. The marked affect of antimony in caesium is in strong contrast with that of gold (§4.3). Fig. 5.3 also presents as a dashed line the concentration dependence of the nearly free electron susceptibility calculated on the basis of one conduction electron per excess caesium atom, and a volume contraction of 50% for the solid compound Cs_3Sb (Gnutzmann et al 1961). Whilst this approach gave good agreement with the data for Cs_xAu_{1-x} there is clearly not even qualitative agreement for Cs_xSb_{1-x}, and caesium-antimony alloys cannot therefore be described in nearly free electron terms over any part of the concentration range.

Although the susceptibility data is rather limited (Steinleitner 1978) and there exists some uncertainty as to the antimony contribution to the total measured susceptibility, a graph of resonance shift against the susceptibility of 1g-atom of caesium atoms with concentration as the implicit variable (Fig. 5.4) produces a straight line over a range corresponding to $0.2 \leq y_{Cs} \leq 0.8$. The antimony susceptibility was assumed to be due to the core susceptibility of Sb^{3+}, shown by Steinleitner (1978) to be consistent with the room temperature measured susceptibility of Cs_3Sb, where any free carrier contribution is negligible. Using equation 2.26

$$K = \frac{\Delta B}{B} = \frac{\bar{A}\chi}{N_A \gamma_e \gamma_n h^2}$$

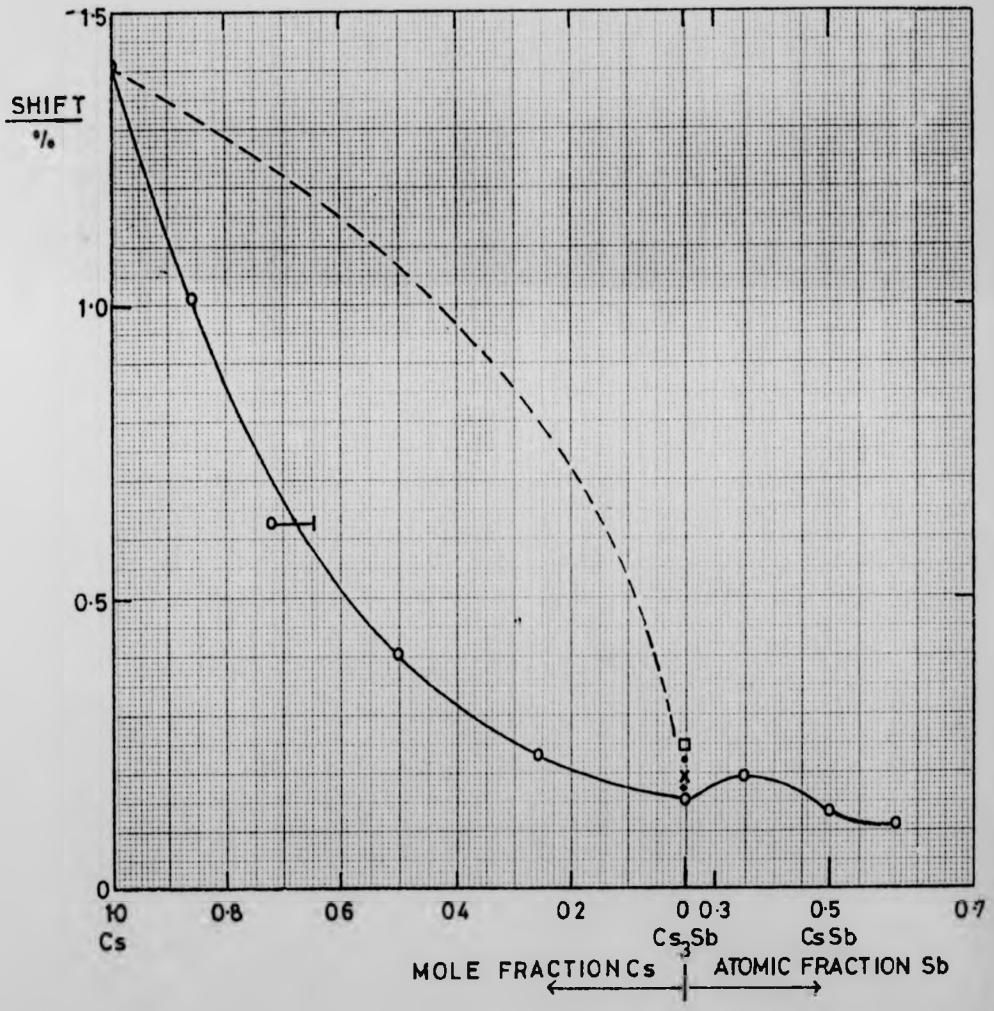

Fig. 5.3: ^{133}Cs resonance shift in Cs_xSb_{1-x} liquid alloys as a function of composition at 1023 K. For $x < 0.75$ the atomic concentration scale is used (right hand side). For $x > 0.75$ an excess mole fraction scale is used (left hand side), and the dashed line gives the form of the calculated free electron shift normalised to pure caesium.

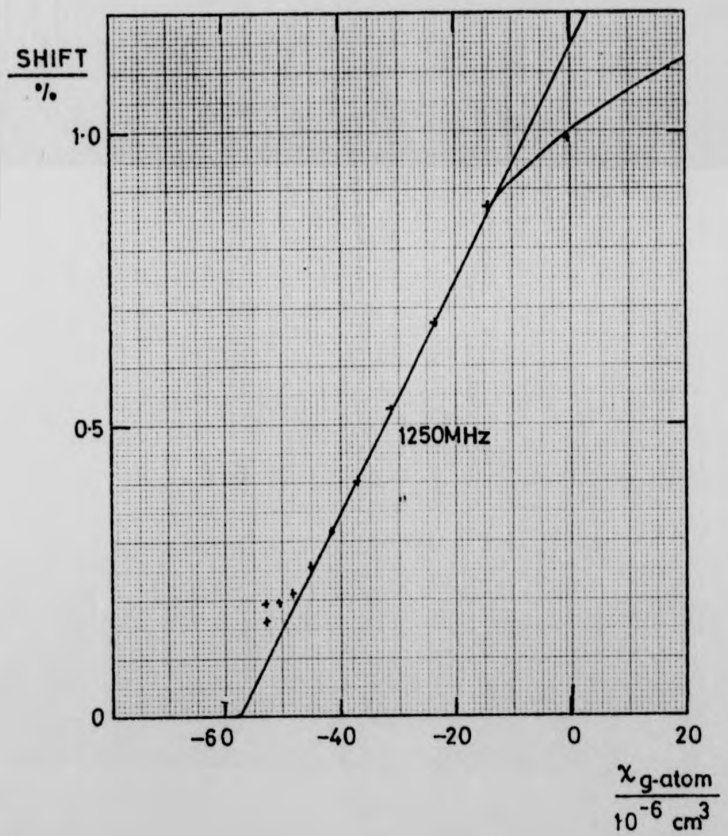

Fig. 5.4: ^{133}Cs resonance shift in $Cs_y(Cs_3Sb)_{1-y}$ liquid alloys at 1023 K versus the magnetic susceptibility of one g-atom of caesium.

the slope of the K, χ graph enables the mean hyperfine field per paramagnetic centre to be deduced. We find from the linear section

$$\overline{A} = (8.3 \pm 1.0) \times 10^{-25} \text{ J.}$$

$$\frac{\overline{A}}{h} = 1250 \text{ MHz.}$$

This value is $\sim$ 60% of the atomic value and is not unreasonable. However, in view of the difficulty in estimating the contribution of antimony to the measured susceptibility an alternative approach to the hyperfine coupling is desirable. Temperature dependence of both NMR shift and susceptibility for the same alloy composition would provide a situation in which the antimony contribution is presumably constant, and hence allow the ^{133}Cs hyperfine coupling to be obtained. However, in most cases where coincident data are available there is negligible temperature dependence of shift and the resulting K, χ plot is nonlinear. The increasing paramagnetism with temperature observed in susceptibility measurements may be associated with bonding changes (molecular dissociation?) and has minimal effect on the resonance shift. The caesium-antimony alloy showing the greatest temperature coefficient of shift was $Cs_{77}Sb_{23}$ and the susceptibility sample most similar in concentration was $Cs_{781}Sb_{218}$. The temperature coefficient of shift at this concentration was therefore estimated to allow a K, χ graph to be plotted with temperature as the implicit parameter. This gave $^{A}/h \simeq (600 \pm 100)$ MHz, or only half the value obtained in Fig. 5.4, suggesting that the susceptibility due to antimony was wrongly accounted for above.

The temperature coefficient of shift in liquid Cs_xSb_{1-x} alloys at $\sim$ 1000 K is always positive, and increases in magnitude as the concentration varies from pure caesium towards Cs_3Sb (Fig. 5.5). However, very close to stoichiometry the value of dK/dT decreases again to a value typical of the other compounds or metal rich alloys investigated. This behaviour contrasts with the temperature coefficient of susceptibility (Steinleitner 1978)

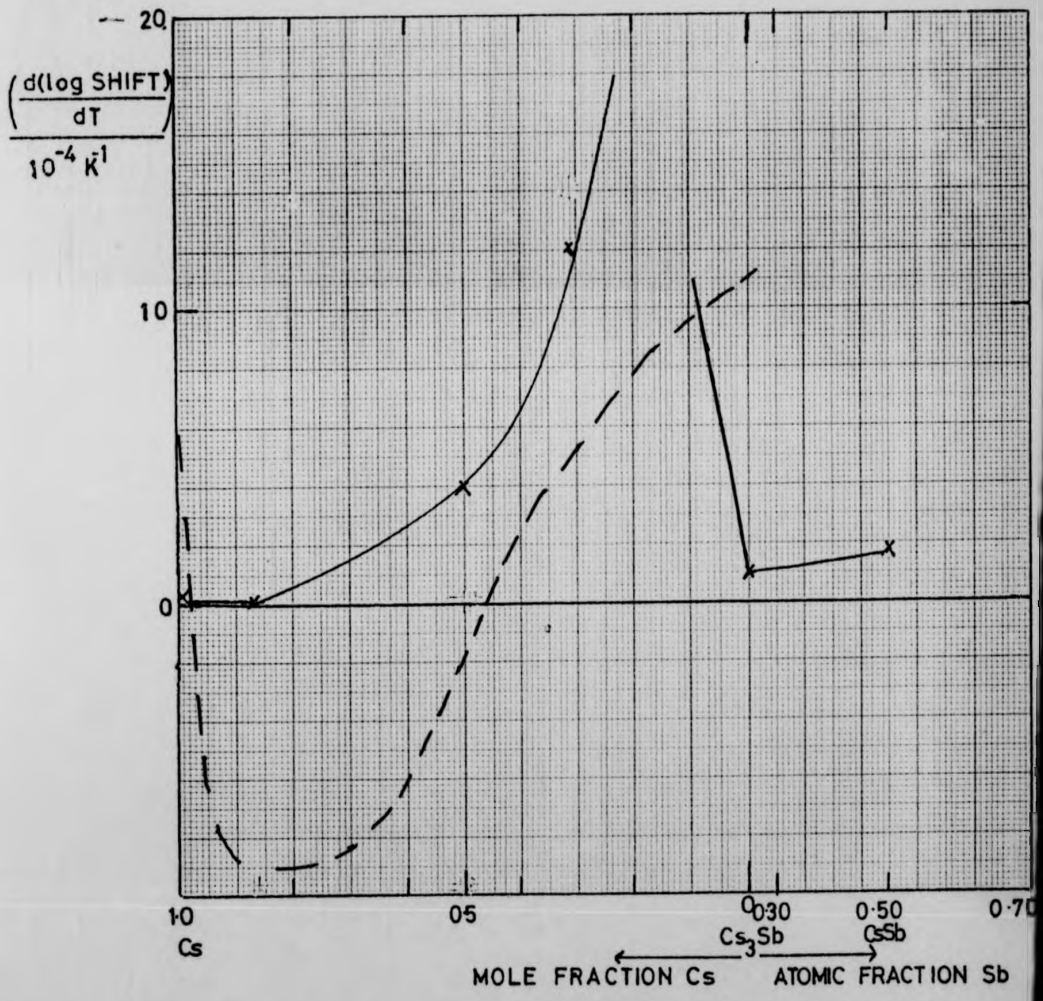

Fig. 5.5: The temperature coefficient of ^{133}Cs shift $\left(\frac{d \ln \text{shift}}{dT}\right)$ versus concentration in Cs-Sb liquid alloys at 1023 K. The dashed line shows the temperature coefficient of susceptibility (Steinleitner 1978) (10^{-1} emu g^{-1} K^{-1})

which has a broad negative minimum near $Cs_{85}Sb_{15}$ but is positive at caesium and Cs_3Sb. This curve is reproduced on Fig. 5.5 as a dashed line.

Fig. 5.6 presents the relaxation time T_1 obtained as a function of composition at 1023 K. There are only small changes in T_1 for Cs-Sb with excess caesium, varying from T_1 = 500 μs at Cs_3Sb to T_1 = 300 μs at $Cs_{0.9}Sb_{0.1}$. Evaluating the Korringa enhancement parameter η (eqn. 2.43)

$$\eta = \frac{K^2 T_1 T_{Korr}}{K^2 T_1 T_{expt.}} = \frac{\tau}{\tau_{\substack{free \\ elect.}}}$$

we find a value of 31 at stoichiometric Cs_3Sb, where the appropriate shift is the experimentally observed value minus the chemical shift (taken to be the room temperature value). η decreases with the addition of caesium to Cs_3Sb. In this region the electrons are mobile but η > 1 reflects an incipient localisation process, in which the correlation time, τ, is increased over its value in a nearly free electron metal like caesium. Fig. 5.7 shows the values of τ calculated from the observed relaxation rates, using a composition dependent value for the free electron correlation time. This approach becomes invalid in the limit of zero excess metal in the stoichiometric compound and for this reason no value of correlation time can be deduced for Cs_3Sb. At y_{Cs} = 0.05, τ is seen to reach the value of a few x 10^{-14} secs and is similar to that observed in the Cs-Au system (Chapter 4).

For Cs_xSb_{1-x} alloys with x < 0.75 the nuclear resonance shift remained small as shown in Fig. 5.3, but the spin-lattice relaxation time increased reaching 3.5 ms for $Cs_{385}Sb_{615}$ at 963 K (Fig. 5.7). In this alloy, which melts near a eutectic at 677 K, $T_1 \neq T_2$ in the liquid and τ decreases slowly with increasing temperature from ∿ 1.4 x 10^{-12} s at the melting

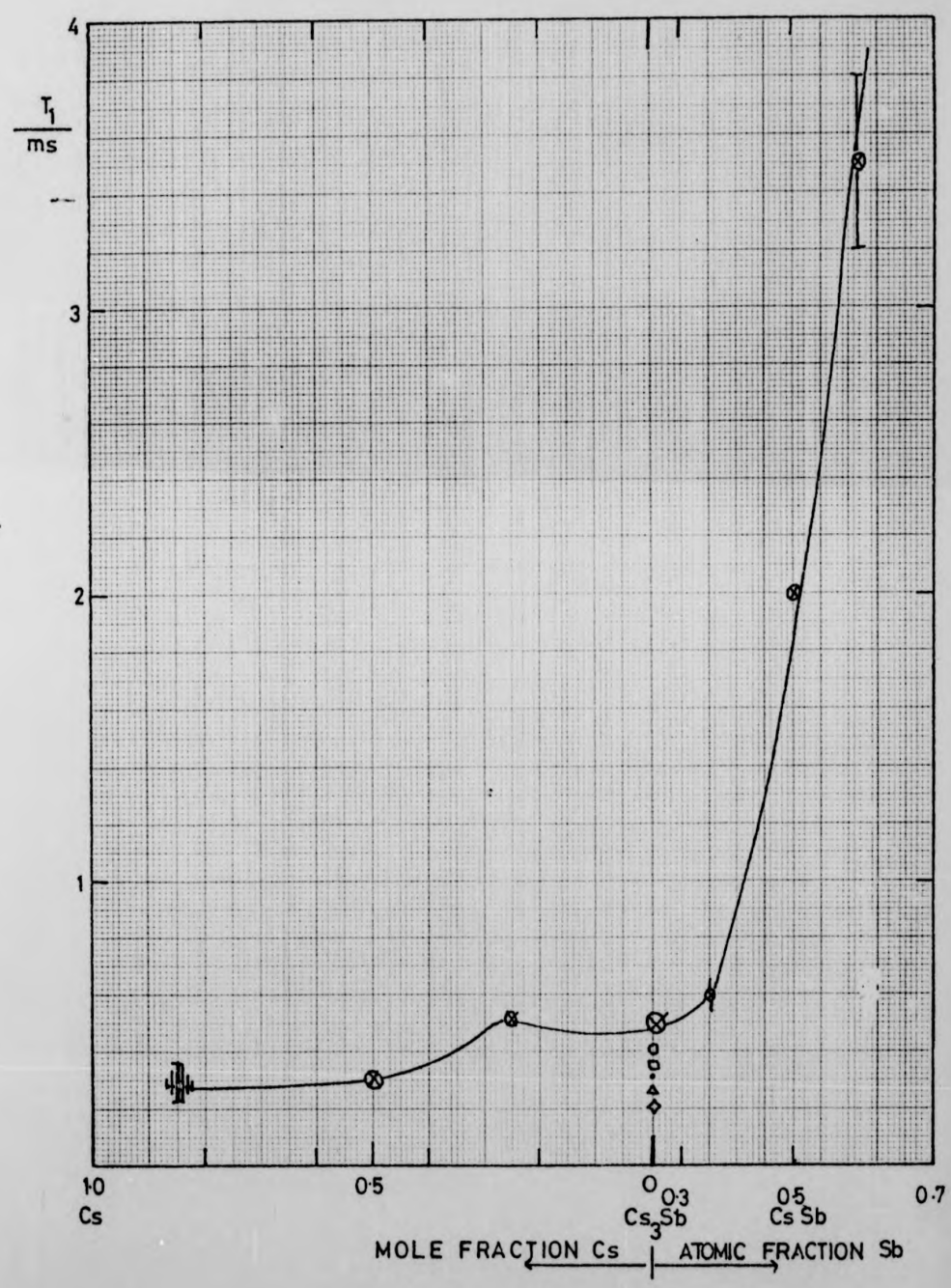

Fig. 5.6: The ^{133}Cs spin lattice relaxation time, T_1, as a function of composition in Cs-Sb liquid alloys at 1023 K.

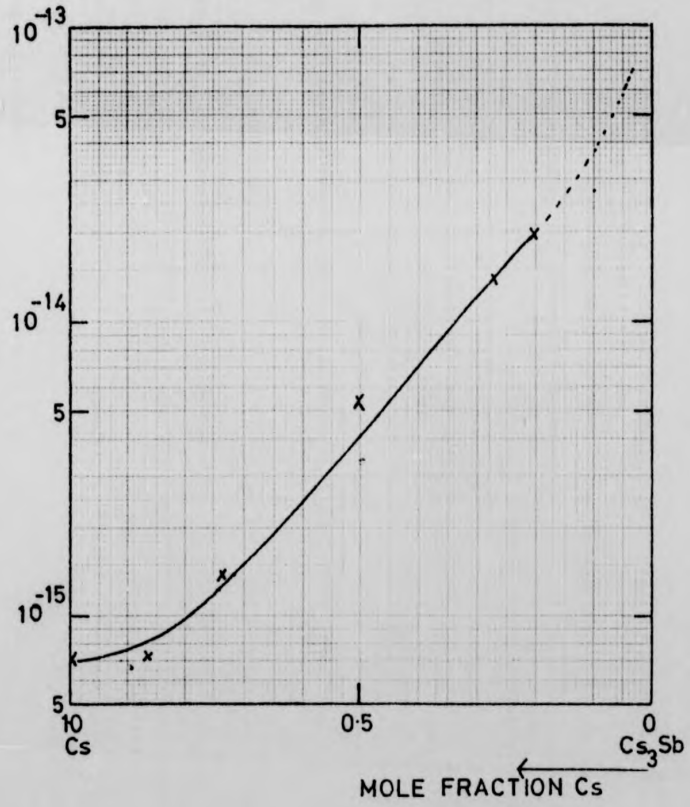

Fig. 5.7: The ^{133}Cs hyperfine field correlation time in liquid $Cs_y(Cs_3Sb)_{1-y}$ alloys as a function of composition at 1023°K.

point to $\sim 1 \times 10^{-12}$ s at 963 K. The long relaxation times, small shifts and long correlation times evident for antimony doped Cs_3Sb and antimony rich alloys suggests that compound formation and chemical bonding are occuring.

Although visible in bulk elemental liquid antimony, the search for both of the antimony isotopes in all alloy compositions studied was unsuccessful. Extensive attempts involving boxcar integration with magnetic field or frequency sweep, and the averaging of the free induction decay, were made at temperatures up to 1100 K over a range of shifts from small diamagnetic values to $\sim$ 1% Knight shift for both stoichiometric compositions and the liquid alloys. Assuming a similar relaxation time to that of caesium, then the observed signal: noise ratio for ^{133}Cs in Cs_xSb_{1-x} implies that the antimony resonance should be readily detectable. That this was not the case suggests that significant line broadening due to extremely rapid nuclear relaxation exceeded the time resolution of the spectrometer. Using the same apparatus at 50 MHz in the study of $BiBr_3$, a Bi resonance with a relaxation time of 3 μs was observed on a single boxcar integrated field sweep with good signal to noise ($\sim$ 10:1) (Dupree and Gardner 1980). The antimony resonance is not expected to be so large since it has lower sensitivity, the skin depth of Cs_xSb_{1-x} alloys attenuates the r.f. compared to the insulating $BiBr_3$, and the $BiBr_3$ sample was contained in a "T-ampoule" in which the B_1 field was generated by a solenoidal rather than Helmholtz coil. However, taking these factors into account it is concluded that an antimony resonance of the same width would be observed and therefore an upper limit for the antimony relaxation time, T_1, is 3 μs.

Such rapid relaxation cannot be magnetic in origin and is ascribed to fluctuating quadrupolar interactions resulting from the tendency to form relatively long lived molecular groups. Assuming motional narrowing, $\omega\tau << 1$, the quadrupolar relaxation rate is given by equation 2.38

$$\frac{1}{T_{1Q}} = \frac{3}{40}.F(I)\left|\frac{e^2qQ}{\hbar}\right|^2.\tau$$

Neither the quadrupolar interaction strength $\left(\frac{e^2qQ}{h}\right)$ or the correlation time are known for Cs_xSb_{1-x} liquid alloys. As one estimate, we take the value $\left(\frac{e^2qQ}{h}\right) \approx 98$ MHz for ^{123}Sb in solid antimony (Hewitt and Williams 1963) and obtain for $T_1 = 3$ μs a correlation time $\tau = 8.5 \times 10^{-11}$ secs. A second estimate is obtained by taking the interaction found for ^{121}Sb in the trihalides (Das and Hahn 1964) and scaling with quadrupole moment to obtain a value of ∿ 450 MHz for ^{123}Sb. This yields $\tau \sim 4 \times 10^{-12}$ secs. Finally, it is reported in §5.3 that room temperature Cs_3Sb showed quadrupolar splitting of the ^{133}Cs resonance. Scaling the interaction with quadrupole moment on the assumption of the same electric field gradient at the antimony site we find $\left(\frac{e^2qQ}{h}\right) \approx 18$ MHz for ^{123}Sb and hence $\tau \sim 2.5 \times 10^{-9}$ sec. All three estimates yield values of the correlation time for the local enviroment of the ^{123}Sb nucleus in caesium alloys at temperatures ≥ 1000 K which are significantly longer than typical liquid diffusion times. These are lower limits for τ and are calculated on the basis of the maximum possible T_1. This means that the local field remains constant for <u>at least</u> a few $\times 10^{-12}$ secs and suggests molecule formation. For comparison the quadrupolar derived correlation time for liquid antimony at 1000 K is $\tau \sim 6 \times 10^{-13}$ s (Warren and Clark 1969).

5.3. <u>NMR in the Stoichiometric Compounds Cs_3Sb and CsSb</u>

As discussed in §5.4 the electrical conductivity of the compound Cs_3Sb is very sensitive to doping by excess metal, and observation of the non-metallic liquid state at 1023 K therefore requires that the exact stoichiometry be achieved. Therefore several samples of the same nominal concentration Cs_3Sb were prepared and investigated. Additionally, powdered Cs_3Sb was obtained from CERAC (99.9% purity) as an independent check on

the range of stoichiometry. Between room temperature and ∿ 380 K the commercial powdered sample and one of the home produced bulk samples showed a quadrupolar splitting of the ^{133}Cs resonance line. The splitting was less marked in the bulk sample: quadrupolar resonance frequency ν_Q = 1.68 kHz, but in the powdered sample the six satellites were well resolved and ν_Q = (7.5 ± 0.14) kHz. Fig. 5.8 presents an averaged frequency sweep of width 56 kHz through the ^{133}Cs resonance at room temperature in the powdered Cs_3Sb sample. Qualitatively the central peak may comprise of two peaks related to the two distinct caesium sites in the crystalline Cs_3Sb lattice, (Jack and Wachtel, 1957) as discussed in §5.4. However, the asymmetry of the satellite spacing about the central peak, the relative peak amplitudes and any possible structure in the central peak are neglected in the calculation of ν_Q.

For a single crystal the first order splitting of the $\Delta m = \pm 1$ transitions from the Larmor resonance frequency is described by (Winter 1971)

$$\Delta\nu = \frac{3}{8}\left(\frac{e^2qQ}{h}\right)\frac{(2m-1)}{I(2I-1)}\left[3\cos^2\theta - 1\right] \quad * \qquad (5.1)$$

where $\Delta\nu$ = frequency shift

$\left(\frac{e^2qQ}{h}\right)$ = nuclear quadrupole interaction strength

I = nuclear spin

m = eigenvalue of I_z, the component of $\underline{I}$ along $\underline{B}_o$

θ = angle between crystal field axis and $\underline{B}_o$.

In a powdered sample the intensity of the transitions is distributed over a range of frequencies and the average value of the angular function is required. For ^{133}Cs, $I = {}^7/_2$ and we deduce $\left(\frac{e^2qQ}{h}\right) = (105 \pm 2)$ * kHz at room temperature. Since the electric quadrupole moment of ^{133}Cs is very small $eQ = -0.004\ e \times 10^{-24}\ cm^2$ (Varian Associates), we conclude that at least some of the caesium sites have non cubic symmetry and experience a

* assuming axial symmetry

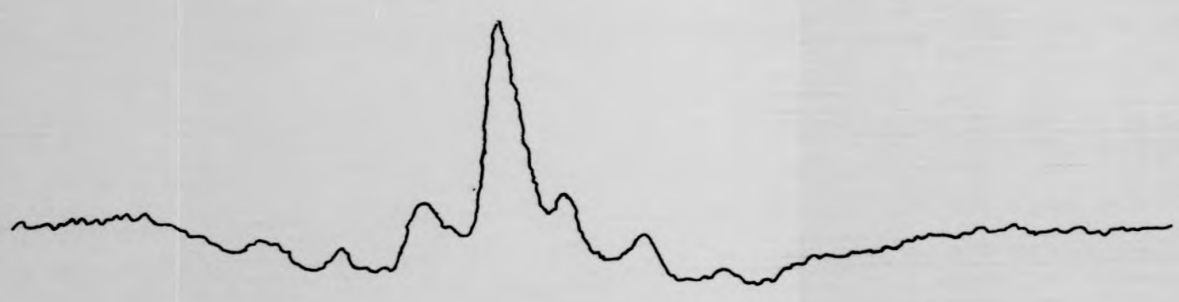

Fig. 5.8: An averaged frequency sweep (width 56 KHz) showing quadrupolar splitting of the ^{133}Cs resonance in the powdered Cs_3Sb sample at room temperature.

large electric field gradient. It is noteworthy that the occurence of quadrupolar splitting of ^{133}Cs NMR is very rare; only one other example occurs in the literature, for Cs_2SO_4 (Haase et al 1977).

Both of the commercially prepared Cs_3Sb samples exploded during the first heating at temperatures of ∿ 600 K and ∿ 660 K. Chemical analysis by Dr. G. R. Willey, Chemistry Department, University of Warwick of the remaining unheated fraction of this material indicated that unreacted antimony metal may have been present. It is postulated that reaction of this with excess caesium or Cs_3Sb at elevated temperature caused the destruction of the samples and cells. The manufacturers deny this interpretation and point to the analysis supplied with the samples as evidence of stoichiometry.

The ^{133}Cs NMR results for the Cs_3Sb samples showed very complicated behaviour in the solid, with a room temperature shift of (0.062 ± 0.005)%. From ∿ 473 K this split into either two or three lines with different temperature dependence of shift as shown on Fig. 5.9. The exact values obtained (across the whole range of temperature) varied from sample to sample and from one heating to the next, but a typical run is plotted. Above ∿ 800 K a line at larger shift with marked $\frac{dK}{dT} > 0$ grew in amplitude at the expense of the other lines. The equilibrium liquid resonance position at 1023 K was also a function of sample and ranged from 0.159% to 0.25%, and it is assumed that the lowest value reflects the closest approach to stoichiometry. Experimentally, the greatest accuracy in weighing etc. that can be hoped for would lead to an uncertainty of about ½% in the atomic concentration, which for $Cs_{.7525}Sb_{.2475}$ corresponds to an excess concentration of caesium y = 0.04. This is a relatively large value and emphasises the difficulty associated in achieving exact stoichiometry.

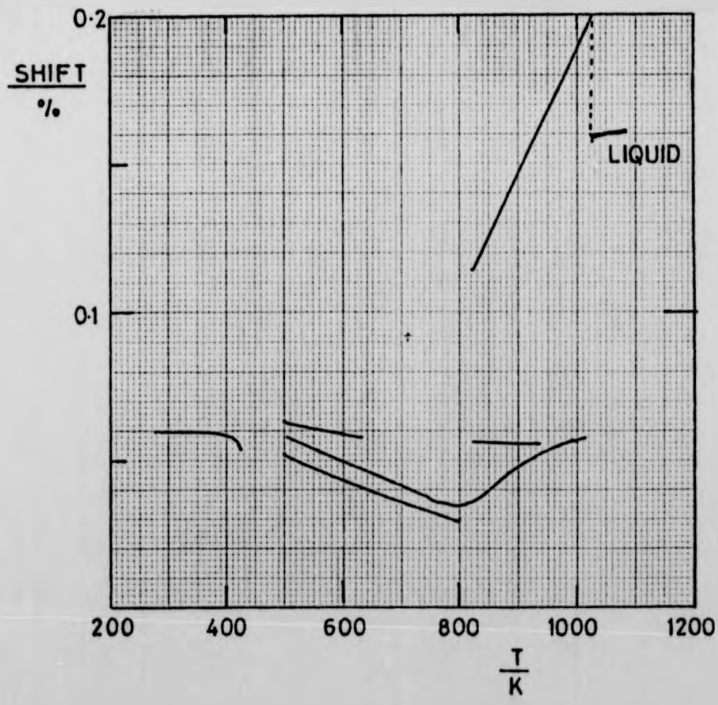

Fig. 5.9: ^{133}Cs resonance shift in the most stoichiometric Cs_3Sb bulk sample as a function of temperature.

Relaxation behaviour was equally complicated. The room temperature spin lattice relaxation time T_1 was often shorter than the values obtained for the largest resonance line after motional narrowing had set in at ∿ 380 K. At room temperature the longest T_1 measured was (108 ± 10)ms, but values ≥ 250 ms were obtained at higher temperatures. With further increase of temperature this value decreased to reach ∿ 500 μs at the melting point and displayed no detectable temperature dependence over 70 K in the liquid.

Comparison of the Cs_3Sb results with those of stoichiometric CsAu (in which the resonance shift was only half as large and relaxation rather stronger) suggest that Cs_3Sb has a larger chemical shift and hence greater covalency in its bonding. (In the limit of pure ionic bonds the chemical shift is zero).

The NMR results for the composition CsSb are similar in many respects to those of Cs_3Sb. A complicated multiple resonance behaviour in the solid gives way to a single resonance in the liquid with a small positive temperature coefficient of shift and almost constant relaxation rate. Relaxation is however a factor of 4 weaker than for Cs_3Sb having the value of T_1 = 2 ms.

5.4. Relation to Other Properties

The solid compound Cs_3Sb crystallises in a compensated interstitial structure related to the NaTl structure (Jack and Wachtel 1957). In this structure (Fig. 5.10) each species is arranged on two interpenetrating diamond sublattices, and for Cs_3Sb the Na sites are occupied by $^2/_3$ of the caesium and the Tl sites by the remaining caesium and all of the antimony. Whether or not the Tl site occupancy is ordered is the subject of some debate (Robertson, 1981). An alternative description of the same arrangement is an sp^3 hybridized covalent structure in which one

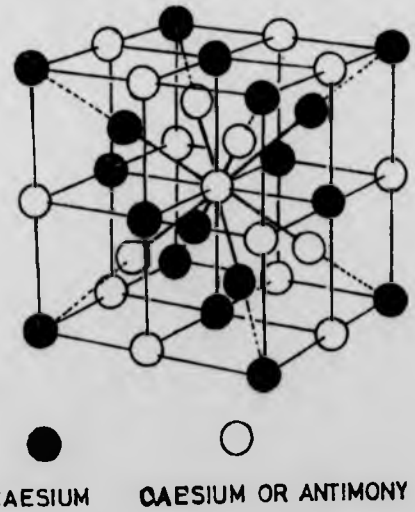

Fig. 5.10: The unit cell of caesium antimonide Cs_3Sb (Jack and Wachtel 1957).

Cs participates with Sb in tetrahedral bonds, and the other two Cs^+ ions occupy interstitial lattice sites.

$$Cs_3Sb \equiv 2Cs^+ + Cs^{3-} + Sb^+$$
$$[6s^0] \quad [6s^1\ 6p^3] \quad [5s^1\ 5p^3]$$

The compound Cs_3Sb is semiconducting with a band gap of 1.6 eV and melts at 1023 K.

The conductivity data for the liquid presented in Fig. 5.1 show a very sharp drop in σ in the narrow range of 24.5 - 25 at % Sb to a value of $\sigma \sim 2\ \Omega^{-1}\ cm^{-1}$; doping of the compound with very small amounts of excess metal gives rise to $\sigma \sim 50\ \Omega^{-1}\ cm^{-1}$. For the stoichiometric compound log σ follows a reciprocal temperature dependent over at least 200 K, giving an activation energy of 0.4 eV and preexponential factor of $500\ \Omega^{-1}\ cm^{-1}$. Within experimental error there is no clear variation of the absolute thermopower with concentration near Cs_3Sb, and the mean value is $S = -20 \pm 10\ \mu VK^{-1}$ (Freyland and Steinleitner 1976). The magnitude of S together with that of the activation energy gives a good indication that electronic conduction should prevail in the liquid, and that the compound is a liquid semiconductor. The analysis of susceptibility shows that the total molar susceptibility of the room temperature solid is equal to the atomic molar susceptibility of the liquid, consistent with the preservation of bonding type through the melting transition.

Fig. 5.11 presents a plot of the resonance shift against the square root of conductivity, and it is seen to follow approximately a straight line over a range of conductivities corresponding to 300 - 3000 $\Omega^{-1}\ cm^{-1}$. This is just the range of σ for which the most general discussions of diffusive transport expect to observe linearity, and indicates that the decrease in the density of states is responsible for both parameters.

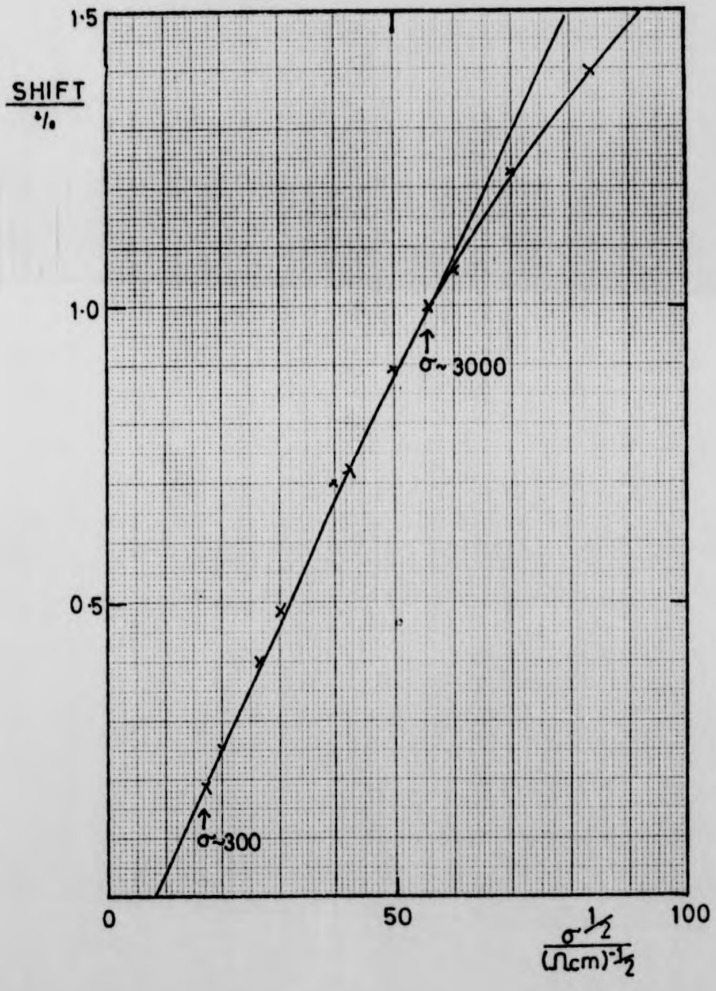

Fig. 5.11: The resonance shift versus (conductivity)$^{\frac{1}{2}}$ in liquid $Cs_y(Cs_3Sb)_{1-y}$ alloys at 1023 K with concentration as the implicit variable.

The reduction in the density of states is described by the Mott g-factor which is obtained from the ^{133}Cs resonance shift and plotted as a function of composition in Fig. 5.12. It is defined by

$$g = \frac{N(E_F)}{N(E_F)_{\substack{\text{Free}\\\text{elec}}}} = \frac{K_{expt} - \sigma_{chemical}}{K_{\substack{\text{Free}\\\text{elec.}}}}$$

Only for stoichiometric Cs_3Sb has the estimated chemical shift ($\sim$ room temperature shift) been subtracted from K_{expt} in evaluating g. Since the K, χ graph was linear over the range $0.2 < y < 0.8$ this implies that $\Omega < |\psi(0)|^2 >$ is constant and the variation in shift is due to a changing density of states. $K_{\substack{\text{Free}\\\text{elec}}}$ was plotted on Fig. 5.3 and was evaluated on the basis of the variation of the free electron concentration, including volume changes, as a function of composition. The resulting susceptibility is taken to be linearly proportional to the shift and normalised to the value for pure caesium. g is seen to fall rapidly from unity at pure caesium to reach the metal non-metal transition value of $^1/_3$ at $y_{Cs} \approx 0.4$. For comparison, the form of g deduced in a similar process from susceptibility data is also plotted as a dashed line (Freyland and Steinleitner 1976). Good agreement is observed although the shift derived values are always larger for any given concentration.

The rapid initial decrease of the ^{133}Cs shift with addition of antimony to caesium can be interpreted in terms of scattering of the conduction electrons by solute "impurity" atoms. This originates in the screening of excess charge in a metal such that long range electrical neutrality is satisfied. The resulting creation of bound impurity states and the occurence of ionicity in metals (host to impurity charge transfer) gives rise to several other experimentally observed effects for many

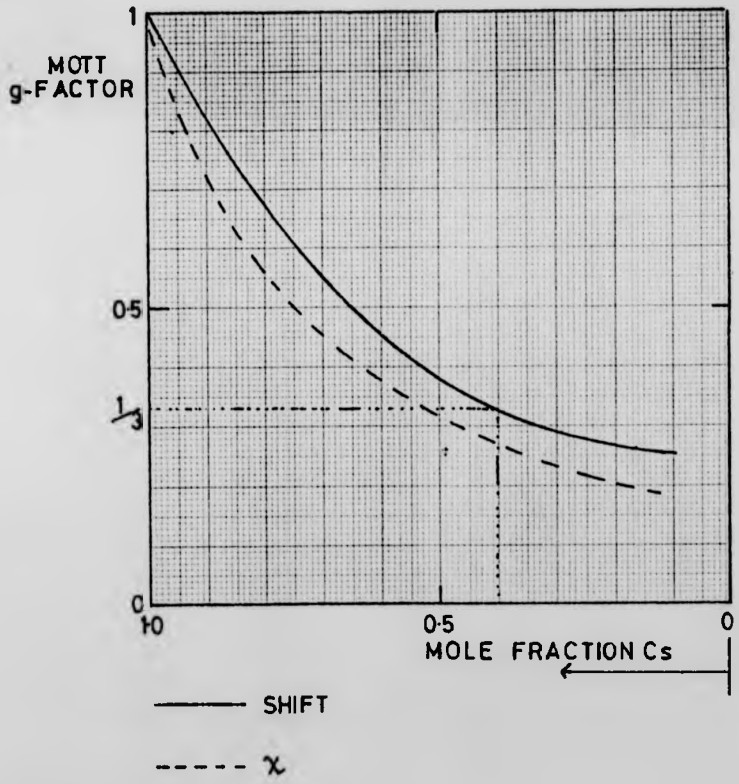

Fig. 5.12: The reduction in caesium density of states described by the Mott g-factor as a function of composition in Cs-Sb liquid alloys at 1023 K

alloy systems: residual resistance (Avci and Flynn 1979), giant diamagnetism (Flynn and Rigert 1973), resonance spin-flip conduction electron scattering (Ball 1973). The scattering amplitudes of the conduction electron partial waves are expressed in terms of phase shifts η_ℓ whose allowed values are controlled by the Friedel sum rule

$$\Delta Z = \frac{2}{\pi} \sum_{\ell=0}^{\infty} (2\ell+1)\eta_\ell \qquad (5.2)$$

where ΔZ is the charge difference between impurity and host.

ℓ is the angular momentum.

A partial wave is most strongly scattered when $\eta_\ell = (n + \frac{1}{2})\pi$, where n is an integer, and in terms of energy the scattering resonance is sharp and has been termed a virtual bound state. If the virtual bound level is close to the Fermi energy then the properties of an alloy can change dramatically with very small changes in electron concentration.

The zeroth order approach to dilute alloying is to simply determine the effect of charge redistribution on the Fermi averaged s-electron density at the nucleus and neglect the variation of susceptibility, but if a large degree of charge transfer occurs then a significant change in the host density of states will occur. Taking both contributions into account, the initial slope of the ^{133}Cs NMR shift as a function of antimony concentration, c, is given by

$$\frac{1}{c}\cdot\frac{\Delta K}{K} = \frac{1}{c}\,\frac{\Delta(\Omega\langle|\psi(0)|^2\rangle)}{\Omega\langle|\psi(0)|^2\rangle} + \frac{1}{c}\cdot\frac{\Delta\chi_p}{\chi_p} \qquad (5.3)$$

where the first term describes the charge redistribution and the second term the change in density of states. The expression for the first term of eqn. 5.3 in terms of phase shifts is given by Blandin and Daniel (1959) and the required structure coefficients tabulated by Thornton and Young (1968). The second term of eqn. 5.3 is given by Ball (1973). Recently Nieminen and

Puska (1980) have calculated these two effects for Ag row impurities in caesium on the basis of a "self consistent density-functional calculation within the spherical solid model developed by Almbladh and von Barth (1976)". For Sb in Cs the p-wave phase shift is nearly resonant, $\eta_1 \sim \pi/2$ and both contributions to ΔK are large and negative, being -1.25 for the charge redistribution and -2.09 for the density of states term. Thus

$$\frac{1}{c}\frac{\Delta K}{K} = -3.34$$

Hence for c = 0.1, the ^{133}Cs resonance shift is calculated to be 0.94% and this is seen to provide rather good agreement with the experimental value of 1.0% (Fig. 5.3).

For Sb (and Sn, Te) in Cs, Nieminen and Puska (1980) describe an incomplete resonance in the conduction band which reduces the ionicity. Addition of impurity diminishes the conduction electron density through charge transfer and weakens the electron screening. Eventually the 5p levels become bound below the conduction band, giving rise to non metallic properties. At high impurity contributions (Sb) the 5p and 5s levels hybridise to form a band and metallic properties are recovered.

5.5. Summary of the Caesium-Antimony system

NMR results have demonstrated the ability of antimony at dilute concentrations in liquid caesium to form molecular groups and remove states from the free electron conduction band. The resulting density of states at the Fermi level is strong reduced, giving rise to very small resonance shifts as the concentration approaches Cs_3Sb from pure caesium. In the sample closest to the stoichiometric composition Cs_3Sb, Korringa enhancement of $\sim$ 30 was observed in the liquid at 1023 K, but in contrast to CsAu no direct evidence of strong electron localisation was observed. The room temperature NMR shift of Cs_3Sb was 0.062%, which is

small compared to typical metallic shifts of 1% but nevertheless significantly greater than values obtained in caesium salts (Haase et al 1977) and also greater than the value found in CsAu, 0.036%. In Cs_3Sb quadrupolar splitting of the ^{133}Cs resonance line was observed indicating the presence of strong electric field gradients. In all concentrations studied neither antimony isotope was observable by NMR due to its very strong quadrupolar relaxation which created a spin lattice relaxation time of < 3 μs. The NMR data implies the presence of directed bonding and is further evidence for the contribution of a covalent aspect to the bonding of Cs_3Sb.

Other experimental data on the caesium-antimony system is relatively scarce, but conductivity, thermopower and magnetic susceptibility favour a covalent interpretation of the structure of stoichiometric Cs_3Sb and a predominantly electronic contribution to transport properties in the liquid. (See for example Freyland and Steinleitner 1977, Steinleitner 1978). The band gap of Cs_3Sb is 1.6 eV at room temperature indicating that this compound is less ionic than CsAu (RT ΔE = 2.2 eV). Theoretical considerations (Robertson 1979, 1980) however suggest that Cs_3Sb is a highly polar ionic compound, and that a band gap can form due to ionicity in the liquid if the system is ordered, even though cation-cation nearest neighbours are inevitable due to the 3:1 composition. It would seem that neither ionic bonding or covalent bonding is dominant in this system.

Away from stoichiometry different behaviour is to be expected for excess caesium and excess antimony in Cs_3Sb. The latter can bond covalently to itself (as in Mg-Sb, Robertson 1979) and therefore maintain a pseudogap in the density of states, but excess caesium will surely enter ionically. From our results, the electron enters the conduction band of Cs_3Sb and gradually the density of states increases.

Compared to related alloy systems, the caesium alloys appear to be relatively ionic. It would be of interest to investigate a less ionic system such as those based on the compounds Na_3Sb or Cs_3Bi, with a view to correlating ionicity and the compound forming characteristics especially in the region near stoichiometry. Since CsAu and Cs_3Sb appear to be on different sides of an ionic/covalent gap it would be especially interesting to study a compound with intermediate properties, but no obvious candidate is available.

CHAPTER SIX

THE SELENIUM-TELLURIUM SYSTEM

§6.1. Introduction

The phase diagram of the selenium-tellurium alloy system Se_xTe_{1-x} is presented in Fig. 6.1. (Hansen 1958). It is clear that the two elements form solid solutions at all concentrations and that no compounds are formed. The liquidus temperature is approximately linear between that of selenium, 493 K, and tellurium, 726 K. The electrical behaviour of the selenium-tellurium alloy system depends monotonically on composition, ranging from nearly metallic for pure tellurium to the insulating character of selenium. Electrical conductivity data (Perron 1967) presented in Fig. 6.2 for various tellurium rich alloys demonstrate semiconducting behaviour over a range of temperature controlled by the composition. The alloy composition $Se_{0.5}$ $Te_{0.5}$ was studied in this work with the intention of investigating the temperature promoted transition from non-metallic conductivities, $\sigma \leq 1\ \Omega^{-1}\ cm^{-1}$, to nearly metallic, $\sigma \geq 10^3\ \Omega^{-1}\ cm^{-1}$. Liquid $Se_{0.4}$ $Te_{0.6}$ was also studied since it is more conducting than liquid $Se_{0.5}$ $Te_{0.5}$ at all temperatures, and so attains metallic values of conductivity approximately 100 K lower. The high temperatures required to reach the metallic regime create an experimental limitation associated with the high vapour pressure of selenium alloys. (The boiling point of selenium at atmospheric pressure is 958 K). Frequently it was found that the quartz sample container had cracked after heating, but in this case the likely explanation is to be found in the volume increase on solidification.

Both ^{77}Se and ^{125}Te are amenable to NMR investigation, although the small γ of ^{77}Se and the low natural abundance (7.5%) of both nuclei ultimately restrict sensitivity. Both nuclei have spin ½, so all higher order multipole interactions are zero. ^{77}Se was studied at approximately

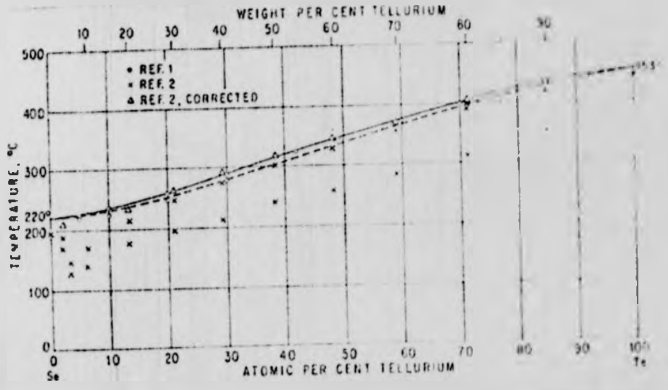

Fig. 6.1: Phase diagram of the selenium-tellurium system (Hansen 1958)

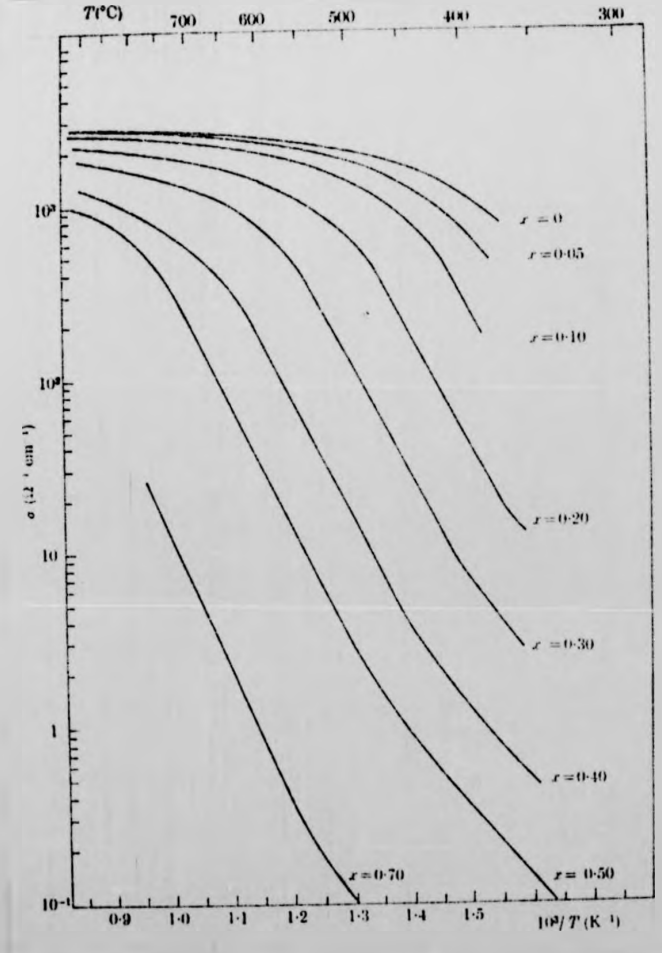

Fig. 6.2: Electrical conductivity of liquid Se_xTe_{1-x} alloys as a function of temperature (Perron 1967).

35 MHz and 59 MHz, and ^{125}Te at 59 MHz. NMR shifts and relaxation rates were measured for both ^{77}Se and ^{125}Te over a temperature range from the supercooled liquid to a maximum restricted by vanishing signal. Contributing to the loss of signal with increasing temperature were the increasing linewidth and the decreasing r.f. skin depth, δ, which drastically reduced the effective sample volume. Assuming effective r.f. penetration to a depth of $\sim 1.5\ \delta$ in a sample of diameter 10 mm, then at 59 MHz equation 3.4 gives

$\frac{\sigma}{\Omega^{-1}cm^{-1}}$	$\frac{\delta}{mm}$	Effective Sample Volume
1	6.55	100%
10	2.06	86%
100	0.66	36%
1000	0.21	12%

It was not found possible to follow the resonance into the truly metallic regime and the highest conductivity at which NMR was observed was $\sim 600\ \Omega^{-1}\ cm^{-1}$ (in the case of ^{77}Se in $Se_{0.4}\ Te_{0.6}$).

Resonance shifts increase with temperature and are defined by

$$\text{shift}_T = \frac{\nu_T - \nu_o}{\nu_o}$$

where ν_T = resonance frequency at temperature T

ν_o = resonance frequency in limit of low T.

Since chemical shifts are not strongly temperature dependent this approach gives directly the paramagnetic shift, which is created in these alloys by a thermally activated concentration of paramagnetic centres at dangling bonds. The time dependence of this interaction provides the major nuclear

relaxation mechanism as described by equations 2.36. The correlation time is sufficiently long at low temperatures that the spin-lattice relaxation time, T_1, is longer than the spin-spin relaxation time, T_2. As the temperature increases T_1 and T_2 become more equal until above $\sim$ 720 K the short correlation time limit is reached and $T_1 = T_2$. Because of the non-axial sample geometry, magnetic field inhomogeneity caused line broadening and for Se $T_2 \neq T_2^*$.

§6.2. NMR in Selenium-Tellurium Liquid Alloys

§6.2.1. $Se_{0.5}$ $Te_{0.5}$

Fig. 6.3 presents the experimental resonance shift of ^{77}Se in $Se_{0.5}$ $Te_{0.5}$ as a function of temperature. The data was obtained at static magnetic fields of 4.4116 T and 7.2036 T and both sets of shift agree well within experimental uncertainty. The corresponding relaxation data at the higher field are presented in Fig. 6.4. For completeness, spin-lattice relaxation times, T_1, obtained at the lower field are also plotted. It is noted in passing that within experimental error these are consistent with the frequency dependence expected for relaxation by localised paramagnetic centres (eqn. 2.36). Fig. 6.5 and Fig. 6.6 present the shift and relaxation data respectively for ^{125}Te in this alloy at 4.4116 T. The character of the data for both nuclei is similar but the tellurium shifts are larger and relaxation stronger, as expected from its larger atomic hyperfine field.

In liquid $Se_{0.5}$ $Te_{0.5}$ the resonance shift arises predominantly from the contact interaction between the nuclear magnetic moment and electronic spin magnetic moment density at the resonating nucleus. Magnetic susceptibility measurements (Gardner and Cutler 1979) have shown the presence of a temperature dependent concentration of paramagnetic centres in these alloys which give rise to an increasing paramagnetic susceptibility contribution with temperature. Since there is good reason to believe that Se-Te

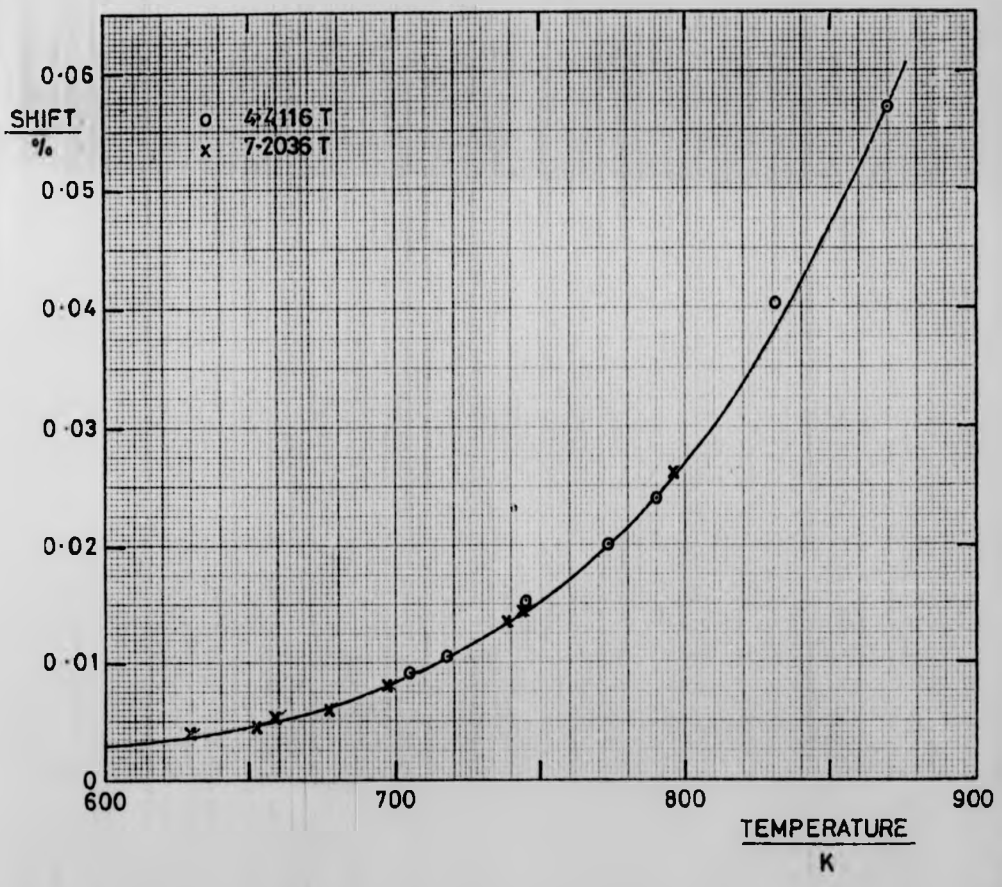

Fig. 6.3: $Se_{0.5}Te_{0.5}$. Temperature dependence of ^{77}Se resonance shift.

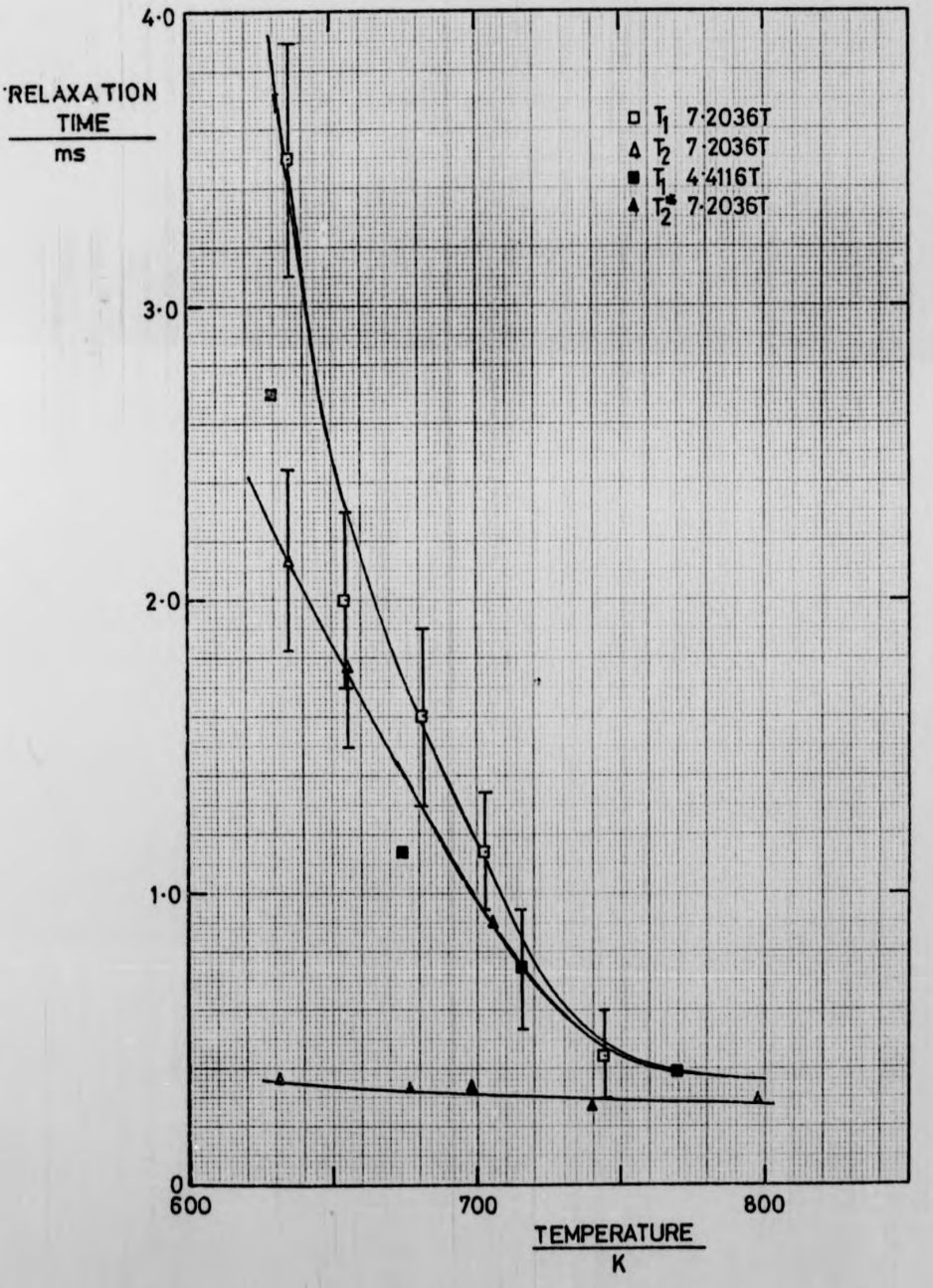

Fig. 6.4: $Se_{0.5}Te_{0.5}$. Temperature dependence of ^{77}Se relaxation times.

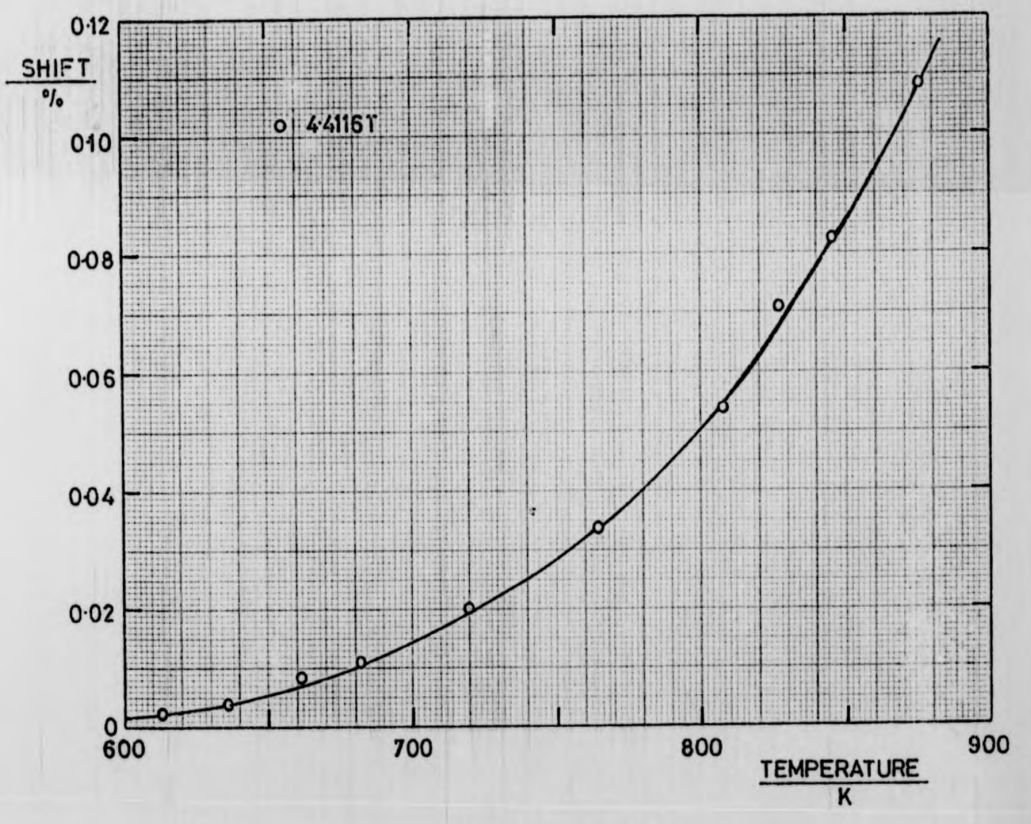

Fig. 6.5: $Se_{0.5}Te_{0.5}$. Temperature dependence of ^{125}Te resonance shift.

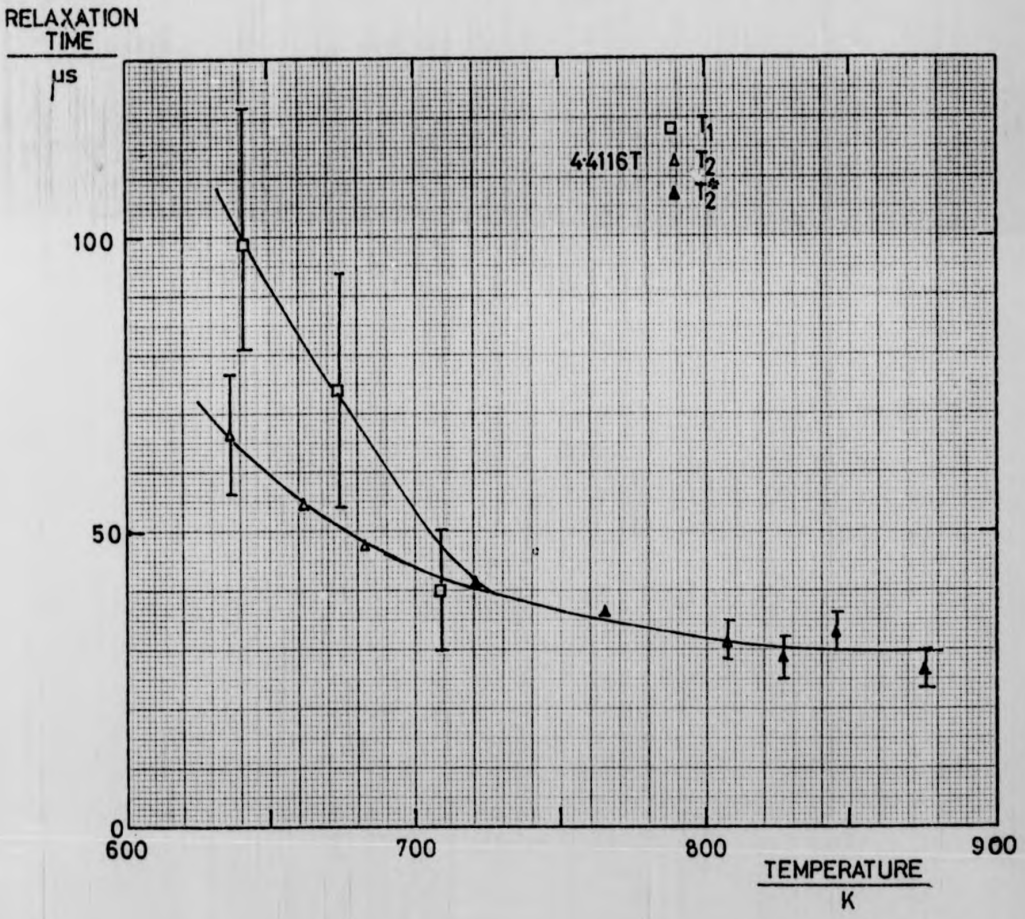

Fig. 6.6: $Se_{0.5}Te_{0.5}$. Temperature dependence of ^{125}Te relaxation times.

alloys are randomly bonded (Cutler 1977) it is assumed that such paramagnetic centres are randomly distributed over selenium and tellurium atoms. However, although the centre is strongly localised, the rapid diffusion of the nuclei and short lifetime of the centre cause the interaction to be averaged over all sites within a time less than the NMR Larmor period. Hence the shift is described by equation 2.30.

$$\frac{\Delta B}{B} = \frac{\mu_o}{2\pi} c \bar{A} \left|\frac{\gamma_e}{\gamma_n}\right| \frac{S(S+1)}{3kT}$$

where $\bar{A} = zA$ as defined in equation 2.30.

Equivalently, writing the Curie-type susceptibility as χ_p

$$\frac{\Delta B}{B} = \frac{\mu_o \bar{A} \chi_p}{2\pi N_A \gamma_e \gamma_n h^2}$$

Fig. 6.7 shows the graph of shift versus susceptibility using the susceptibility values reported for the Se-Te system by Gardner and Cutler (1979). The gradient yields the mean hyperfine coupling constant per paramagnetic centre, $\bar{A}$. We find:

For ^{77}Se, $\bar{A} = (4.8 \pm 0.5) \times 10^{-25}$ J or in frequency units 726 MHz.

For ^{125}Te, $\bar{A} = (1.45 \pm 0.05) \times 10^{-24}$ J or 2187 MHz.

As expected the heavier tellurium atom has a larger hyperfine coupling energy. The fitted curve to the resonance shift of Fig. 6.3 and 6.5 are calculated from these values of coupling constant.

Using these values of hyperfine coupling constant in the expression for the temperature dependence of resonance shift (equation 2.30) the molar concentration of paramagnetic centres, C, is obtained as a function of temperature. This is shown by Gardner and Cutler (1979) to be of the form

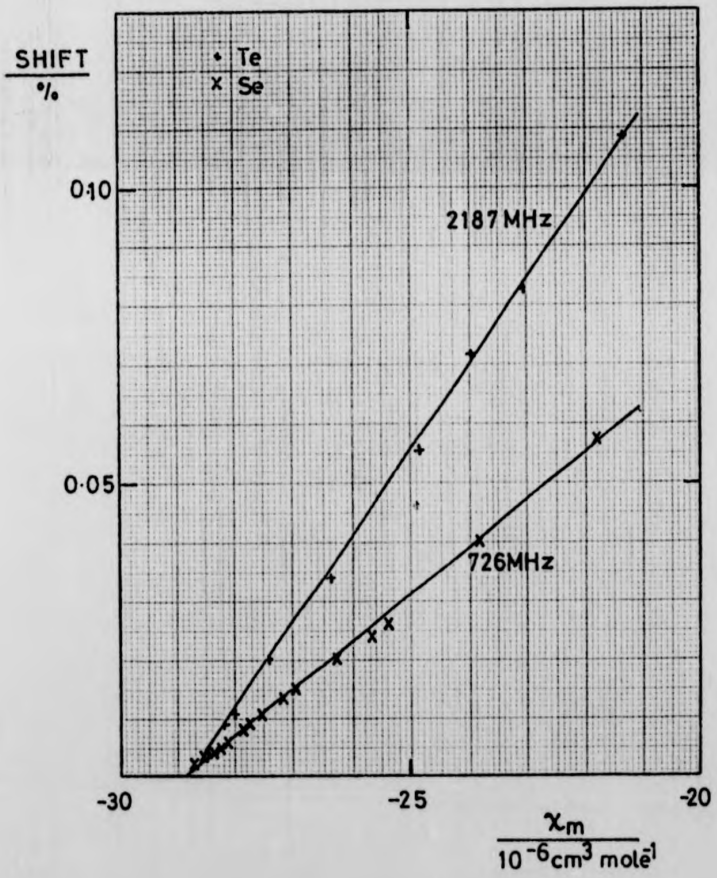

Fig. 6.7: $Se_{0.5}Te_{0.5}$. NMR shift versus magnetic susceptibility for both ^{77}Se and ^{125}Te .

$$c \propto \exp\left(\frac{F}{kT}\right) = \exp\left(\frac{S_o}{k}\right).\exp\left(\frac{E}{kT}\right)$$

where S_o is the concentration dependent entropy associated with bond breaking.

E is the concentration independent activation energy.

The 'zero' of paramagnetic resonance shift is chosen in order that the plot is linear on a log c versus $^1/_T$ graph. This requires the assumption of a small paramagnetic value for the shift ν_o, (defined in §6.1) of typically 0.003% corresponding to a molar concentration of centres of the order of 5×10^{-4} at the lowest temperatures studied. Using the density data of Thurn and Ruska (1976) this yields a number density of centres $\sim 1.3 \times 10^{19}$ cm^{-3} at 625 K. Fig. 6.8 presents the concentration of centres deduced as a function of reciprocal temperature and they are seen to agree well with those obtained from susceptibility measurements. The small deviation from linearity apparent at low temperature is within the experimental uncertainty of small resonance shift measurements. The flattening of the shift versus temperature graph at low temperatures reflects primarily the small fractional change of c with temperature, and solidification of the melt prevents access to the very gradually decreasing shift at even lower temperatures. A further factor which may complicate determination of paramagnetic shifts is the difficulty of accurately separating diamagnetic contributions to the observed shift.

Whilst generally it is a good approximation to assume temperature independence of chemical shifts, this may not be true in this system since bonding configurations are thought to be temperature dependent, (see for example Thurn and Ruska 1976, Cutler 1977). A particularly relevant example is found in the study of pure selenium (Warren and Dupree 1980) where the marked non-linearity of the shift (K) versus susceptibility (χ) graph enabled low temperature chemical shifts to be determined. The change in chemical shift was linked with a possible structural transformation in

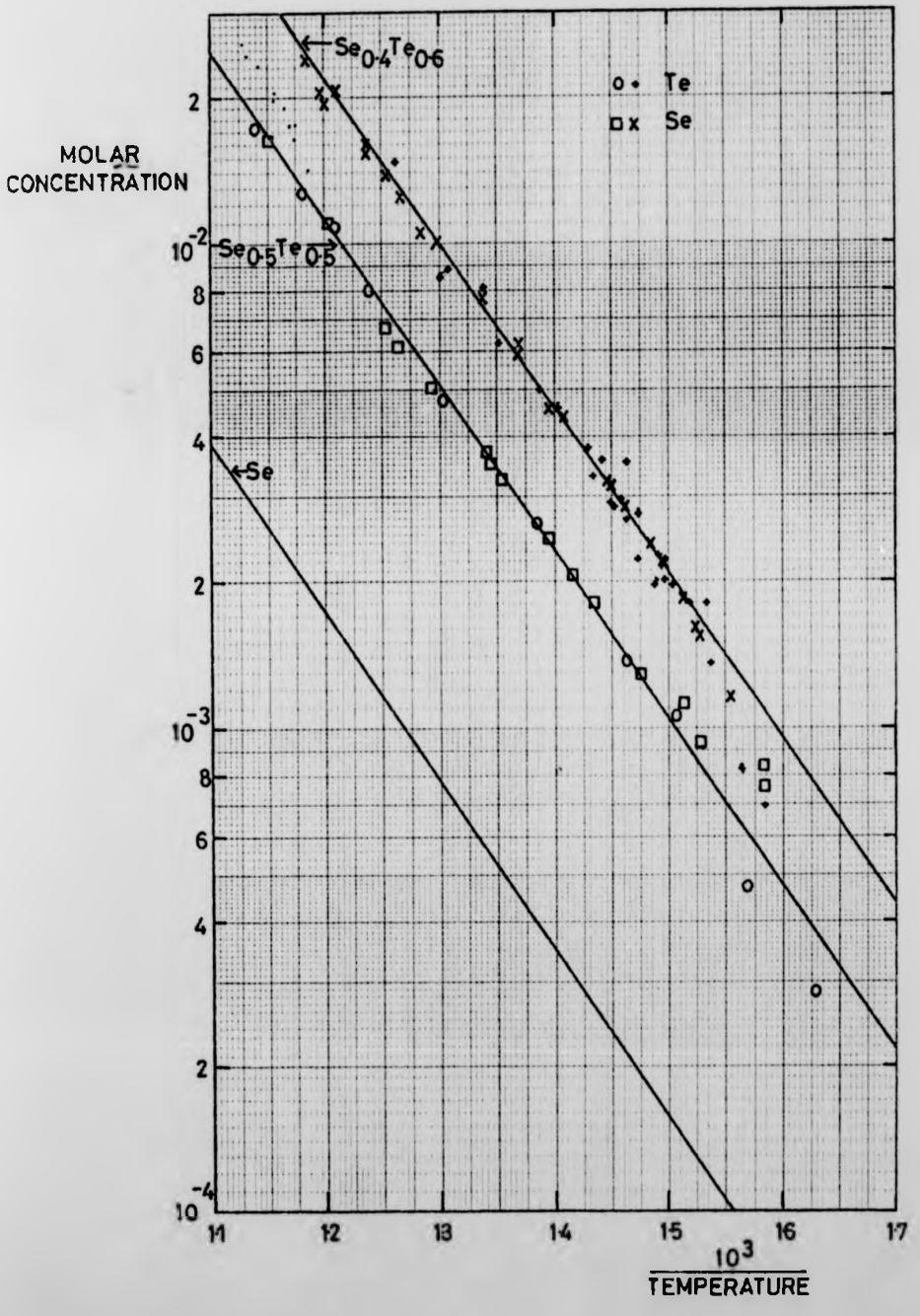

Fig. 6.8: Molar concentration of paramagnetic centres in liquid Se_xTe_{1-x} alloys as a function of temperature. Values obtained in this work (data points) are compared with those obtained from magnetic susceptibility (solid lines) (Gardner and Cutler, 1979).

which the Se_8 ring concentration decreases in favour of chain polymer molecules. In this work however the K, χ graphs are linear within the limits of experimental uncertainty at low temperatures, implying that such dramatic structural changes do not occur.

The electronic centres also provide the dominant relaxation mechanism, described by equations 2.36 provided that the correlation time is short enough that a nucleus cannot relax completely during a single encounter with a centre (Richards 1978).

$$\frac{1}{T_1} = \frac{2}{3} S(S+1)\, c\, \frac{\overline{A^2}}{h^2} \left[\frac{\tau}{1 + (\omega_s - \omega_I)^2 \tau^2} \right]$$

$$\frac{1}{T_2} = \frac{1}{3} S(S+1)\, c\, \frac{\overline{A^2}}{h^2} \left[\tau + \frac{\tau}{1 + (\omega_s - \omega_I)^2 \tau^2} \right]$$

The inequality of T_1 and T_2 is rather unusual for a liquid conductor and indicates a correlation time for the interaction of the nucleus with its surroundings such that $\tau \geq \omega_s^{-1}$, where ω_s is the electron resonance frequency. Values of the correlation time τ are directly obtained from the experimental spin-lattice and spin-spin relaxation times by means of equation 2.37. These are plotted in Fig. 6.9 where it is observed that $\tau > 10^{-12}$ s at the lowest temperature studied, and the fluctuating field correlation time at the tellurium nucleus exceeds that at the selenium site. At 650 K, $\tau_{Te} = (1.3 \pm 0.2)$ ps and $\tau_{se} = (0.7 \pm 0.2)$ ps. Making use of the c and τ values already derived, the spin-lattice relaxation time then enables an estimate of the mean squared hyperfine coupling energy, $\overline{A^2}$, to be made. Alternatively, by forming the product of the experimental parameters K and T_1, the concentration c is eliminated and $\overline{A^2}$ is given in terms of τ and $\overline{A}$

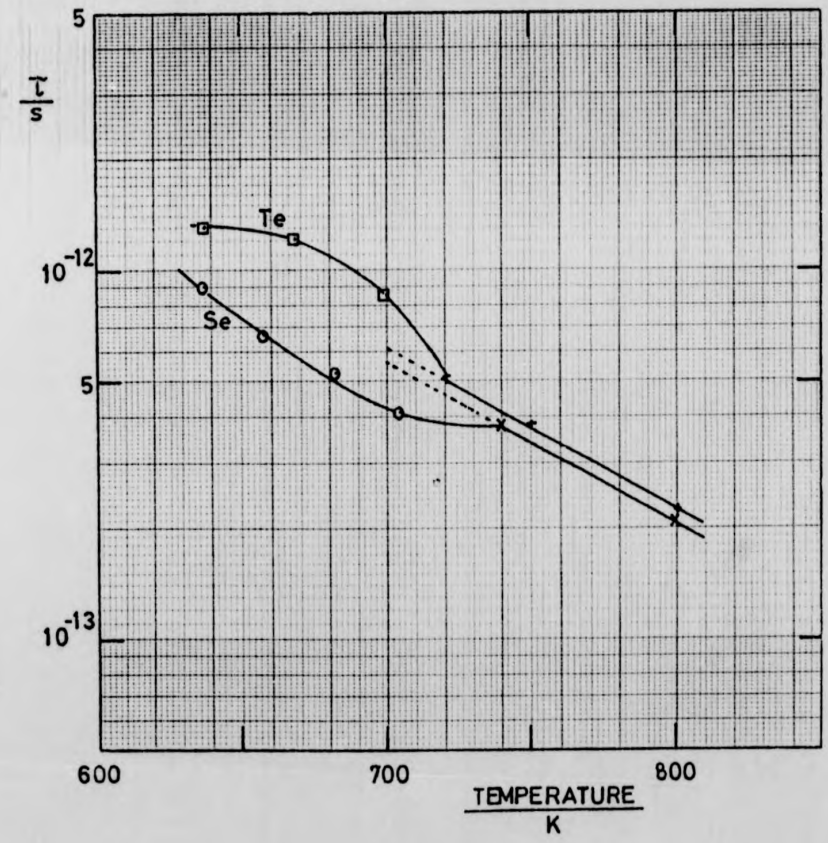

Fig. 6.9: The correlation time of the hyperfine field experienced by ^{77}Se and ^{125}Te in liquid $Se_{0.5}Te_{0.5}$ as a function of temperature.

$$\overline{A^2} = \frac{\gamma_e}{\gamma_n}\frac{h^2}{2k}\left(\frac{1+\omega^2\tau^2}{\tau}\right)\frac{\overline{A}}{KT_1T}$$

Defining $(\overline{A^2})^{\frac{1}{2}} = A_{r.m.s.}$ we find:

For ^{77}Se: $A_{r.m.s.} = (1.63 \pm 0.04) \times 10^{-25}$ J, $\frac{A_{r.m.s.}}{\overline{A}} = 0.34 \pm 0.05$

For ^{125}Te: $A_{r.m.s.} = (6.4 \pm 0.5) \times 10^{-25}$ J, $\frac{A_{r.m.s.}}{\overline{A}} = 0.44 \pm 0.04$

These values are temperature independent within experimental uncertainty. Assuming the constancy of the ratio $A_{r.m.s.}/\overline{A}$ into the motionally narrowed regime an estimate of the hyperfine correlation time is obtained, and this is also plotted on Fig. 6.9. Within the range of temperature measured τ falls to $\sim 10^{-13}$ s (at > 850 K). Within experimental uncertainty τ_{Te} is approximately equal to τ_{Se} in the motionally narrowed regime, although at lower temperatures the similar values of τ for each nucleus are just distinguishable with $\tau_{Te} > \tau_{Se}$. There exist several possibilities as to the mechanism responsible for the time τ. Motional or rotational correlation times in this polymeric liquid are unlikely to give rise to such short values. Electron spin relaxation times (obtainable from electron spin resonance experiments) are not available for this alloy and cannot be excluded a priori, but the required correlation time is likely to be the shorter of the residence time of an electron at a particular nucleus (or "chain-end-lifetime"), and the electron spin fluctuation time. Increasing concentration of electronic centres resulting from broken bonds and shorter chains would lead to the observed decrease of τ with increasing temperature if the electron-electron exchange fluctuation time is responsible, and this is considered to be the more probable explanation, (as was thought to be the case for pure selenium).

§6.2.2. $Se_{0.4}\ Te_{0.6}$

A similar analysis to that for $Se_{0.5}\ Te_{0.5}$ in §6.2.1. is employed for the liquid alloy $Se_{0.4}\ Te_{0.6}$. The resonance shift and relaxation data are shown in the following figures:

Fig. 6.10: ^{77}Se shift at 7.2036 T as a function of temperature.

Fig. 6.11: corresponding ^{77}Se relaxation times.

Fig. 6.12: ^{125}Te shift at 4.4089 T as a function of temperature.

Fig. 6.13: corresponding ^{125}Te relaxation times.

For comparison the shift graphs also show the shift observed in the $Se_{0.5}\ Te_{0.5}$ liquid alloy. It is apparent that both ^{77}Se and ^{125}Te show increased shifts in $Se_{0.4}\ Te_{0.6}$ compared to $Se_{0.5}Te_{0.5}$ at the same temperature. The mean hyperfine coupling constants obtained from the shift versus susceptibility graph, Fig. 6.14, are

For ^{125}Te: $\bar{A} = (1.43 \pm 0.05) \times 10^{-24}$ J, $\bar{A}/h = 2158$ MHz.

For ^{77}Se: $T \leq 836$ K $\bar{A} = (3.66 \pm 0.3) \times 10^{-25}$ J, $\bar{A}/h = 552$ MHz.

$T \geq 836$ K $\bar{A} = (5.60 \pm 0.5) \times 10^{-25}$ J, $\bar{A}/h = 845$ MHz.

The value of $\bar{A}$ for tellurium in $Se_{0.4}\ Te_{0.6}$ is the same as that found in $Se_{0.5}\ Te_{0.5}$ within experimental uncertainty, but the selenium K, χ graph shows a different slope at low and high shifts (corresponding to low and high temperatures). Although a continuously changing slope cannot be entirely discounted, two straight lines are drawn with a change at $\sim$ 836 K. The molar concentration of free spins (deduced as before) for this alloy is presented in Fig. 6.8 and the correlation times in Fig. 6.15. Relaxation data for ^{125}Te in this alloy were restricted by experimental difficulty to measurement of T_2^* and T_1. The values of T_2 required for correlation time calculations were therefore obtained by correcting the free induction decay time T_2^* by a constant magnetic field inhomogeneity contribution calculated from observation of the selenium resonance in this alloy, and both nuclei in $Se_{0.5}\ Te_{0.5}$. A comparative discussion of the nuclear magnetic

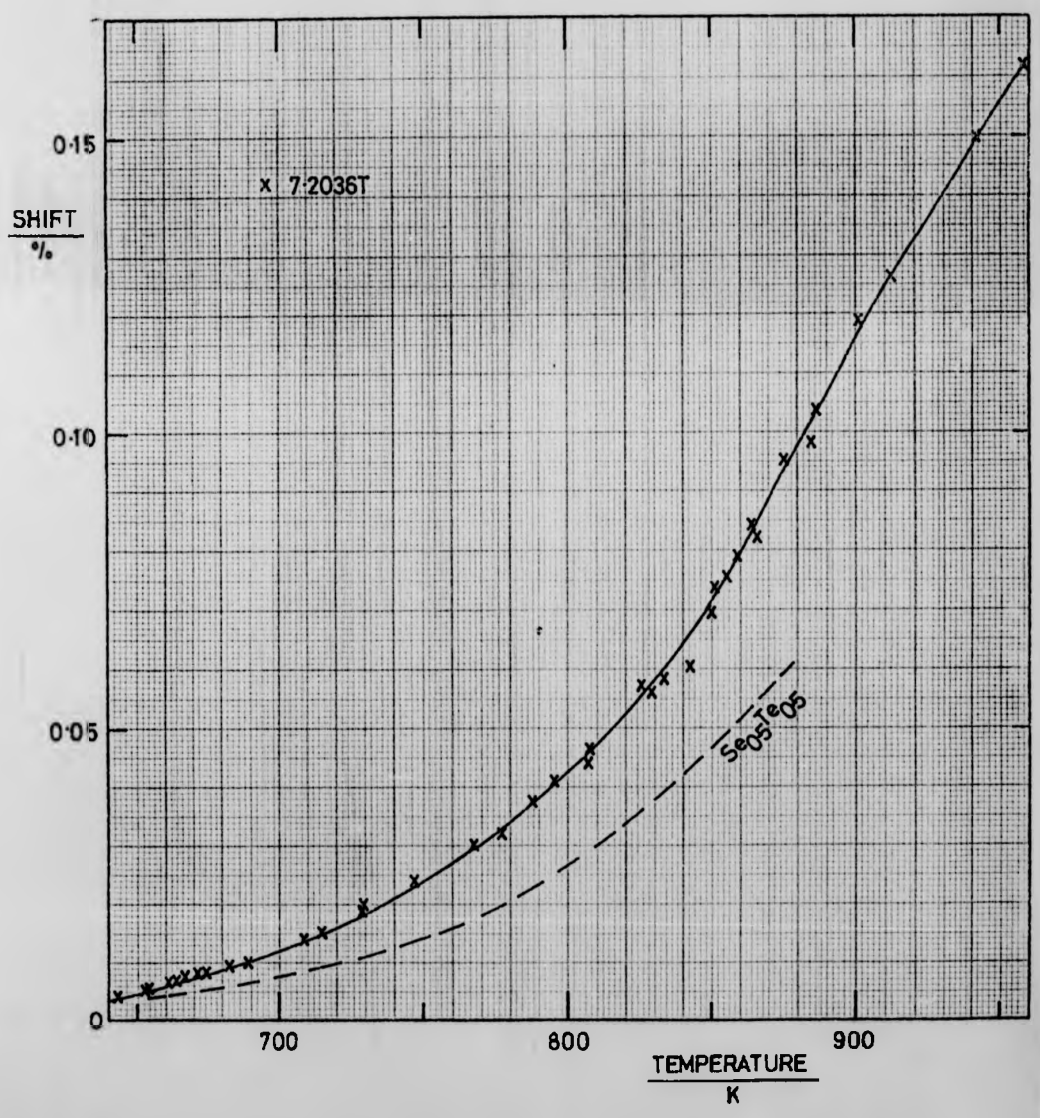

Fig. 6.10: $Se_{0.4}Te_{0.6}$. Temperature dependence of ^{77}Se resonance shift.

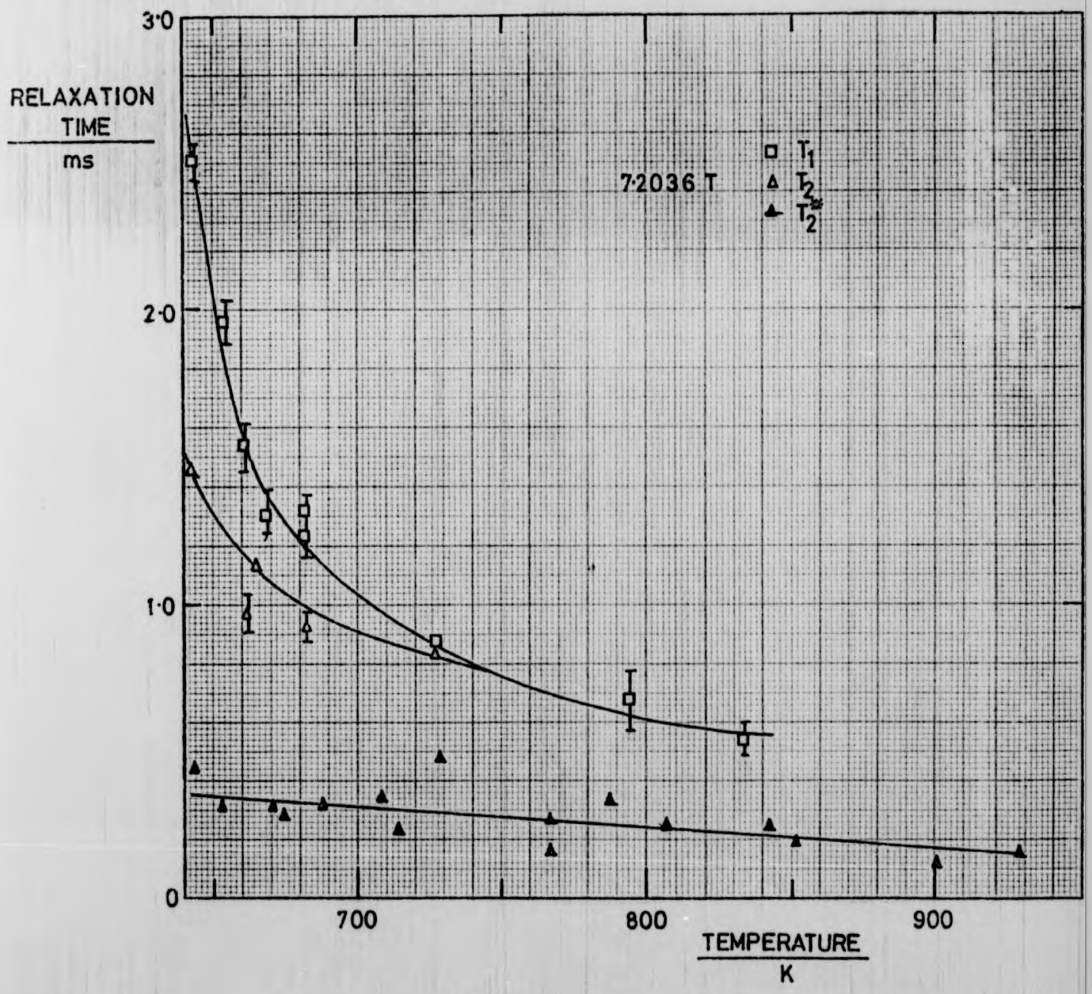

Fig. 6.11: $Se_{0.4}Te_{0.6}$. Temperature dependence of ^{77}Se relaxation times.

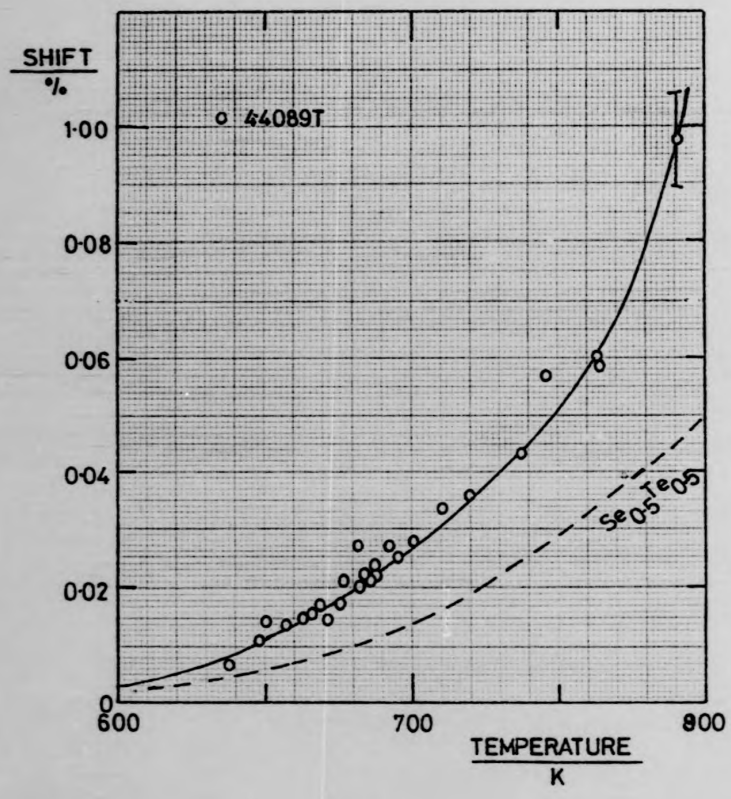

Fig. 6.12: $Se_{0.4}Te_{0.6}$. Temperature dependence of ^{125}Te resonance shift.

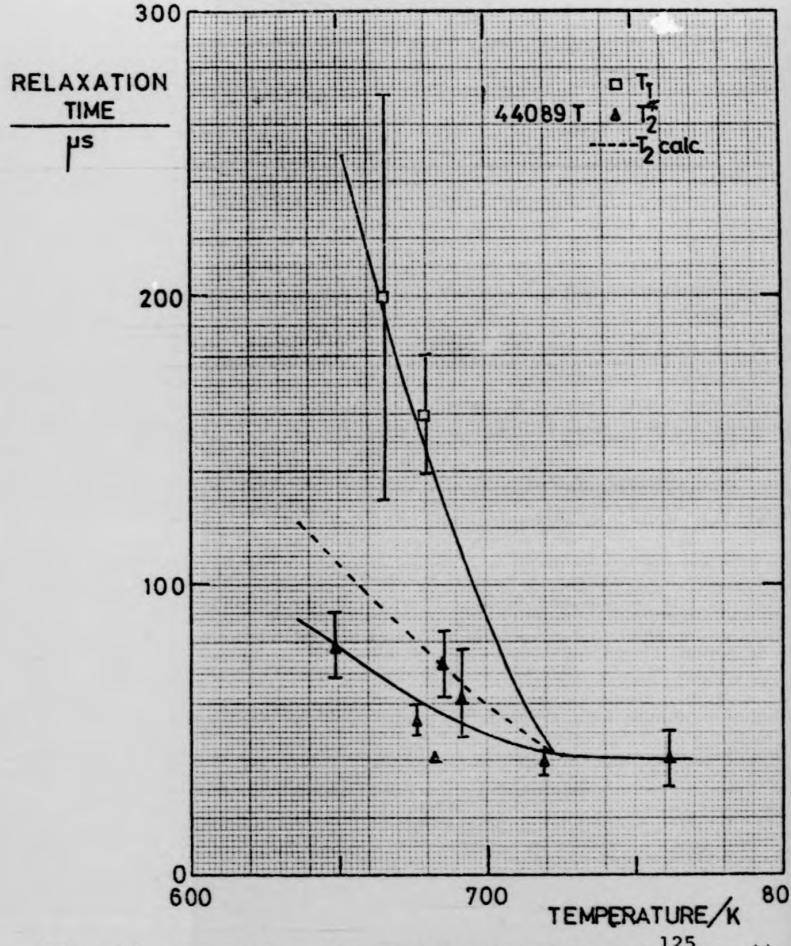

Fig. 6.13: $Se_{0.4}Te_{0.6}$. Temperature dependence of ^{125}Te relaxation times.

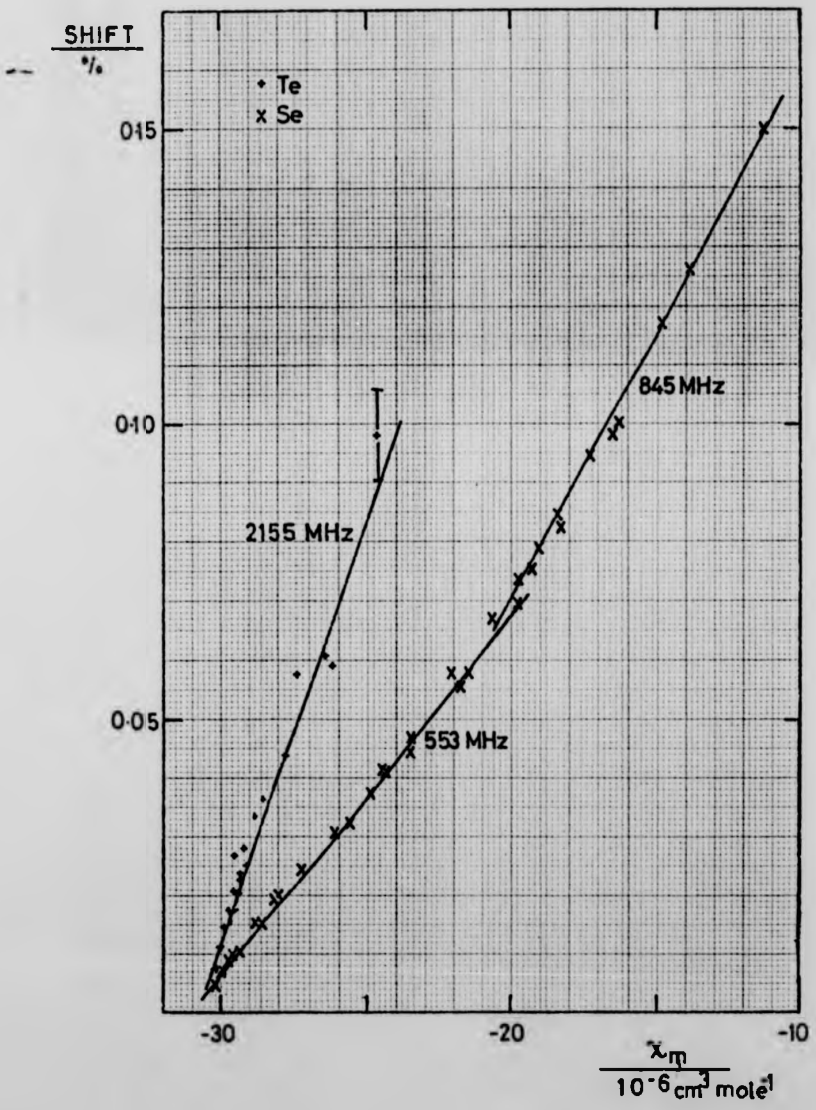

Fig. 6.14: $Se_{0.4}Te_{0.6}$. NMR shift versus magnetic susceptibility for both ^{77}Se and ^{125}Te.

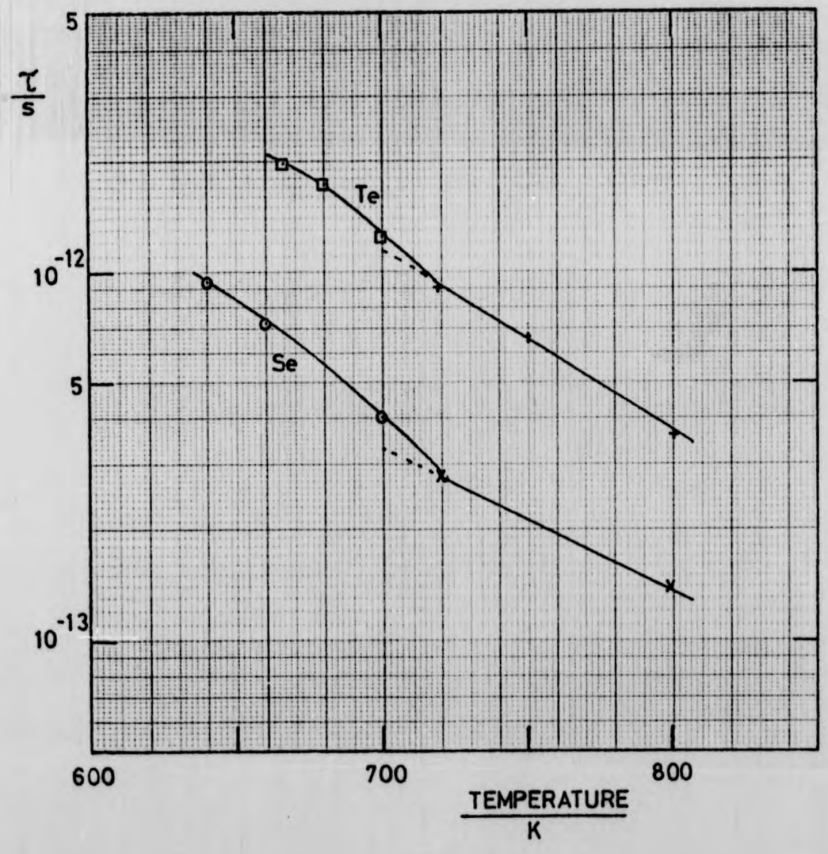

Fig. 6.15: The correlation time of the hyperfine field experienced by ^{77}Se and ^{125}Te in liquid $Se_{0.4}Te_{0.6}$ as a function of temperature.

resonance results for both alloy compositions, together with other measurements on $Se_x Te_{1-x}$ alloys, is now presented.

§6.3. Relation to Other Properties

In view of the smooth variation with composition displayed by the phase diagram one might expect $Se_x Te_{1-x}$ alloy properties to be intermediate between the two elemental extremes. It is therefore worthwhile briefly noting the characteristics of liquid selenium and tellurium with a view to interpretation of the NMR data of the liquid alloys presented in §6.2. The topic is fully covered in the recent text of Gerlach and Grosse (1979).

Liquid selenium has a predominantly chainlike structure consisting of 2-fold bonded atoms, and possibly a fraction of 8 membered rings as found in sulphur. Near the melting point there are $\sim 10^5$ atoms per chain, and increasing temperature decreases the chain length, although the coordination number remains constant. The bond equilibrium theory based on Eisenberg and Tobolsky (1960) and Gee (1952) is generally accepted, in which an equilibrium constant with activation energy E_d describes the dangling bond concentration. The intrinsic electrical behaviour is more nearly insulating than semiconducting. Below about 1000 K the electronic properties are controlled by impurities, in particular oxygen, but the activated bond-breaking process generates holes. Near the melting point a temperature independent diamagnetism is observed (Busch and Vogt 1957, Gardner and Cutler 1979) in spite of the expected presence of paramagnetic broken bonds. The explanation is to be found in the suggestion of Anderson (1975) that an effective negative electron-electron correlation energy creates diamagnetic charged defect states from the paramagnetic neutral dangling bonds. The process may be summarised as

$$2D_3^o \rightleftharpoons D_3^+ + D_1^-$$

where D_y^x represents a defect state of charge x and coordination number y. Neutral states such as D_1^o and D_3^o are therefore excited states and are thermally generated (Steet and Mott 1975, Kastner et al 1976). Fig. 6.16 indicates schematically a chalcogen chain showing the branching nature of a D_3^+ defect and the chain-terminating nature of the D_1^- defect. A neutral dangling bond is also shown. The influence of temperature and pressure on pure liquid selenium NMR has been studied by Warren and Dupree (1980).

Liquid tellurium on the other hand is almost describable in nearly free electron terms. It is a poor metal at the melting point and becomes a better metal as heated due to a temperature dependent density of states at the Fermi energy. The NMR study of Warren (1972) indicates that a diffusive model for electronic transport is applicable below $\sim$ 900 K. The neutron diffraction experiments of Tourand and Breuil (1970), and Tourand et al (1972), have shown that the nearest neighbour coordination number of liquid tellurium rises to $\sim$ 6 at 1973 K. In their discussion of the properties of liquid tellurium, Cabane and Friedel (1971) suggested a decrease of coordination number, z, from the observed value of 3 at 873 K towards 2 at the melting poing as the structural basis for the electronic properties. However Tourand (1975) has shown that z remains near to 3 down to 673 K. Cutler (1977) has suggested that a bonding resonance occurs within the low temperature liquid, comprised of an equal number of instantaneously three-fold bonded, 3F, and one fold bonded, 1F, atoms. On the basis of an independent band model in which the liquid at higher temperatures consists of cross-linked chains of various lengths terminated in dangling bonds, Cutler (1977) suggests that the number of 3F atoms is less than the number of 1F (dangling bond) atoms. The excess increases with temperature and is responsible for electrical conduction. A third bond is stable in the presence of dangling bonds since the extra electron can enter an empty state in the valence band rather than the

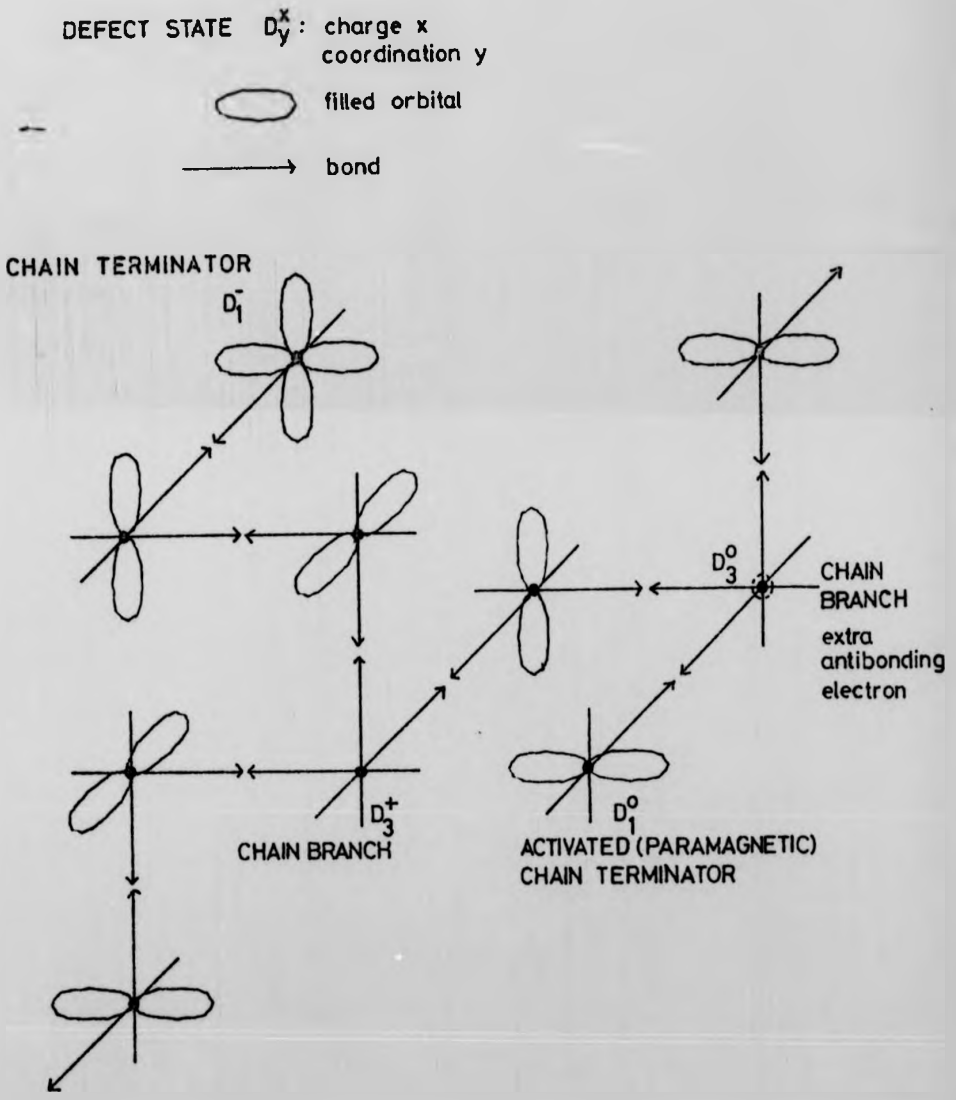

Fig. 6.16: Schematic representation of a chalcogen polymer chain showing the different defect states which form by changing the local bonding configuration.

energetically unstable antibonding levels. Note that dangling bond interactions are generally neglected in bonding models.

The selenium-tellurium liquid alloy system has been extensively studied: Perron (1967) measured thermoelectric properties, which have been extended to high temperature and pressure by Yao et al (1980a), Ioffe and Regel (1960) viscosity; Thurn and Ruska (1976) density; Gardner and Cutler (1979) susceptibility; Yao et al (1980b) compressibility; Seymour and Brown (1973) NMR. In the latter work a concentration dependence of resonance shift in Se_xTe_{1-x} liquid alloys was presented in the limited temperature range of 450°C-500°C. For $x > 0.3$ no temperature dependence of shift was observed, and the data interpreted in terms of interaction with localised electron spins at chain ends.

Structurally, the average coordination number ~ 2 in selenium-rich alloys independent of composition, but increases with tellurium content in tellurium-rich alloys. (Hoyer et al (1975)). Semiconducting electrical behaviour is observed in Se_xTe_{1-x} up to a maximum temperature which increases with selenium content. In the limit of high temperature and pressure nearly metallic conductivities are achieved. It is generally observed that the influence of increasing temperature and of increasing tellurium content are qualitatively similar. This reflects the preference of selenium for loosely packed atoms (2F) and that of tellurium for a more highly coordinated structure. The anomalous increase in density with temperature is strong evidence for increasing coordination, and supports the structural transformation model for the metal-nonmetal transition in these alloys. The recently reported compressibility maxima as a function of temperature and concentration imply that there exists large density fluctuations near the transition region due possibly to the coexistence of various types of bond configuration in the melt.

The (small) electronegativity difference between selenium and tellurium

$$\Delta X = X_{Se} - X_{Te} = 0.3 \qquad \text{(Pauling)}$$

suggests that the Se-Te bond is to be preferred, and therefore mixed bonding will occur in the long disordered chains. Mössbauer studies (Boolchand and Suranyi 1973) have shown that in amorphous Se_xTe_{1-x}, the bond energy of Se-Te is ≥ 0.07 eV greater than the average of Se-Se and Te-Te, and therefore the alloy will consist of as many Se-Te bonds as possible. It is reasonable to suggest therefore that a change in Se_xTe_{1-x} properties will occur when $x < 0.5$ since only then can the weakest Te-Te bonds form. As tellurium is added to selenium it is thought that the proportion of 3F atoms increases and hence there is a transition towards metallic properties. In terms of band structure, the electron band is an acceptor band which is entirely absorbed into the valence band in the metallic range. Fig. 6.17 shows a possible band structure model for Se-Te alloy at different conductivities. Cutler (1977) presents a discussion of the electrical properties in these alloys.

Table 6.1 summarises the hyperfine field and correlation time data obtained in this work in the alloys $Se_{0.5}Te_{0.5}$ and $Se_{0.4}Te_{0.6}$ and compares them with the values obtained in the pure liquid elements at the same temperature (Se: Warren and Dupree 1980, Te: Warren 1972)

The amplitude of the hyperfine coupling constant for selenium in the alloys is increased over its value in the pure element, but it is still much less than the free spin value for 4s electrons (Bennett et al 1971). Hence the s-p ratio at the selenium site is larger in the alloy but in both cases predominantly p character is present. The well-defined increase in the value of $\bar{A}$ for Se in the $Se_{0.4}Te_{0.6}$ alloy occurs in the neighbourhood of 836 K. This is within ∿ 20 K of the approximately coincident compressibility and molar volume maxima observed in this alloy and the conductivity at this temperature is ∿ 90 Ω^{-1} cm^{-1}. The likely interpretation of this effect is a structural transition from a selenium-like to tellurium-like liquid.

a) LOW TEMP.
b) HIGH TEMP.
Upper band is conduction band.

c)-f)
Growth with increasing temperature of an acceptor band.

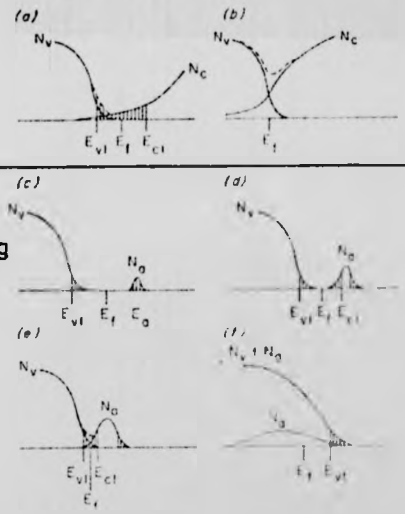

Fig. 6.17: Overlapping band models for Se-Te alloys (Cutler, 1977). Hatching indicates possible regions of localised states: E_v and E_c being the mobility edges for holes and electrons respectively.

Se_xTe_{1-x}	^{77}Se			^{125}Te		
x	$\bar{A}$ (J)	$\frac{A_{rms}}{\bar{A}}$	τ(S) @ 650 K	$\bar{A}$ (J)	$\frac{A_{rms}}{\bar{A}}$	τ(S) @ 650 K
0	-	-	-	(1.07 ±) x 10^{-24}	0.37	2 x 10^{-16}
0.40	T ≤ 836 K (3.7 ± 0.3) x 10^{-25}	0.46 ± 0.05	0.85 x 10^{-12}	(1.43 ± 0.05) x 10^{-24}	0.22	2.3 x 10^{-12}
	T ≥ 836 K (5.6 ± 0.5) x 10^{-25}					
0.50	(4.8 ± 0.5) x 10^{-25}	0.34 ± 0.05	0.7 ± 0.2 x 10^{-12}	(1.45 ± 0.05) x 10^{-24}	0.44 ± 0.04	(1.3 ± 0.2) x 10^{-12}
1.00	2.87 x 10^{-25}	0.59	8 x 10^{-12}	-	-	-

Table 6.1

The density data shows a volume minimum approximately 200 K higher and thereafter shows a slope similar to that observed in pure tellurium. Thus the structural transition occurs over a wide range of temperature, in the middle of which the conductivity data starts to be no longer activated ($\geq 400\ \Omega^{-1}\ cm^{-1}$) and eventually saturates. The maximum temperature at which resonance data was obtained in this work corresponds to $\sigma \approx 600\ \Omega^{-1}\ cm^{-1}$. A plot of resonance shift against $\sigma^{\frac{1}{4}}$ is presented in Fig. 6.18. The ^{77}Se data in $Se_{0.4}Te_{0.6}$ is linear over a range of conductivity from approximately $20\ \Omega^{-1}\ cm^{-1}$ to $500\ \Omega^{-1}\ cm^{-1}$. These limits are rather lower than generally considered for the diffusive transport regime, where linearity of this plot is predicted, but this may be characteristic of liquids where the number of carriers at the mobility edge is small (Mott and Davis, 1979). These authors observe that the extrapolation of log σ versus $^{1}/T$ for Se-Te without assuming ambipolar conduction gives a similar low value of $\sigma_o \sim 10\ \Omega^{-1}\ cm^{-1}$. The upper limit, which reflects the transition to NFE behaviour, occurs when $k_F\lambda \sim 1$, where k_F is the fermi wavevector and λ is the electronic mean free path. Using the density data together with the concentration of centres deduced in this work we find $k_F \sim 3.5 \times 10^7\ cm^{-1}$, and from equation 1.6

$$\sigma = \frac{S_F e^2 \lambda}{12\pi^3 h}$$

we obtain $\sigma = 900\ \Omega^{-1}\ cm^{-1}$.

The tellurium hyperfine coupling energy is also increased in the alloys over its value in the pure element and both alloys investigated give the same value of $\bar{A}_{Te}$. It was not possible to follow the tellurium resonance shift to sufficiently high temperatures to observe any structural transition.

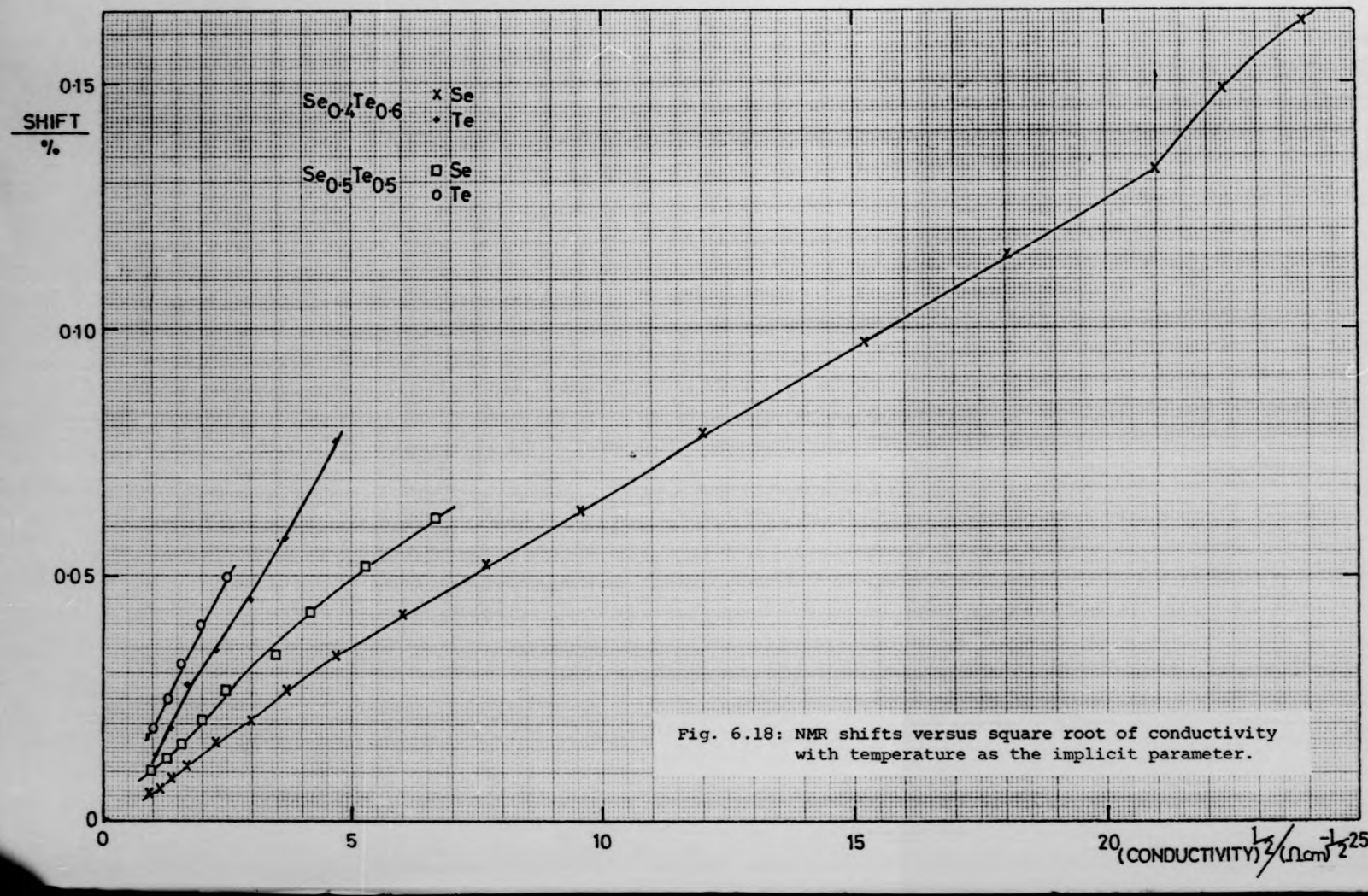

Fig. 6.18: NMR shifts versus square root of conductivity with temperature as the implicit parameter.

The similarity of the ratio $A_{rms}/\bar{A}$ for both nuclei in $Se_{0.5}Te_{0.5}$ implies that the nature of the electronic centre at a tellurium site is similar to that at a selenium site. Further the fractional value < 1 implies that more than one nucleus experiences the hyperfine field created by the centre. If z nuclei experience the local field we have $z^{\frac{1}{2}} A_{rms} = \bar{A}$ and for example z = 6 for $A_{rms}/\bar{A} = 0.41$. Some contribution to the hyperfine field may therefore be postualted as being due to the presence of relatively delocalised dangling bonds: for example threefold coordinated neutral defects D_3^o have no more than 0.15 of their amplitude at any one atom (Vanderbilt and Joannopolous 1979). However, as in the study of selenium (Warren and Dupree 1980), the magnitude of $\bar{A}$ suggests that the major hyperfine interaction occurs at the nucleus of the chain-end-atom due to the D_1^o defect localised there.

The value of $A_{rms}/\bar{A}$ for Te in the $Se_{0.4}Te_{0.6}$ alloy is particularly surprising, and sceptism is most suitably directed at the values of $\overline{A^2}$ and τ derived from relaxation data. It was not possible to measure spin-spin relaxation times, T_2, directly for Te in this alloy but the values deduced from FID T_2^* are thought to be fairly reliable. The major source of error originates in the spin-lattice relaxation data and its associated large uncertainty. However, irrespective of the actual values obtained for the correlation time for tellurium in the alloys, it is of interest to compare the markedly shorter time in elemental tellurium. The tendency to show less metallic behaviour in the alloys is reflected in the Korringa enhancement parameter, η, obtained from the relaxation data. Fig. 6.19 presents a plot of η against conductivity based on the plot of Warren and Dupree (1980b). It is observed that the data for both nuclei in both alloys falls approximately on the extrapolated line described by tellurium and selenium in the degenerate regime of the pure elements.

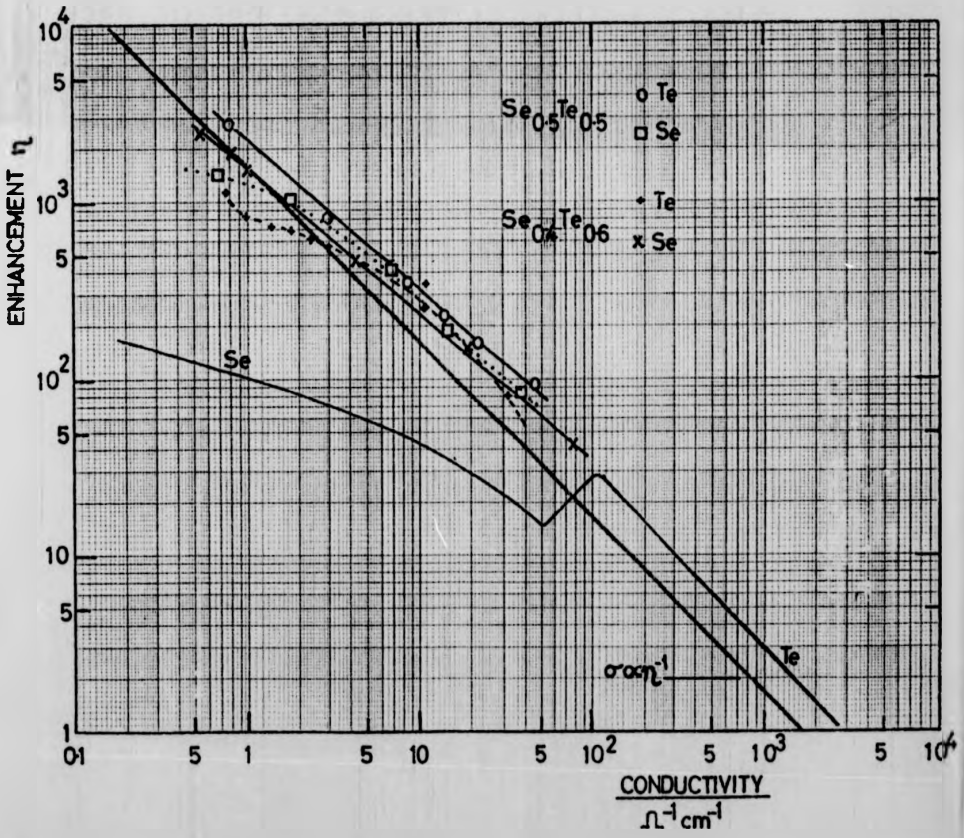

Fig. 6.19: Relaxation enhancement, η, versus conductivity σ. (Based on the plot of Warren and Dupree, 1980).

In both alloys the low temperature tellurium correlation time is apparently longer than that of selenium implying that the unpaired electron stays constant near a tellurium atom for a longer time relative to selenium. If this is the true situation then a random bonding model is not entirely appropriate. Since Te-Te bonds are the weakest available in the system one might expect chain end atoms to be preferentially tellurium, and that this effect would be more significant in $Se_{0.4}Te_{0.6}$ than $Se_{0.5}Te_{0.5}$ since the excess of tellurium requires Te-Te bonding. Qualitatively this may explain the observed behaviour of τ, but more NMR data as a function of concentration and temperature is required before a quantitative model can be established.

6.4. Summary of the Selenium Tellurium System

The ^{77}Se and ^{125}Te NMR results in both of the Se-Te liquid alloy samples studied demonstrate qualitatively similar behaviour as a function of temperature. The paramagentic resonance shift and relaxation arise from the interaction between the nucleus and unpaired electrons and a thermally activated concentration of such electrons explains the observed rapid increase of shift and relaxation rate with temperature. The larger shifts for both nuclei in $Se_{0.4}Te_{0.6}$ compared to $Se_{0.5}Te_{0.5}$ support the idea that the roles of additional tellurium and increasing temperature are similar in these liquid alloys. The basis for this lies in the crucial role played by bonding in determining the alloy properties. Selenium prefers 2-fold coordination and the strong Se-Te bond maintains this low coordination in Se_xTe_{1-x} with $x < 0.5$. Tellurium favours higher coordination and so excess Te disrupts the polymeric chain structure creating bonding defects in a similar manner to increasing temperature. The wide range of electrical behaviour exhibited by Se_xTe_{1-x} liquid alloys as a function of composition and temperature is thus due to a structural change from Se-like (non metallic) to Te-like (nearly metallic). A change

in the hyperfine field at the ^{77}Se nucleus in the liquid alloy $Se_{0.4}Te_{0.6}$ was observed in this work as a function of temperature, and this was correlated with the start of the structural transition. It was not found possible to follow NMR for ^{77}Se in $Se_{0.5}Te_{0.5}$, or for ^{125}Te in either alloy, to high enough temperatures to observe any similar effect.

The initial assumption made in this work of random bonding and of an unpaired electron being equally probable on either selenium or tellurium is brought into question by the characteristics of the hyperfine field detected by NMR. At temperatures near the melting point the correlation time at the tellurium site is longer than at the selenium site. It seems likely that non random bonding occurs with unpaired electrons being located preferentially at tellurium.

Further NMR study of the Se_xTe_{1-x} liquid alloy system, including a wider range of concentrations and temperature, is clearly desirable, and the greatest difficulty in acquiring data is in overcoming the problem of loss of signal with increasing temperature. Since this is due in part to reduced r.f. skin depth, then dispersal of samples with insulating material may prove beneficial. Interpretation of the mechanism responsible for the hyperfine field correlation time would be aided by the as yet unavailable ESR data on these alloys.

References

Abragam, A. (1961). "The Principles of Nuclear Magnetism", O.U.P. London.

Allgaier, R.S. (1969). Phys. Rev. 185, 227.

Almbladh, C. O., and von Barth, U., Phys. Rev. B13, 3307.

Anderson, P.W. (1958). Phys. Rev. 109, 1492.

Anderson, P.W. (1975). Phys. Rev. Lett. 34, 953.

Angell, C.A. (1971). A Rev. Phys. Chem., 22, 429.

Avci, R. and Flynn, C.P. (1979). Phys. Rev. B 19, 5967.

Ball, M.A. (1973) Phil. Mag. 28, 1365.

Bennett, L. H., Watson, R.E., and Carter, G.C. (1971) "Electronic Density of States" (ed. Bennett, L.H.), p.601, Bureau of Standards, Washington, Special Publ. 323.

Bhatia, A.B., and Thornton, D.E., (1970), Phys. Rev. B2, 3004.

Blandin, A. and Daniel, E. (1959), J. Phys. Chem. Solids, 10, 126.

Bloch, F., Hansen, W.W., and Packard, M., (1946). Phys. Rev. 70, 474.

Bloembergen, N., Purcell, E.M., and Pound, R.V. (1948), Phys. Rev. 73, 679.

Bloembergen, N. (1949) Physica, 15, 386.

Boolchand, P., and Suranyi, P. (1973) Phys. Rev. B7, 57.

ten Bosch, A., Moran-Lopez, J. L. and Bennemann, K. H. (1976) Ber. Bunsenges. Phys. Chem. 80, 792.

Bredig, M.A. (1964). "Molten Salt Chemistry" (ed. Blander, M.), p.367, Wiley, New York.

Brovers, F., Holzhey, C., and Franz, J. (1980), J.de.Phys. 41, c8-56.

Busch, G., and Vogt, O. (1957). Helv. Phys. Acta. 30, 224.

Butcher, P. N. (1974) J. Phys. C7, 879.

Cabane, B., and Friedel, J. (1971), J. Phys. 32, 73.

Carr, H.Y., and Purcell, E.M. (1954). Phys. Rev. 94, 630.

Carver, G.P., Holcomb, D.F. and Kaeck, J.A. (1976) Phys. Rev. 164, 410.

Cheshnovski, O., Even, U., and Jortner, J. (1977) Solid State Comm. 22, 745.

Clark, W.G. (1964) Rev. Sci. Inst. 35, 316.

References

Abragam, A. (1961). "The Principles of Nuclear Magnetism", O.U.P. London.

Allgaier, R.S. (1969). Phys. Rev. 185, 227.

Almbladh, C. O., and von Barth, U., Phys. Rev. B13, 3307.

Anderson, P.W. (1958). Phys. Rev. 109, 1492.

Anderson, P.W. (1975). Phys. Rev. Lett. 34, 953.

Angell, C.A. (1971). A Rev. Phys. Chem., 22, 429.

Avci, R. and Flynn, C.P. (1979). Phys. Rev. B 19, 5967.

Ball, M.A. (1973) Phil. Mag. 28, 1365.

Bennett, L. H., Watson, R.E., and Carter, G.C. (1971) "Electronic Density of States" (ed. Bennett, L.H.), p.601, Bureau of Standards, Washington, Special Publ. 323.

Bhatia, A.B., and Thornton, D.E., (1970), Phys. Rev. B2, 3004.

Blandin, A. and Daniel, E. (1959), J. Phys. Chem. Solids, 10, 126.

Bloch, F., Hansen, W.W., and Packard, M., (1946). Phys. Rev. 70, 474.

Bloembergen, N., Purcell, E.M., and Pound, R.V. (1948), Phys. Rev. 73, 679.

Bloembergen, N. (1949) Physica, 15, 386.

Boolchand, P., and Suranyi, P. (1973) Phys. Rev. B7, 57.

ten Bosch, A., Moran-Lopez, J. L. and Bennemann, K. H. (1976) Ber. Bunsenges. Phys. Chem. 80, 792.

Bredig, M.A. (1964). "Molten Salt Chemistry" (ed. Blander, M.), p.367, Wiley, New York.

Brovers, F., Holzhey, C., and Franz, J. (1980), J.de.Phys. 41, c8-56.

Busch, G., and Vogt, O. (1957). Helv. Phys. Acta. 30, 224.

Butcher, P. N. (1974) J. Phys. C7, 879.

Cabane, B., and Friedel, J. (1971), J. Phys. 32, 73.

Carr, H.Y., and Purcell, E.M. (1954). Phys. Rev. 94, 630.

Carver, G.P., Holcomb, D.F. and Kaeck, J.A. (1976) Phys. Rev. 164, 410.

Cheshnovski, O., Even, U., and Jortner, J. (1977) Solid State Comm. 22, 745.

Clark, W.G. (1964) Rev. Sci. Inst. 35, 316.

Cohen, M.H., and Thompson, J.C. (1968). Adv. Phys. 17, 857.

Cohen, M. H., Fritzsche, H., and Ovshinsky, S.R. (1969) Phys. Rev. Lett. 22, 1065.

Cohen, M.H., and Jortner, J. (1973) Phys. Rev. Lett. 30, 699.

Cohen, M.H., and Jortner, J. (1974). Proc. Int. Conf. Amorphous Liquid Semiconductors, 5th Garmisch Partenkirchen, p167.

Coulson, C.A. (1961). "Valence", 2nd ed. O.U.P., London.

Cusack, N.E. (1978). "The Metal Non-Metal Transition in Disordered Systems" (Proc. S.U.S.S.P.19) ed. Friedman, L.R., and Tunstall, D.P., S.U.S.S.P., Edinburgh.

Cutler, M., and Mott, N.F. (1969), Phys. Rev. 181, 1336.

Cutler, M. (1971a). Phil. Mag. 24, 381.

Cutler, M. (1971b). Phil. Mag. 24, 401.

Cutler, M. (1976), Phys. Rev. B14, 5344.

Cutler, M. (1977) Liquid Semiconductors. Academic Press, New York.

Das, T.P., and Hahn, E.L. (1958). "Nuclear Quadrupole Resonance Spectroscopy", Solid State Physics Supp. 1, Academic Press, New York.

Davis, E.A., and Mott, N.F. (1970). Phil. Mag. 22, 903.

Deverell, C., and Richards, R.E. (1966). Mol. Phys. 10, 551.

Dupree, R. and Gardner, J.A. (1980), J. de Phys. 41, C8, 20.

Dupree, R., and Seymour, E.F.W. (1972). "Liquid Metals" (Ed. Beer, S.Z.) p.461, Marcel Dekker, New York.

Economou, E.N., Cohen, M.H., Freed, K.F., and Kirkpatrick, E.S. (1974), "Amorphous and Liquid Semiconductors" (ed. Tauc, J.), p.101, Plenum, New York.

Edwards, F.G., Enderby, J.E., Howe, R.A., and Page, D.I. (1975), J. Phys. C. 8, 3483.

Edwards, P.P., and Sienko, M.J. (1978) Phys. Rev. B17, 2575.

Eggarter, T.P., and Cohen, M.H. (1970), Phys. Rev. Lett. 25, 807.

Eisenberg, A. and Tobolsky, A.V. (1960), J. Polym. Sci. 46,19.

Elliott, R.P., (1965). "Constitution of Binary Alloys", 1st Supp. McGraw-Hill, New York.

Enderby, J.E. (1968). "Physics of Simple Liquids", (ed. Temperley, H.N.V., Rawlinson, J.S., and Rushbrooke, G.S., North Holland, Amsterdam.

Enderby, J.E., and Simmons, C.J. (1969), Phil. Mag. 20, 125.

Enderby, J.E., and Collings, E.W. (1970), J. Non-Cryst. Solids 4, 161.

Enderby, J.E. (1973) "Band Structure Spectroscopy of Metals and Alloys", Academic Press, London (ed. Fabian, D.J., and Watson, L.M.).

Enderby, J.E. (1974) "Amorphous and Liquid Semiconductors", (ed. Tauc, J.) Plenum, London.

Enderby, J.E. (1978). "The Metal Non-metal Transition in Disordered Systems", (Proc. S.U.S.S.P.19) ed. Friedman, L. R. and Tunstall, D.P. S.U.S.S.P., Edinburgh.

Evans, R., and Telo da Gama, M.M. (1980). Phil. Mag. B. 41, 3, 351.

Faber, T.E., and Ziman, J.M. , (1965) Phil. Mag. 11, 153.

Faber, T. E. (1972) "Introduction to the Theory of Liquid Metals". C.U.P., London and New York.

Flynn, C. P., and Rigert, J. A. (1973) Phys. Rev. B7, 3656.

Franz, J. R., Brovers, F., and Holzhey, C. (1980). J. Phys. F, 10, 235.

Freyland, W., and Steinleitner, G. (1976), Ber. Bunsenges. Phys. Chem. 80, 810.

Freyland, W., and Steinleitner, G. (1977). "Liquid Metals", (ed. Evans, R., and Greenwood, D.A.) p.436, Inst. of Physics Conf. Ser. 30, London.

Friedman, L. (1971). J. non-cryst Solids 6, 329.

Fritzsche, H. (1978) "The Metal Non-Metal Transition in Disordered Systems", (Proc. S.U.S.S.P.19), ed. Friedman, L. R. and Tunstall, D.P. S.U.S.S.P., Edinburgh.

Gardner, J. A. and Cutler, M. (1976). Phys. Rev. B14, 4488.

Gardner, J. A., and Cutler, M. (1979). Phys. Rev. B 20, 2, 529.

Gaskell, T. (1978). Phys. Chem. Liq., 8, 23.

Gee, G. (1952), Trans. Faraday Soc. 48, 515.

Gerlach, E., and Grosse, P. (ed) (1979). "Selenium and Tellurium", Springer, Berlin.

Glazov, V. M., Chizhevskaya, S. N., and Glagoleva, N. N. (1969). "Liquid Semiconductors", Plenum, New York.

Gordy, W., and Thomas, W. J. O. (1956), J. Chem. Phys. 24, 439.

Grutzmann, G., Dorn, F. W., and Klemm, W. (1961), Anorg. Allg. Chem. 309 210.

Gubanov, A. I. (1965). "Quantum Theory of Amorphous Conductors". Consultants Bureau, New York.

Haase, A. R., Kerber, M. A., Kessler, D., Kroenenbitter, J., Krüger, H., Lutz, O., Miller, M., and Nolle, A., (1977), Z. Natur. 32a, 952.

Hahn, E. L. (1950). Phys. Rev. 80, 580.

Halperin, B. I., and Lax, M. (1966). Phys. Rev. 148, 722.

Halperin, B. I., and Lax, M. (1967) Phys. Rev. 153, 802.

Hansen, M. and Anderko, K. (1958). "Constitution of Binary Alloys", 2nd ed. McGraw Hill, New York.

Hasegawa, A., and Watabe, M. (1977), J. Phys. F., 7, 75.

Heighway, J., and Seymour, E.F.W. (1971), Phys. Kondens, Materie, 13, 1.

Hensel, F. (1977), Can. J. Chem. 55, 2225.

Hensel, F. (1979). Adv. Phys. 28, 555-94.

Hewitt, R. R., and Williams, B. W., (1963), Phys. Rev. 129, 1199.

Hodgkinson, R. J. (1971), Phil. Mag. 23, 673.

Hodgkinson, R. J. (1973), Proc. Int. Conf. Amorphous Liquid Semiconductors, 5th Garmisch Partenkirchen, p.841.

Holcomb, D. F. (1978), "The Metal Non-metal Transition in Disordered Systems", (Proc. S.U.S.S.P.19) ed. Friedman, L. R., and Tunstall, D. P., S.U.S.S.P. Edinburgh.

Holzhey, C., Brovers, F., and Franz, J. R. (1981), J. Phys. F. (in press).

Hoshino, H., Schmutzler, R. W., and Hensel, F. (1975), Phys. Lett. A51, 7.

Hoult, D. I. and Richards, R. E., (1976), J. Mag. Res. 24, 71.

Hoyer, W., Thomas, E., and Wobst, M. (1975), Z. Natur. 30a, 1633.

Huang, H. M., and Liu, T. J. (1971), Phys. Lett. A, 46, 293.

Hubbard, J., (1964). Proc. R. Soc. A. 277, 237.

Ichikawa, K. and Warren W. W. Jr., (1979), Phys. Rev. B20, 1.

Ioffe, A. F., and Regel, A. R. (1960). Progr. Semicond. 4, 238.

Jack, K. H., and Wachtel, M. M. (1957). Proc. R. Soc. 239 A, 46.

Kastner, M., Adler, D., and Fritzsche, H. (1976), Phys. Rev. Lett. 37, 1504.

Kaye, G.W.C., and Laby, T.H. (1968). "Tables of Physical and Chemical Constants", Longmans, London.

Kienast, G., and Verma, J. (1961), Z. Anorg. Allg. Chemie. 310, 143.

Kittler, R. C., and Falicov, L. M., (1976), J. Phys. C. 9, 4259.

Knight, W. D. (1949), Phys. Rev. 76, 1259.

Knight, W. D. (1956), Solid State Physics 2 (ed. Seitz, F. and Turnbull, D.T.) p.93.

Korringa, J., (1950), Physica, 16, 601.

Krüger, K. D., and Schmutzler, R. W., (1976). Ber. Bunsenges. Phys. Chem. 80, 816.

Krüger, K. D., Fischer, R., and Schmutzler, R. W., (1977). "Liquid Metals", (ed. Evans, R., and Greenwood, D. A.) Inst. of Physics Conf. Ser. 30, I.O.P., Bristol.

Lewis, M. H., (1980), private communication.

Littlewood, P.B., (1981), private communication.

Lowe, I. J., and Norberg, R. A. (1957), Phys. Rev. 107, 46.

Lowe, I. J., and Tarr, C. E., (1968), J. Sci. Inst. (2), 1, 320.

March, N. H. (1968), "Liquid Metals", Pergamon, Oxford.

Martin, W., Freyland, W., Lamparter, P., and Steeb, S. (1980). Phys. Chem. Liq., 10, 49.

Miller, A., and Abrahams, S. (1960), Phys, Rev. 120, 745.

Mitchell, A. H. (1957), J. Chem. Phys. 26, 1714.

Mollwo, E. (1948), Z. Phys. 124, 118.

Mott, N. F. (1949). Proc. Phys. Soc. A62, 416.

Mott, N. F. (1961), Phil. Mag. 6, 287.

Mott, N. F. (1967), Adv. Phys. 16, 49.

Mott, N. F. (1968), Phil. Mag. 17, 1269.

Mott, N. F. (1969), Phil. Mag. 19, 835.

Mott, N. F., and Davis, E. A. (1971). "Electronic Processes in Non-Crystalline Materials", O.U.P., London and New York.

Mott, N. F. (1972), Phil. Mag. 26, 1015.

Mott, N. F. (1974). "Metal-Insulator Transitions", Taylor-Francis, London.

Mott, N. F. (1978). Phil. Mag. B 37, 377.

Mott, N. F., and Davis, E. A. (1979), "Electronic Processes in Non-Crystalline Materials", 2nd ed., O.U.P., London and New York.

Münster, P., and Freyland, W., (1979). Phil. Mag. B39, 93.

Nachtrieb, N. H. (1962), J. Phys. Chem. 66, 1163.

Nikoloso, N., Schmutzler, R. W., and Hensel, F., (1978), Ber. Bunsenges. Phys. Chem., 82, 621.

Nieminen, R. M. and Puska, M. (1980), Solid State Comm. 33, 463.

Noer, R. J., and Knight, W. D. (1964). Rev. Mod. Phys. 36, 177.

North, D. M., Enderby, J. E., and Egelstaff, P. A. (1968), J. Phys. C: Solid State Phys. 1, 1075.

Overhof, H., Knecht, J., Fisher, R., and Hensel, F. (1978), J. Phys. F, 8, 1607.

Pauling, L. (1960). "The Nature of the Chemical Bond", 3rd ed. Cornell Univ. Press, Ithaca, New York.

Pearson, W. B. (1972), "The Crystal Chemistry and Physics of Metals and Alloys", Wiley, New York.

Perron, J. C. (1967). Adv. Phys. 16, 657.

Phillips, J. C. (1970), Rev. Mod. Phys, 42, 317.

Phillips, J. C. (1973), "Bonds and Bands in Semiconductors", Academic Press, New York.

Pines, D. (1955), "Solid State Physics", ed. Seitz, F., and Turnbull, D., Academic, New York, Vol. 1.

Pings, C. J. (1968), "Physics of Simple Liquids", ed. Temberley, H. N. V., Rowlinson, J. S., and Rushbrooke, G. S., p. 387, North-Holland, Amsterdam.

Pitzer, K. S. (1962), J. Am. Chem. Soc. 84, 2025.

Purcell, E. M., Torrey, H. C., and Pound, R. V. (1946), Phys. Rev., 69, 37.

Rabi, I. I., Ramsey, N. F., and Schwinger, J. (1954), Rev. Mod. Phys., 26, 167.

Ramsey, N. F. (1950), Phys. Rev., 78, 699.

Richards, P. M. (1978). Phys. Rev. B 18, 6358.

Rigert, J. A., and Flynn, C. P. (1971), Phys. Rev. Lett., 26, 1177.

Robertson, J. (1979), Phil. Mag. B., 39, 6, 479.

Robertson, J. (1981), Private Communication.

Roth, L. M. (1975), Proc. Liquid Met. Conf. Mexico, Jan. 1975.

Roth, L. M. (1977), Liquid Metals, 1976, Conference Series, 30, ed. Evans, R., and Greenwood, D. A., I.O.P., Bristol.

Ryter, C., (1960), Phys. Rev. Lett. 5, 10.

Schmutzler, R. W., Fischer, R., Hoshino, H., and Hensel, F. (1975). Phys. Lett. A, 55, 67.

Schmutzler, R. W., Hoshino, H., Fischer, R., and Hensel, F. (1976), Ber. Bunsenges, Phys. Chem., 80, 113.

Schmutzler, R. W. (1978), Habilitationschrift, Philipps-Univ., Marburg, Germany.

Schumacher, R. T., and Slichter, C. P., (1957), Phys. Rev. 101, 58.

Seidel, H., and Wolf, H. C. (1968), "Physics of Colour Centres", ed. Fowler, W. B., p.538, Acad. Press, New York.

Seymour, E. F. W., and Brown, D. (1973), Proc. Int. Conf. Properties Liquid Met. 2nd, Tokyo, 399.

Sholl, C. A. (1967), Proc. Phys. Soc. 91, 130.

Slichter, C. P. (1978), "Principles of Magnetic Resonance", 2nd ed., Harper, New York.

Sommer, F., Schmutzler, R. W., Predel, B. and Eschenweck, D. (1979). see Schmutzler (1978)

Sotier, S., and Warren, W. W. Jr. (1980), J. de Phys. 41, C8, 40.

Spicer, W. E., Sommer, A. H., and White, J. G. (1959), Phys. Rev. 115, 57.

Steinleitner, G., and Freyland, W. (1975). Phys. Lett. A, 55, 163.

Steinleitner, G. (1978). Thesis, Philipss-University, Marburg, Germany.

Street, R. A., and Mott, N. F. (1975), Phys. Rev. Lett. 35, 1293.

Stuke, J. (1969), Festkörperprobleme, 9, 46.

Tauc, J. (ed.) (1974). "Amorphous and Liquid Semiconductors", Plenum New York.

Thornton, D. E., and Young, W. H. (1968), J. Phys. C., 1, 1097.

Thouless, D. J. (1972), J. Non-Cryst. Solids, 8-10, 461.

Thurn, H., and Ruska, J. (1976). J. Non-Cryst Solids, 22, 331.

Tinelli, G. A., and Holcomb, D. F. (1978), J. Sol. State. Chem. 25, 157.

Tourand, G., and Brevil, M. (1970), C. R. Acad. Sci. Paris, B270, 109.

Tourand, G., Cabane, B., and Brevil, M. (1972), J. Non-Cryst. Solids, 8-10, 676.

Tourand, G. (1975), Phys. Lett. A54, 209.

Townes, C. H., Herring, C., and Knight, W. D. (1950). Phys. Rev. 77, 852.

Vanderbilt, D., and Joannopoulos, J. D. (1979), Phys. Rev. Lett. 42, 1012.

Warren, W. W. Jr., and Clark, W. G. (1969), Phys. Rev. 177, 600.

Warren, W. W. Jr., (1971), Phys. Rev. B3, 11, 3708.

Warren, W. W. Jr., (1972a), Phys. Rev. B6, 2522.

Warren, W. W. Jr., (1972b), J. Non-Cryst. Sol. 8-10, 241.

Seidel, H., and Wolf, H. C. (1968), "Physics of Colour Centres", ed. Fowler, W. B., p.538, Acad. Press, New York.

Seymour, E. F. W., and Brown, D. (1973), Proc. Int. Conf. Properties Liquid Met. 2nd, Tokyo, 399.

Sholl, C. A. (1967), Proc. Phys. Soc. 91, 130.

Slichter, C. P. (1978), "Principles of Magnetic Resonance", 2nd ed., Harper, New York.

Sommer, F., Schmutzler, R. W., Predel, B. and Eschenweck, D. (1979). see Schmutzler (1978)

Sotier, S., and Warren, W. W. Jr. (1980), J. de Phys. 41, C8, 40.

Spicer, W. E., Sommer, A. H., and White, J. G. (1959), Phys. Rev. 115, 57.

Steinleitner, G., and Freyland, W. (1975). Phys. Lett. A, 55, 163.

Steinleitner, G. (1978). Thesis, Philipss-University, Marburg, Germany.

Street, R. A., and Mott, N. F. (1975), Phys. Rev. Lett. 35, 1293.

Stuke, J. (1969), Festkörperprobleme, 9, 46.

Tauc, J. (ed.) (1974). "Amorphous and Liquid Semiconductors", Plenum New York.

Thornton, D. E., and Young, W. H. (1968), J. Phys. C., 1, 1097.

Thouless, D. J. (1972), J. Non-Cryst. Solids, 8-10, 461.

Thurn, H., and Ruska, J. (1976). J. Non-Cryst Solids, 22, 331.

Tinelli, G. A., and Holcomb, D. F. (1978), J. Sol. State. Chem. 25, 157.

Tourand, G., and Brevil, M. (1970), C. R. Acad. Sci. Paris, B270, 109.

Tourand, G., Cabane, B., and Brevil, M. (1972), J. Non-Cryst. Solids, 8-10, 676.

Tourand, G. (1975), Phys. Lett. A54, 209.

Townes, C. H., Herring, C., and Knight, W. D. (1950). Phys. Rev. 77, 852.

Vanderbilt, D., and Joannopoulos, J. D. (1979), Phys. Rev. Lett. 42, 1012.

Warren, W. W. Jr., and Clark, W. G. (1969), Phys. Rev. 177, 600.

Warren, W. W. Jr., (1971), Phys. Rev. B3, 11, 3708.

Warren, W. W. Jr., (1972a), Phys. Rev. B6, 2522.

Warren, W. W. Jr., (1972b), J. Non-Cryst. Sol. 8-10, 241.

Warren, W. W. Jr., (1980), "Adv. in Molten Salt Chem", (ed. Mamantou, G., and Braunstein, J.), 4, Plenum, New York.

Warren, W. W., Jr., and Dupree, R., (1980a), Phys. Rev. B22, 5, 2257.

Warren, W. W. Jr., and Dupree, R., (1980b), J. De Phys. 41, C8, 85.

Waseda, Y., and Tamaki, S., (1975), Phil. Mag. 32, 951.

Weiss, A., and Witte, H. (1973), "Magnetochemie", Verlag Chemie, Weinheim.

Wilson, A. H., (1931), Proc. Roy. Soc. 133, 458.

Winter, J., (1971), "Magnetic Resonance in Metals", Clarendon, Oxford.

Wotten, F., and Condas, G. A., (1963), Phys. Rev. 131, 657.

Yao, M., Suzuki, K., and Endo, H., (1980a), Sol. State Comm. 34, 187.

Yao, M., Misonou, M., Tamura, K., Ishida, K., Tsuji, K., and Endo, H., (1980b), J. Phys. Soc. Japan, 48, 1, 109.

Yafet, Y., and Jaccarino, V., (1964), Phys. Rev. 133, A1630.

Ziman, J. M., (1961), Phil. Mag. 6, 1013.